Hadronization of quarks and gluons into hadron jets at high energies

V. G. Grishin

Joint Institute of Nuclear Research, Dubna (Moscow Province)
Usp. Fiz. Nauk **148**, 221–287 (February 1986)

The available data on the formation of quarks and gluons in hard interactions of particles and their hadronization into hadron jets at high energies are reviewed. Data on the structure functions, fragmentation properties, and interactions of partons are examined. Modern theoretical interpretations of the parton hadronization stage and estimates of the strong interaction constant are presented. The universality of the characteristics of a hadron jet in soft and hard interactions of particles is pointed out.

CONTENTS

1. INTRODUCTION

The rapid development of high-energy physics in recent years has completely altered our understanding of the nature of particles and their interactions. The multiplicity of hadrons and the virtually unrelated directions of research and models were replaced by a unified approach to the description of fundamental interactions.[1,2] This approach is based on the fact that the universe surrounding us is made up of quarks and leptons, which interact by means of the exchange of γ quanta (electromagnetic interactions), gluons (strong interactions), and intermediate bosons (weak interactions), discovered in 1983. This picture of the universe already contains a unified theory of weak and electromagnetic interactions, and for the time being, only a fragment of the theory of strong interactions—the so-called quantum chromodynamics (QCD).[1–4]

QCD successfully describes the interaction of colored partons (quarks and gluons) at small distances ($r \ll R$), where because of a remarkable property of this theory—asymptotic freedom—the interaction is weak and perturbation theory (PT) can be used.[1)] At large distances ($r \sim R$) the interaction becomes so strong that it probably does not allow the colored quarks (gluons) to be in a free state. Only their colorless (white) states—hadrons—are observed in experiments. It is precisely the description of this stage of all processes, at which hadrons form from colored quarks, that is the main unsolved problem of the theory of strong interactions (the confinement problem). For this reason the experimental data are, as a rule, analyzed by using QCD perturbation theory at small distances and phenomenological models for the transitions of quarks into hadrons at $r \sim R$ (see Sec. 2). Because of this symbiosis of the theory and phenomenology even the main strong interaction constant $\alpha_s(Q^2)$, extracted from experiments, is model dependent. It is therefore important to study the formation of hadrons at high energies both in order to determine the structural elements required for constructing a complete theory and in order to check QCD at small distances.

This review is concerned with hadron jets at high energies. Jets are a group of hadrons whose transverse momenta ($p_\perp$) are much smaller than their longitudinal momenta ($p_\parallel$) relative to the axis of the jet (ΣP_i). It is evident that the terminology is borrowed from the standard representations of a jet of liquid or gas ($p_\perp \ll p_\parallel$). Their formation is not, however, a simple problem in the physics of particles (see Sec. 3). Partons indeed do not exist in a free state, whereas at high energies they transform into jets of hadrons, which reflect their properties more fully than individual hadrons.[3,4] The study of hadron jets at high energies is therefore one of the main problems investigated on all the largest accelerators. Hadron jets were discovered in the so-called hard processes, in which a high momentum ($Q^2 \gtrsim 10\ \mathrm{GeV}^2$) is transferred to the partons. These processes include e^+e^- annihilation, deep-inelastic *lN* interactions, production of particles and jets with high transverse momenta in hadronic interactions, etc.

The discovery of hadron jets in accelerators with collid-

 0038-5670/86/020126-40$01.80

ing beams (e^+e^-, pp, $\bar{p}p$) in hard processes showed immediately that two different temporal (or spatial) stages of these reactions can be studied. At first, partons with high momenta are formed over a very short time $\tau \sim 1/Q$, and QCD PT is applicable here. Then, over a longer time $t \sim 1/m$, they transform into hadrons, and this stage is described with the help of models (m is the hadron mass).[2)] For example, already at $Q^2 \gtrsim 10$ GeV^2 these stages appear in substantially different regions: $C\tau \lesssim 0.1$ fm and $ct \gtrsim 1$ fm. In addition, the experimental data show that the characteristics of hadron jets largely coincide with the properties of the partons generating them. This was the origin of the hypothesis of soft decolorization, in which it is assumed that when the partons are hadronized their momenta and quantum characteristics are transferred to the hadron jet (see Secs. 4 and 5), i.e., in the first approximation the formation and hadronization of partons with high momenta can be regarded as independent processes. In the opposite case the picture would be very complicated, and it is unlikely that such spectacular results would have been obtained over a relatively short time.

The observed universality of hadron jets, produced in weak, electromagnetic, and strong interactions, also serves as a confirmation of this hypothesis—the hadronization of partons occurs independently of the method by which they are formed. It is therefore desirable to study jointly (see Sec. 5) the properties of the hadron jets produced in different interactions (see Sec. 4).

The physics of hadron jets is linked primarily with hard processes, which comprise only a small relative fraction ($\lesssim 1\%$) of all hadron interactions. However, soft collisions of hadrons ($Q^2 \sim m^2$), which have now been studied for more than 30 years in cosmic rays and in accelerators, have played an important role in understanding the physics of hadron jets. These processes do not have a hard stage and QCD PT is not applicable. They are described with the help of phenomenological models.[5–9] However, the soft stage of hard processes—the hadronization of partons—has much in common with soft collisions of hadrons.[3)] Many models of parton hadronization, moreover, make use of the basic characteristics of these processes: the limitation of the transverse momentum of the hadrons, the quasiplateau in the rapidity in the central region, the approximate scaling in the fragmentation region, and the short-range correlation between the hadrons. The unity of the physics of soft and hard processes is well reflected in the parton model,[8,9] which is widely used in their interpretation. In this connection we shall briefly discuss the basic characteristics of soft hadron collisions, which clearly have a general character, in Sec. 2.

In our presentation we assume that the reader is familiar with the fundamentals of the theory of the interactions of leptons and quarks.[1–4] The phenomenology of soft collisions is presented in Refs. 5–7 and the original parton model is presented in Refs. 8–9. Some questions regarding the formation of hadron jets are discussed in review articles in Usp. Fiz. Nauk [Sov. Phys. Usp.] and Fiz. Elem. Chastits At. Yadra [Sov. J. Part. Nucl.].[10–13] The main results obtained up to 1982 are presented in these papers. Since then the period of pessimism regarding the existence of jets in hadronic interactions (Sec. 3) has passed. Jets were separated in pp interactions in 1982 (CERN). Now, with the successful operation of the collider at CERN with colliding beams of protons and antiprotons (270×270 GeV^2). We have entered the period of jet production: hadron jets can be seen, as they say, with the naked eye. We shall therefore devote our principal attention to the latest results obtained on accelerators with colliding beams.

2. FUNDAMENTALS OF THE PARTON MODEL AND QCD

The discovery of scaling (1968) in experiments on deep inelastic electroproduction was the first direct experimental indication of the existence of new point particles inside nucleons. These results served as the foundation for the parton model (1969), which is widely used to describe the interaction of high-energy particles.[8–9] It has now been established that these new particles—partons—are quarks (q_i) and gluons (g).[1–4] Basically, a hadron consists of two (mesons) or three (baryons) valence quarks (q_v) and gluons. The quantum numbers of the valance quarks determine the quantum numbers of the hadrons. In addition, a hadron contains a so-called "sea" of ($q_s \bar{q}_s$) pairs, which have zero quantum numbers and arise as a result of vacuum fluctuations. This picture of hadron structure was obtained from deep-inelastic processes.[3,4]

In the parton model all interactions of particles reduce to the interaction of their constituents—partons. It successfully describes both soft processes and the characteristic features of hard collisions.[1–19] In particular, the formation of hadron jets at high energies, which are the subject of this review, was predicted on the basis of this model. The possibility of a unified approach to the description of all interactions is an attractive feature of the parton model, which is for the time being inaccessible to QCD.

On the other hand, the parton model of hard processes is only the zeroth-order approximation of QCD. Indeed, at high energies and $Q^2 \to \infty$, because of the asymptotic freedom of QCD, the partons can be regarded as free particles, which is the starting postulate of this model.[8,9] Thus the parton model is the first stage in the theoretical description of all interactions, and we shall examine its basic hypotheses and results for both soft (see Sec. 2.1) and hard processes (see Sec. 2.2).

Soft processes are studied because their properties have been investigated most fully, and they have been widely used in the formulation of the parton hadronization stage in hard processes. In addition, in the last few years it has been shown experimentally that hadron jets form universally in any interactions, which undoubtedly indicates the unity of the physics underlying their production, which for the time being cannot be given a rigorous theoretical interpretation.

The hard stage of jet formation is described by QCD.[1–4] We shall therefore study the simplest gluon-quark interaction diagrams, as well as a modification of the formulas of the parton model taking into account the effects of QCD (see Sec. 2.3).

2.1. Soft processes

2.1.1. Experimental characteristics

The hypotheses of the parton model (of which there are more than fifteen) concerning the momentum characteristics of the partons in hadrons, are largely based on the experimental data on the properties of soft ($Q^2 \sim m^2$) hadronic collisions at high energies ($s^{1/2} \gtrsim 10$ GeV).[8,9, and 4] For this reason, following the historical development of the present understanding of the parton nature of interactions, we shall briefly present the basic characteristics of these processes.[5-7]

The single-particle

$$a + b \to c + X, \tag{2.1}$$

and the two-particle

$$a + b \to c_1 + c_2 + X \tag{2.2}$$

multiple processes, where a and b are the primary particles, c_1 and c_2 are the secondary hadrons, and X is any hadronic accompaniment, have been studied in detail in the inclusive approach.[5-9] They are described by the corresponding invariant distributions[5)]

$$\frac{E_c}{\sigma_{in}} \frac{d\sigma_c^{ab}}{dp_c} = f_c^{ab}(s^{1/2}, p_c), \tag{2.3}$$

$$\frac{E_{c_1}E_{c_2}}{\sigma_{in}} \frac{d\sigma_{c_1c_2}^{ab}}{dp_{c_1}\,dp_{c_2}} = f_{c_1c_2}^{ab}(s^{1/2}, p_{c_1}, p_{c_2}), \tag{2.4}$$

which in the general case depend on three (2.3) and six (2.4) kinetic variables and the quantum numbers of the primary (a, b) and secondary (c_1, c_2) particles.[6)] Aside from the total energy ($s^{1/2}$) of the collision, different sets of kinematic variables, depending on the region of the phase space of the reactions (2.1) and (2.2) studied, are usually used. They are discussed in detail in Refs. 5–7. For our purposes it is sufficient to study only two characteristic regions: the central and fragmentation regions, where the functions (2.3) and (2.4) behave differently. In these cases the variables

$$x = \frac{p_\parallel^*}{p_{max}^*} \approx \frac{2p_\parallel^*}{s^{1/2}}, \tag{2.5}$$

$$y = \frac{1}{2} \ln \frac{E + p_\parallel}{E - p_\parallel} \tag{2.6}$$

and $p_\perp$ are used.[7)] Here x is Feynman's variable; $p_\parallel^*$, p_{max}^* are the longitudinal and maximum possible momenta of the secondary particles in the center of mass system, and y is the longitudinal rapidity (or simply the rapidity), which is convenient for studying slow particles ($v \approx p/E \ll 1$) in the central region. The boundary between these regions is very uncertain, but with the energies of existing accelerators it may be assumed that in the central region $x \lesssim 0.1$–0.05 or $|y| \lesssim |y_{min}^{max}| - 2$.[5-7] The structure functions of the process (2.1) in these variables have the following form:

$$f(s^{1/2}, p) = \frac{E^* d^3\sigma(s)}{\sigma_{in}(s)\,\pi p_{max}^*\,dx\,dp_\perp^2} \approx \frac{2E^*}{\pi s^{1/2}\sigma_{in}(s)} \frac{d^2\sigma(s)}{dx\,dp_\perp^2}, \tag{2.7}$$

$$f(s^{1/2}, p) = \frac{1}{\pi\sigma_{in}(s)} \frac{d^2\sigma(s)}{dy\,dp_\perp^2}. \tag{2.8}$$

The form of the distribution (2.8) remains unchanged under longitudinal Lorentz transformations, and only the origin is shifted by a constant amount $y_0 = (1/2) \ln [(1 + v_0)/(1 - v_0)]$, where v_0 is the relative velocity of the frames of reference. Having introduced the basic concepts of the inclusive description of multiple processes we shall list their basic characteristics[14-19]:

1. The transverse momenta $p_\perp$ of the secondary hadrons are limited ($p_\perp \lesssim 1$) GeV and $\langle p_\perp \rangle = 0.4 - 0.5$ GeV in a wide range of energies ($s^{1/2} = 10 - 540$ GeV), while $p_\parallel^* \sim s^{1/2}$.[5-7,14] The double-jet picture of soft hadronic collisions at high energies ($p_\perp \ll p_\parallel^*$) follows from here[5-7,14] This remarkable result was first obtained in experiments with cosmic rays for long-lived particles ($\tau \gtrsim 10^{-10}$ s), primarily for π mesons ($\langle p_\perp \rangle \approx 0.35 \pm 0.05$ GeV).[6] In experiments on accelerators it was found that short-lived ($\tau \lesssim 10^{-22}$ s) states—resonances (R)—form the main fraction ($\approx 80\%$) of the secondary particles, while the long-lived hadrons (π and K mesons and baryons) are, as a rule, products of their decay.[5] The distributions of the direct reaction products—resonances—over $p_\perp^2$ are described by the simple formula

$$\frac{1}{\sigma_{in}} \frac{d\sigma(R)}{dp_\perp^2} = \langle n(R) \rangle\, e^{-B(R)p_\perp^2}, \tag{2.9}$$

where $B(R) = 3.4 \pm 0.2$ GeV^{-2}, which corresponds to $\langle p_\perp(R) \rangle = 0.47 \pm 0.02$ GeV. The formula (2.9) is valid for resonances with $M(R)$ from 0.55 GeV (η mesons) to 1385 MeV ($\Sigma^{*\pm}$) and direct pions.[5 8)] The limitedness of the transverse momentum of the hadrons discovered experimentally is widely employed in models and still does not have a satisfactory theoretical explanation.

2. In the central region the invariant distributions of the hadrons are virtually independent of the quantum numbers of the primary and secondary particles, with the exception of the values of $\langle n(R) \rangle$. They have for $s^{1/2} = 23 - 63$ GeV a quasiplateau in y:

$$f(s, p_\perp^2, y) = A_c \left(\frac{s}{s_0}\right)^\alpha (1 - \beta\,|\,y\,|)\, e^{-Bm_\perp}, \tag{2.10}$$

where $m_\perp^2 = m^2 + p_\perp^2$, $s_0 = 1$ GeV^2, $\alpha \approx 0.2$, $\beta \approx 0.1$, $B \approx 7$ GeV^{-1}.[9)] The width and height of this quasiplateau increase with energy as $\sim \ln s$ and s^α (or $\sim \ln s$), respectively.[5,14] The growth in the average multiplicity of the hadrons is linked precisely with this behavior:

$$\langle n(s) \rangle \sim \int f(s, p_\perp^2, y)\, dp_\perp^2\, dy \sim \ln^2 s. \tag{2.11}$$

The universality of $f(s, p_\perp^2)$ for different processes and the existence of a quasiplateau in y are employed in parton models.[10)]

3. In the fragmentation region the invariant functions (2.7) are virtually independent of the total collision energy $f(p_\perp^2, x)$. This phenomenon is called Feynman scaling or the scale invariance of strong interactions.[8] It was discovered in experiments performed on accelerators at the Institute of High Energy Physics (Serpukhov) and CERN (Geneva).[5,6]

The distributions $f(x, p_\perp^2)$ for $x = 0.2$–0.8 are satisfactorily described by the formula

$$f(x, p_\perp^2) = A(p_\perp^2)(1 - x)^m, \tag{2.12}$$

where m depends on the quantum numbers of the primary and secondary hadrons.[6] Possible explanations for the values of m for different processes are given on the basis of the quark-parton models.

4. Correlations in the production of two particles (2.2) have been studied with the help of the functions:

$$C_2(y_1, y_2) = \frac{1}{\sigma_{1n}} \frac{d^2\sigma}{dy_1\, dy_2} - \frac{1}{\sigma_{1n}^2} \frac{d\sigma}{dy_1} \frac{d\sigma}{dy_2}, \qquad (2.13)$$

$$R_2(y_1, y_2) = \frac{C_2(y_1, y_2)}{\sigma_{1n}^{-2} (d\sigma/dy_1)\, d\sigma/dy_2} = \frac{\sigma_{1n}\, d^2\sigma/dy_1\, dy_2}{(d\sigma/dy_1)\, d\sigma/dy_2} - 1, \qquad (2.14)$$

for different sets of primary and secondary particles.[11)] These correlation functions vanish if the hadrons are created independently.[12)] Numerous experiments have demonstrated a short-range correlation in the production of the long-lived hadrons in the variables Δy, $\Delta p_\perp$ and $\Delta\varphi$ ($\Delta\varphi = \varphi_1 - \varphi_2$ is the difference of the azimuthal emergence angles of the particles).[5,6] The correlation lengths (L) are: $L(\Delta y) \approx 2$, $L(\Delta\varphi) \approx 0.2$–$0.3$ and $L(\Delta p_1) \approx 0.15 - 0.2$ GeV^{-1}. They are largely explained by the kinematic decay of the resonances. Unfortunately data on the correlations of the direct products of the collisions—resonances—have not yet been obtained.

The intervals of compensation of different quantum numbers of the secondary hadrons (charge, isotopic spin, baryon number, etc.) in the kinematic variables (x, y, $p_\perp$) have also been studied. They have a short-range character (the so-called local compensation).

The long-range correlations with respect to the multiplicity in the production of hadrons, emerging into different hemispheres in the center of mass system, have been observed in $p\bar{p}$ interactions with $s^{1/2} = 540$ GeV. These basic characteristics of soft processes were obtained as a result of multiyear studies of cosmic rays and on accelerators, including also the CERN collider (1984).[14] When the parton model was created (1969–1973)[8,9] not all of them were known. In particular, the large contribution of the resonances and the relatively fast growth of $f(y = 0, s)$ and $\langle n(s)\rangle$ with energy were discovered in recent years. This does not, however, affect the foundations of the model, and its further modifications take these features into account.

2.1.2. The parton model

The main hypothesis of the parton model is that a real particle with a high momentum (p) can be regarded as a collection of some number ($n \sim \ln(p/\mu)$) of virtually noninteracting point partons with limited masses (μ) and transverse momenta ($k_\perp$). The longitudinal momenta ($k_\parallel$) of the partons vary from p to $k_\parallel \sim \mu$ (Fig. 1a).[8,9] In this case the fast particle is weakly coupled with the fluctuations of the vacuum, which appear over short time intervals ($\tau \sim 1/k$) and are important only for slow partons ($k \sim \mu$). Thus a hadron in the limit $p \to \infty$ consists of a jet of partons ($k_\perp \ll k_\parallel$), moving in the direction $\mathbf{p}$ (see Fig. 1a).

Further, hypotheses on the momentum distributions of the partons are formulated based on the experimental data on multiple processes (see Sec. 2.1.1) and model assumptions[8,9]:

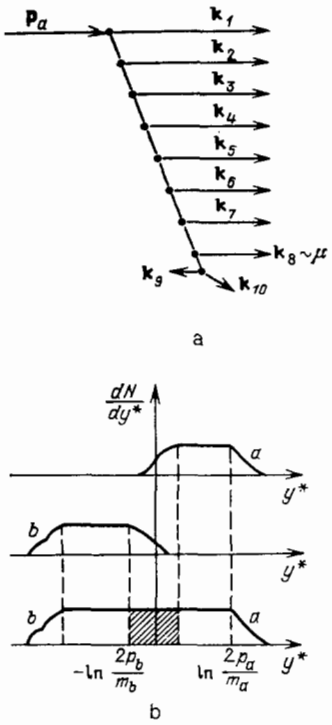

FIG. 1. a) Parton scheme of hadrons with $p \to \infty$. b) Rapidity distribution of partons in hadrons (a,b) before and after a collision.

1. The structure function of a hadron $F_h^q(p, k_\perp^2, k_\parallel)$ in the limit $p \to \infty$ depends only on $x = k_\parallel/p$, i.e., scale invariance holds. It is convenient to represent it in the form $F_h^q(x, k_\perp^2) = xq(x, k_\perp^2)$, where $q(x, k_\perp^2)$ is the probability density for finding partons with x and $k_\perp^2$.

2. The distribution of partons over the transverse momenta is limited and $\langle k_\perp\rangle = 0.3 - 0.5$ GeV.

3. In the central region the parton distribution is universal for all hadrons and is independent of x:

$$F_h^q(x, k_\perp^2) = \text{const}, \quad q(x) \sim \frac{1}{x}.$$

This means that the parton rapidity distribution ($F_h^q(y, p_\perp^2)$) has a plateau (Fig. 1b).

4. In the fragmentation region $F_h^q(x) \sim (1 - x)^m$ where m depends on the quantum numbers of the partons and hadrons.

5. Partons interact with one another only if $\Delta y \approx 1 - 2$ (short-range correlations).

As we can see, the main hypotheses of the model (items 1–5 above) are consistent with the established characteristics of multiple processes (see Sec. 2.1), with the exception of a strong breakdown of scale invariance of the hadron distribution in the central region (growth of the height of the plateau with s). This breakdown is linked with the wave nature of the interactions and is described by QCD.

In the model the hadrons interact via slow partons:

$$\sigma \sim \pi\lambda^2 \sim (s_{12})^{-1} \sim e^{-\Delta y_{12}}, \qquad (2.15)$$

where σ is the cross section for the interaction of point par-

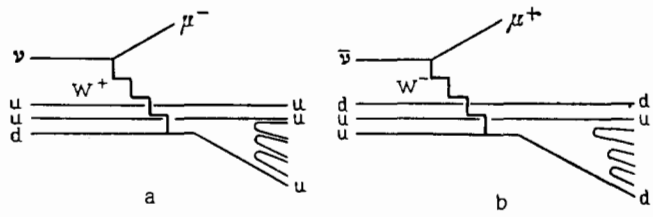

FIG. 2. Diagrams of deep-inelastic interaction of ν (a), $\bar{\nu}$ (b), and $l^{\pm}$ (c) with protons p (uud).

tons, $\hbar$ is the wavelength, $s_{12}^{1/2}$ is the total energy, and Δy_{12} is the relative rapidity of these partons. Therefore only slow partons with $\Delta y_{12} \lesssim 1-2$ can interact with a large cross section. As a result of their interaction all other partons can no longer assemble into the starting hadrons; they will move apart in space, producing as a result of their decays and decolorization, hadrons with rapidities in the interval from 0 to $\ln(2p/m)$ (see Fig. 1b). Because the interaction between the partons has a short range the hadron rapidity distribution will reproduce the distribution of the starting partons. This is what determines the agreement in the overall characteristics of soft processes between the model and the experiment. The mechanism for the transition of partons into hadrons is itself unknown, and for this reason additional assumptions must be made in order to make more specific predictions about the characteristics of the hadrons.[15-19]

The space-time picture of the interactions is also described quite simply in the parton model.[9] In the absence of a theory this is especially important in order to understand the physics of the decolorization processes and to study collisions between particles and spatially extended objects—nuclei.[20-22] The picture of the formation of a jet (see Fig. 1a) as a result of the successive emission of partons with $k_{\perp} \sim \mu$ and $k_{\parallel}$ yields a distribution which is characteristic for diffusion in the plane perpendicular to **p**:

$$\varphi(\rho, y) = \frac{C(y)}{\pi\gamma(y_p - y)} \exp\left[-\frac{\rho^2}{\gamma(y_p - y)}\right], \qquad (2.16)$$

where ρ is the impact parameter of the collision and $n = \gamma(y_p - y)$ is the number of partons in the interval $\Delta = y_p - y$ and $y_p = \ln(2p/m)$. From here it follows that slow partons ($y \approx 0$) have the widest distribution, and the transverse size of a fast hadron is

$$R_{\perp} \approx (\gamma y_p)^{1/2} = \left(\gamma \ln \frac{2p}{m}\right)^{1/2}, \qquad (2.17)$$

which leads to the well-known growth of $R_{\perp}$ in the limit $p \to \infty$. In the longitudinal direction (z) each parton with $k_{\parallel}^{i}$ is distributed in the interval $\Delta z \sim 1/k_{\parallel}^{i}$, and the longitudinal dimensions of the hadron are once again determined by slow partons:

$$R_{\parallel} \approx \frac{1}{k_{\parallel}} \sim \frac{1}{\mu}. \qquad (2.18)$$

Thus a fast hadron is a disk with a radius $R_{\perp}$ and thickness $R_{\parallel} \sim 1/\mu$. The total hadron interaction cross sections are determined by the dimensions of the hadrons and $\sigma \sim \pi R_{\perp}^2 \sim \gamma \ln(2p/m)$.

In this space-time picture the concept of the lifetime of one or another parton fluctuation is also meaningful, and hence also the "lifetimes" of partons

$$\tau \sim \frac{k_i}{\mu^2} \sim \tau_0 \frac{k_i}{\mu}, \qquad (2.19)$$

where τ_0 is the characteristic lifetime of a parton in its rest system.[9] It is evident from (2.19) that the lifetime of partons increases with momentum and their hadronization occurs at increasingly larger distances, which is taken into account in the study of hadron-nuclear interactions.[20-22]

These basic hypotheses of the parton model[8,9] regarding the structure of the hadrons are widely employed in the analysis of soft and hard processes at high energies.[1-9] To describe transitions of partons into hadrons the so-called fragmentation functions $D_q^h(z, p_{\perp}^2,)$ whose properties are in many ways analogous to those of $F_h^q(x, k_{\perp}^2)$, are introduced.[13)] The specific form of the functions D_q^h and F_h^q is determined from the experimental data on hard processes (see Sec. 2.2). The quantum numbers (charge, strangeness, etc.) of the partons and their corresponding hadron jets are related to one another, which is what makes it possible to measure them experimentally (see Sec. 4).

2.2. Hard processes

2.2.1. Types of processes

At the present time the main information on hard processes is obtained from the study of deep inelastic l N interactions (Fig. 2), e^+e^- annihilation into hadrons (Fig. 3), and hh collisions (Fig. 4).

In the parton model l N interactions are regarded as being the result of incoherent elastic interaction of leptons with a jet of quarks making up the hadrons. The cross sections of these processes are therefore determined by the known cross sections for the interactions of leptons with charged point quarks ($\sigma(lq \to lq)$) and by the momentum distribution of the quarks in the nucleon ($q(x)$).[1,2] As can be seen from Fig. 2, in this case two jets ($J_i(h)$) of hadrons, associated with the fragmentation of the "knocked out" quark

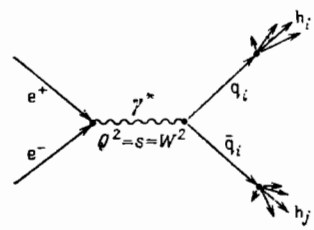

FIG. 3. Diagram of e^+e^- annihilation into two hadron jets.

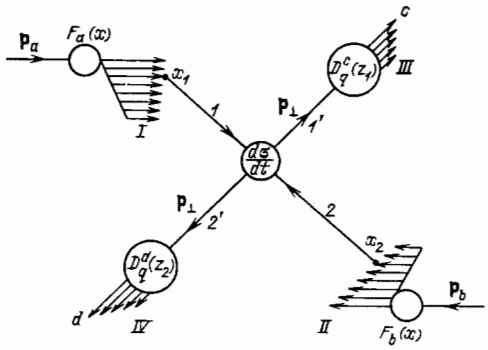

FIG. 4. Scheme of the formation of four (I–IV) hadron jets in hard hh collisions.

($D^{h}_{q_i}(z)$) and the remaining diquark ($D^{h}_{qq}(z)$), are formed.[14)]

In e^+e^- annihilation (see Fig. 3), in the simplest case, two hadron jets are formed in the decay of a virtual γ^* quantum ($Q^2 = s = W^2$) into a $q\bar{q}$ pair. The hadron distributions in the jets are described by the quark and antiquark fragmentation functions $D^{h}_{q(\bar{q})}(z)$.

Finally, the third and most complicated type of hard processes are the hh interactions (see Fig. 4). They are determined by the structure functions of the interacting hadrons ($F^{q}_{a,b}(x)$), by the parton interaction cross section, and by the quark and gluon fragmentation functions ($D^{h}_{q}(z)$. Here four jets of hadrons are formed. Two jets (I, II) are associated with the partons which did not enter into the reaction; they are usually called the spectator jets (J_s (h)). The other two jets (III, IV) are formed with the fragmentation of the scattered partons and, as a rule, have high transverse momenta or energies. These jets can be seen only at high energies $s^{1/2} \gtrsim 20 - 30$ GeV.

Thus hard processes yield quite complicated information on quark and gluon formation and fragmentation, which at first glance appears to refer to entirely different situations. In all these reactions, however, there are two stages: the formation of partons at very short distances ($r \sim 1/Q$) and their transformation into hadrons at large distances ($R \sim 1/m$). The experiments show that in the first approximation these stages are independent of one another. The formation of partons and their fragmentation into hadrons can therefore be studied separately. In this case different hard processes can be analyzed at the same time and data on the structure functions of the hadrons, parton interaction cross sections, and parton fragmentation into hadrons can be obtained.

2.2.2. Momentum distributions of quarks in hadrons (deep-inelastic l N interactions)

The study of inclusive processes

$$l + N \to l' + X, \tag{2.20}$$

with large transfers of momentum (Q) and energy (ν) enables the measurement of the momentum distributions of quarks in nucleons ($q(x)$), which form the starting data for the analysis of any hard collisions with the participation of hadrons.[1–4] In electromagnetic interactions ($l \equiv e, \mu$) the cross section of (2.20) can be represented in the form

$$\frac{d^2\sigma}{dx\,dy} = \sigma_0(x, y) \sum_i e_{q_i}^2 q_i(x), \tag{2.21}$$

with $x = Q^2/2m\nu, y_h = q\,p/m = \nu/E, \nu = E - E'$, m is the nucleon mass, and e_{q_i} is the charge of a quark in units of the electron charge (see Fig. 2).[1,2 15)] Physically x is the relative fraction of the momentum of the nucleon carried away by the quark ($0 \leqslant x \leqslant 1$), and y_h is the relative fraction of the energy of the lepton transferred to the hadron in the laboratory coordinate system. The first factor in (2.21) corresponds to the cross section of the elementary process (for example, $e\mu \to e\mu$), taking into account the fact that the square of the total energy in an lq interaction is $\hat{s} = xs$:

$$\sigma_0(x, y) = \frac{2\pi\alpha^2}{sx} \frac{1 + (1 - y_h)^2}{y_h^2}, \tag{2.22}$$

where $\alpha = 1/137$.[16)] Thus in the parton model the cross section of the lN interaction is the product of the known cross section for scattering of point particles and the momentum distribution function of the quarks in the nucleon. Therefore, using (2.21), information on $\Sigma e_{q_i}^2 q_i(x)$ can be obtained from the data.

Measurements of lN interactions on protons and deuterons with Q^2 ranging from 1 to 200 GeV^2 and x ranging from 0.03 to 0.9 have now been performed.[23–26] As a result it was found that scaling breaks down (see for example, Fig. 5). As Q^2 increases the function $F_2(x, Q^2)$ increases in the region $x < 0.2$ and decreases in the region $x > 0.2$. This effect is linked with the interaction of partons and is explained in QCD. It was also established that the valence-quark distribution $d_v(x)$ in the proton is narrower than $u_v(x)$.[24] As an approximation it can be assumed that

$$\frac{d_V(x)}{u_V(x)} \approx 0.57\,(1 - x). \tag{2.23}$$

More detailed information on $q(x)$ can be obtained from experiments on $\nu(\bar{\nu})$N interactions. Because of the law of conservation of leptonic charge ν interacts with d, s, and $\bar{u}$ quarks, while $\bar{\nu}$ interacts with u, s, and $\bar{d}$ quarks in the nucleon.[1,2] For example the cross section for $\nu_\mu\, p \to \mu^- X$ is equal to

$$\frac{d^2\sigma}{dx\,dy_h} = \frac{G^2 sx}{\pi}\,[d(x) + s(x) + \bar{u}(x)\,(1 - y_h)^2], \tag{2.24}$$

where $G = 10^{-5} m_p^{-2}$ is the Fermi constant and the first factor in (2.24) is the cross section for scattering of ν by a quark taking into account the fact that $\hat{s} = sx$. Analogous formulas for $\bar{\nu}p$, νn, and $\bar{\nu}n$ interactions include other combinations of $q_i(x)$.[1,2] The combined study of these processes therefore enables obtaining the momentum distributions

$$xu_V(x),\ xd_V(x),\ x\left[\bar{u}(x) + \frac{3}{4}s(x)\right],$$
$$x\left[\bar{d}(x) + \frac{3}{4}s(x)\right]$$

in the proton (Fig. 6, $\langle Q^2 \rangle \approx 8$ GeV^2).[17)]

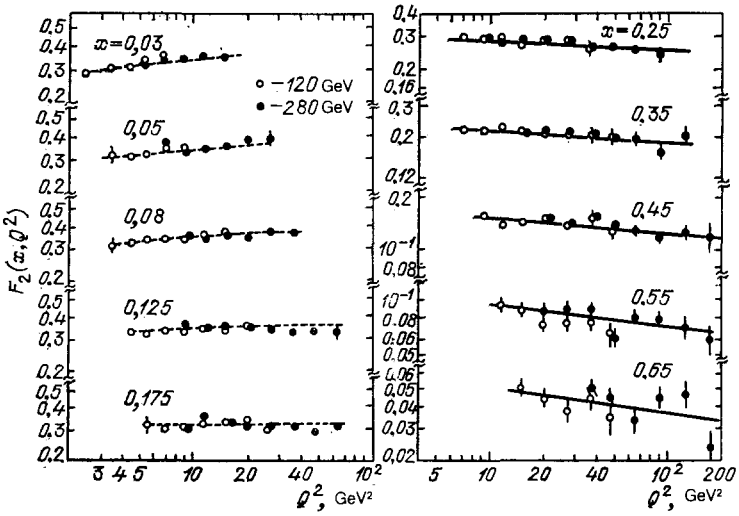

FIG. 5. $F_2(x,Q^2)$ as a function of Q^2 for different values of x (E_μ = 120 and 280 GeV). The broken and solid curves show the QCD approximation of the data.

We shall list the basic results obtained by studying lN interactions, which we shall require in order to analyze the formation and fragmentation of partons.[24–26]

1. The sea quarks and antiquarks u_s ($\bar{u}_s$); d_s ($\bar{d}_s$), s($\bar{s}$) have low momenta $x_s \lesssim 0.3$ (see Fig. 6), they carry about 0.08 of the momentum of the nucleon, and $q_s(x) \sim 1/x$. Within the limits of error ($\sim 30\%$) there is no difference between the quark distributions $\bar{u}_s(x)$ and $\bar{d}_s(x)$.[25,26] The contribution of the momentum of the sea quarks in the nucleon is estimated to be ~ 0.005.[24]

2. The distribution of the valence u_v quarks over x is wider than that of the d_v quarks (2.23).[24] The average relative fractions of the proton momentum carried off by the u_v and d_v quarks are equal to 0.24 and 0.09, respectively (with an uncertainty of $\sim 10\%$). The total momentum carried away by the quarks and antiquarks is equal to 0.45 ± 0.03.

3. The gluons carry approximately one-half of the momentum of the nucleon. From data on νN interactions, taking into account the effects of QCD, it was found that

$$G(x, Q_0^2) = xg(x, Q_0^2) = 2.62\,(1+3.5x)\,(1-x)^{5.9}, \qquad (2.25)$$

with $\langle Q_0^2 \rangle = 5$ GeV^2.[25,26] As expected, the gluons are found in the same region of x as the sea quarks ($\langle x_g \rangle \approx 0.16$).

4. It was found that the quark distribution in the nucleon depends on Q^2 ($q_i(x, Q^2)$).

Thus the quark and gluon momentum distributions in nucleons are known in the first approximation with $\langle Q^2 \rangle \approx 5 - 10$ GeV^2. For example, they are parameterized in the form

$$\left.\begin{aligned} xu(x) &= 2.13x^{1/2}(1-x)^{2.3} + 0.27\,(1-x)^{3.1}, \\ xd(x) &= 1.26x^{1/2}(1-x)^{3.8} + 0.27\,(1-x)^{3.1}, \\ x\bar{u}(x) &= x\bar{d}(x) = 0.27\,(1-x)^{3.1}, \\ xs(x) &= x\bar{s}(x) = 0.5x\bar{u}(x), \end{aligned}\right\} \qquad (2.26)$$

where it is assumed that the strange sea quarks comprise approximately one-half of the u_s or d_s quarks. This parametrization is used to find $q_i(x, Q^2)$ when $Q^2 \geqslant 100$ GeV right up to the collider energies ($s^{1/2} = 540$ GeV).[10]

The structure functions of the pions were studied in processes of the Drell-Yan type:

$$\pi^\pm + N \to \mu^+\mu^- + X, \qquad (2.27)$$

with $E_\pi \geqslant 150$ GeV and effective masses $M(\mu^+\mu^-) = 4.2 - 8.5$ GeV.[3,4,24,27] The cross section of (2.27) is determined by the nucleon structure functions ($F_N^{q_i} \sim (1-x)^m$ with $m_{u(d)} \approx 3(4)$), by the cross section of the annihilation process $\bar{q}q \to \mu^+\mu^-$, and by the pion structure functions ($F_\pi^q(x)$). Using the known functions $F_N^q(x, Q^2)$ it was found from the data on the process (2.27) that

$$F_\pi^{\bar{u}_V}(x) = x\bar{u}^{\pi^-} \sim x^{0.41 \pm 0.04}\,(1-x)^{0.95 \pm 0.05}, \qquad (2.28)$$

where $\langle Q^2 \rangle = \langle M^2(\mu^+\mu^-) \rangle = 25$ GeV^2.[27] The valence-

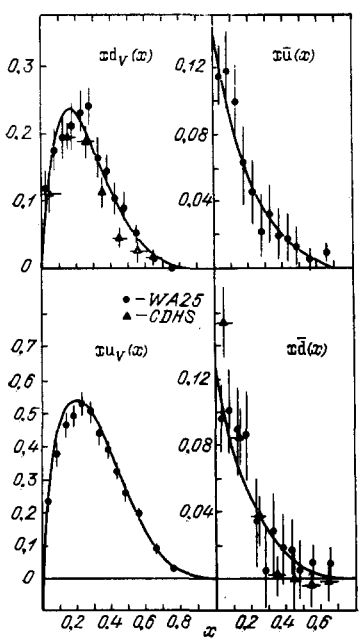

FIG. 6. Momentum distributions ($xq(x)$) of the valence (d_v, u_v) and sea ($\bar{u}$, $\bar{d}$) quarks in a proton, obtained from data on $\nu(\bar{\nu})$N interactions.

quark distribution $u(x)$ in the π^- meson turned out to be wider ($m \sim 1$) than $u_v(x)$ in the proton ($m \approx 3$). There are still no data on $q_i(x)$ in other hadrons.

2.2.3. Parton fragmentation functions

Quark fragmentation functions are most simply measured in e^+e^- annihilation processes:

$$e^+ + e^- \to \gamma^* \to q_i + \bar{q}_i \to J_{q_i}(z) + J_{\bar{q}_i}(z), \quad (2.29)$$

where two hadron jets are formed (see Fig. 3).

In this case, the parton model makes clear predictions regarding the characteristics of the production of quarks, which have been verified experimentally, and the relatively simple kinematics of the reaction enables separating clearly the hadron jets. Colored quarks and gluons were "discovered" precisely in the study of e^+e^- annihilation ($e^+e^- \to q\bar{q}g$; $s^{1/2} = W \leqslant 45$ GeV).

The total cross section for jet formation in (2.29) with $s^{1/2} \gg m_{q_i}$ can be written in the form[2]:

$$\sigma_{tot}(e^+e^- \to X) = \sigma_{tot}(e^+e^- \to \mu^+\mu^-) \cdot 3 \sum e_{q_i}^2, \quad (2.30)$$

where

$$\sigma_{tot}(e^+e^- \to \mu^+\mu^-) = \frac{4\pi\alpha^2}{3s}, \quad (2.31)$$

while the factor of 3 represents the number of quark colors. In this model quarks are created as free point particles with spin 1/2, charge e_{q_i}, and three different colors. The ratios between different types of quarks in the reaction (2.29) are determined by e_q^2:

$$d : u : s : c : b = 1 : 4 : 1 : 4 : 1, \quad (2.32)$$

if $s^{1/2} \gg m_b$. The angular distributions of the quarks (and, therefore, of the hadron jets also) relative to the e^+e^- collision axis in the center of mass system have the form

$$\frac{d\sigma(e^+e^- \to q\bar{q})}{\sigma_{tot}(e^+e^- \to X)\, d\,|\cos\vartheta|} = \frac{3}{4}(1 + \cos^2\vartheta). \quad (2.33)$$

The hadron momentum distributions in the jets

$$e^+e^- \to J_{q_i}(h) + J_{\bar{q}_i}(h) \to \sum_{q_i} h_{q_i}(z) + \sum_{\bar{q}_i} h_{\bar{q}_i}(z) \quad (2.34)$$

are determined by the expression

$$\frac{d\sigma(e^+e^- \to h(z)\, X)}{\sigma_{tot}(e^+e^- \to X)\, dz} = \frac{\sum e_{q_i}^2 [D_{q_i}^h(z) + D_{\bar{q}_i}^h(z)]}{\sum e_{q_i}^2}, \quad (2.35)$$

where $D_{q_i(\bar{q}_i)}^h(z)$ are the fragmentation functions of the quarks and antiquarks.[18] They are normalized by the following conditions:

$$\int \sum_h D_{q_i(\bar{q}_i)}^h(z)\, dz = \langle n_{q_i(\bar{q}_i)}^h \rangle, \quad (2.36)$$

$$\int \sum_h D_{q_i}^h(z)\, z\, dz = 1, \quad (2.37)$$

where $\langle n_{q_i(\bar{q}_i)}^h \rangle$ is the average number of hadrons formed in the fragmentation of quarks (q_i) and antiquarks ($\bar{q}_i$). The relation (2.37) expresses the law of conservation of momentum ($\Sigma z_i = 1$).

In deep inelastic $l(\mu)N$ interactions (see Fig. 3)

$$l + N \to \gamma^* + q_i + (qq)_j \to J_{q_i}^h(z) + J_{(qq)_j}(z') \quad (2.38)$$

two hadron jets are formed.[19] The normalized cross sections of this process can be written in the form

$$\frac{1}{\sigma_{tot}(\gamma^*N)} \frac{d\sigma(\gamma^*N \to hX)}{dz} = \frac{\sum_i e_{q_i}^2 q_i(x) [D_{q_i}^h(z) + D_{(qq)_j}^h(z')]}{\sum_i e_{q_i}^2 q_i(x)}, \quad (2.39)$$

where $\sigma_{tot}(\gamma^*N)$ is the total cross section of the $\gamma^* q_i(x)$ interaction, $z = p_h/xp$ and $z' = p_h/(1-x)p$ in the center of mass system (γ^*N).

Analogous formulas for quark fragmentation in $\nu(\bar{\nu})p$ interactions[1,2]

$$\frac{1}{\sigma_{tot}} \frac{d\sigma(\nu p \to \mu^- hX)}{dz} = \frac{d(x) D_u^h(z) + (1/3)\bar{u}(x) D_{\bar{d}}^h(z)}{d(x) + (1/3)\bar{u}(x)}, \quad (2.40)$$

$$\frac{1}{\sigma_{tot}} \frac{d\sigma(\bar{\nu}p \to \mu^+ hX)}{dz} = \frac{u(x) D_{\bar{d}}^h(z) + (1/3)\bar{d}(x) D_{\bar{u}}^h(z)}{u(x) + (1/3)\bar{d}(x)} \quad (2.41)$$

contain different combinations of $q_i(x) D_{q_i}^h(z)$, which is what makes it possible to distinguish jets of hadrons associated with definite quarks.[20] For example, for $x \gtrsim 0.3$, where there are no sea quarks,

$$\frac{1}{\sigma_{tot}} \frac{d\sigma(\nu p \to \mu^- hX)}{dz} = D_u^h(z) \quad (2.40')$$

$$\frac{1}{\sigma_{tot}} \frac{d\sigma(\bar{\nu}p \to \mu^+ hX)}{dz} = D_{\bar{d}}^h(z), \quad (2.41'')$$

and the hadron momentum distributions $h(z)$ are the fragmentation functions of the u and d quarks.

Thus lN interactions and e^+e^- annihilation yield rich information about the fragmentation of partons into hadrons. Combined analysis of the data on these processes yields the basic characteristics of the processes by which quarks and gluons transform into hadrons (see Sec. 5).

2.2.4. Hard hadron collisions

Four hadron jets form in hard ab interactions (see Fig. 4):

$$a + b \to J_{q_i}(h) + J_{q_j}(h) + J_s(a) + J_s(b), \quad (2.42)$$

two of which ($J_{q_i}(h)$ and $J_{q_j}(h)$) have high transverse momenta $p_\perp$ (J) or transverse energies $E_\perp(J) = \Sigma E_i \sin\vartheta_i$. In the parton model this process is viewed as being the result of the scattering of two partons

$$q_i(x_1) + q_j(x_2) \to q_k(x_1) + q_l(x_2) \quad (2.43)$$

by large angles in the center of mass system of (ab) followed by their fragmentation into hadrons.[1-3] The description of (2.42) therefore requires knowing the hadron structure functions ($F_a^{q_i}(x_1)$, $F_b^{q_i}(x_2)$), the parton scattering cross section in (2.43), and the partons-into-hadrons fragmenta-

tion functions ($D^{h}_{q_k}(z)$, $D^{h}_{q_l}(z)$). As we have already discussed, the $F^{q}_{h}(x)$ and $D^{h}_{q}(z)$ functions are measured in e^+e^- annihilation and deep-inelastic lN interaction processes. Therefore the great interest in hard hadron collisions is associated primarily with the possibility of obtaining direct data on parton interactions at high energies.

Hadron jets are usually distinguished in the inclusive processes

$$a+b \to c_{tr}(p_\perp^{tr}) + X, \tag{2.44}$$

$$a+b \to \sum_i c_i^{tr}(E_{\perp i}) + X, \tag{2.45}$$

by recording the particles c_{tr} with high transverse momenta or groups of particles $\Sigma_i c_i^{tr}$ with high transverse energy ($E_\perp(J)$). The cross section (2.44) can be written in the form[2,3]

$$E_c \frac{d\sigma}{dp_c} = \sum_{i,j,k} \int F_a^{q_i}(x_1) F_b^{q_j}(x_2) \frac{D^c_{q_k}(z)}{\pi z} \frac{d\hat{\sigma}_{ijk}}{d\hat{t}} dx_1 dx_2, \tag{2.46}$$

where the summation extends over different types of partons (i, j, k), and D^{c}_{k} is a function characterizing the fragmentation of the parton k into the hadron c. All kinematic variables in (2.46) are expressed in terms of x_1 and x_2—the relative fractions of the momenta of the primary particles (a, b) carried away by the ith and jth partons:

$$\left.\begin{aligned} &z = -\frac{1}{s}\left(\frac{t}{x_1} + \frac{u}{x_2}\right), \\ &t = (P_c - P_a)^2, \quad u = (P_c - P_b)^2, \\ &\hat{t} = \frac{x_1 t}{z}, \quad \hat{s} = x_1 x_2 s, \end{aligned}\right\} \tag{2.47}$$

where $\hat{t}$ and $\hat{s}$ are the squares of the transferred momentum and total energy in the reaction (2.43) and P_a, P_b, and P_c are the four-momenta of the hadrons. The inclusive formation of jets with energy $E_\perp$ (J) is obtained from (2.46) by integrating over z [10]:

$$E_\perp(J) \frac{d\sigma}{dp_\perp(J)} = \sum_{i,j} \int F_a^{q_i}(x_1) F_b^{q_j}(x_2) \frac{\hat{s}}{\pi} \delta(\hat{s} + \hat{t} + \hat{u}) \times \frac{d\hat{\sigma}_{ijk}}{d\hat{t}} dx_1 dx_2. \tag{2.48}$$

The ratio between the cross sections for the formation of the hadron jet (2.48) and of the trigger particle (2.46) is determined by the fragmentation function $D^{c}_{k}(z)$ and for $z > 0.9$ is equal to about 100.[3,5]

It is evident from these formulas that the basic characteristics of hard collisions are determined by parton scattering (2.43). The differential cross section for (2.43) in lowest order in $\alpha_S(p_\perp^2)$ has the form[2,3,10,13]

$$\frac{d\hat{\sigma}_{ijk}}{d\hat{t}} = \pi \alpha_S^2(p_\perp^2) \frac{|A_{ijk}|^2}{\hat{s}^2}, \tag{2.49}$$

where the amplitudes A_{ijk} are dimensionless, are averaged over color and spin, and depend on the specific process of the type (2.43).[10] In the observation of trigger particles (c_{tr}) with $\vartheta \approx 90°$ their production cross sections obey the simple scaling law:

$$E_c \frac{d\sigma}{dp_c} = \frac{1}{p_\perp^4} f(x_\perp), \tag{2.50}$$

where

$$x_\perp = \frac{2p_\perp}{s^{1/2}} \tag{2.51}$$

and $x_\perp \approx x_1 \approx x_2$. It is evident from here that the bulk of the change in (2.50) with increasing $x_\perp$ is determined by the x dependence of the structure functions, which decrease rapidly as $x \to 1$ (Sec. 2). Increasing the energy with fixed $p_\perp$ decreases $x_\perp$ and, therefore, increases the inclusive cross sections (2.46) and (2.48). All these characteristic features of hard processes have been observed in $p\bar{p}$ collisions at $s^{1/2} = 20$–63 GeV, and especially clearly in $p\bar{p}$ interactions at $s^{1/2} = 540$ GeV (see Sec. 4).

We shall end our brief review of the basic ideas of the parton model here. The deviations from the formulas of this model (for example, breakdown of scaling) are associated with the field picture of the interaction of partons and are described by QCD.

2.3. Interaction of partons in QCD

Strong interactions of quarks and gluons at high Q^2 are described by QCD PT.[1-4,10-13] Their interaction constant in the so-called leading logarithm approximation has the form

$$\alpha_S(Q^2) = \frac{g_S^2}{4\pi} = \frac{12\pi}{(33-2n_q)\ln(Q^2/\Lambda^2)}, \tag{2.52}$$

where n_q is the number of quarks with $m_q^2 \ll Q^2$ and Λ is the main parameter determining the applicability of perturbation theory ($\alpha_S \ll 1$).[21] Estimates show that for $Q^2 \geqslant 100$ GeV^2 $\alpha_S(Q^2) \approx 0.2$. As is evident from (2.52), in the limit $Q^2 \to \infty$ the partons do not interact ($\alpha_S \to 0$) and the formulas of the parton model are applicable without breakdown of scaling ($F(x)$, $D(z)$). For finite values of Q^2 breakdown of scaling of the logarithmic type is expected in the perturbation theory[3,4]:

$$F(x) \to F(x, t), \quad D(x) \to D(x, t),$$

where $t = \ln(Q^2/\Lambda^2)$.

The value of Λ can in principle be determined from chromodynamic effects in hard collisions. In deep inelastic lN interactions they determine the breakdown of scaling[3]:

$$F_N^q(x, t) = \int_x^1 \frac{dx'}{x'} F_N^q(x', t_0) W^q\left(\frac{x}{x'}, \frac{t}{t_0}\right), \tag{2.53}$$

where W^q is the probability that after the transition from the probing momentum Q_0 to the momentum Q a parton with a relative fraction of the momentum x instead of x' will be recorded.[22] However, for values of Q^2 which are now accessible corrections reflecting the physics at large distances ($\alpha_S \to 1$) which decay in a power-law fashion $\sim (1/Q^2)^n$, are important. For this reason the structure functions of the nucleons, measured in lN interactions with Q^2 varying from 1 to 200 GeV^2 and x from 0.03 to 0.9, are usually described by the expression[25,26]:

$$F_N(x, Q^2) = F_N^{QCD}(x, Q^2)\left(1 + \frac{h(x)}{Q^2}\right), \quad (2.54)$$

$$h(x) = \frac{x^2}{(1-x)^2}, \quad (2.55)$$

which takes into account the evolution of $F_N^{QCD}(x, Q^2)$ according to the perturbation theory (2.53) and corrections of the power-law type (they are called twists). As is evident from (2.54), they are significant for $x \gtrsim 0.5$. The value of Λ obtained from here falls into the range 50–250 MeV.[25,26] Since at the present time there is no systematic method for taking twists into account, the value of Λ determined from these experiments is not reliable.[23)] Nevertheless, the good description of the data by the expression (2.54) permits using $F_N^{QCD}(x, Q^2)$ for higher values of Q^2 also, in particular, at collider energies ($Q^2 \sim 10^4$ GeV^2) (see Sec. 4).[10]

The results obtained from the study of e^+e^- annihilation into hadrons at high energies $s^{1/2} \leqslant 45$ GeV provided the *most spectacular confirmation of QCD.*[2–4] *The point* colored quarks and gluons were "discovered" here and rich information about hadron jets was obtained.[11,12,28–31] In particular, the study of three-jet events

$$e^+ + e^- \to q + \bar{q} + g \to \sum_q h + \sum_{\bar{q}} h + \sum_g h \quad (2.56)$$

gives direct information about $\alpha_S(Q^2)$. Indeed, the cross section of the process of hard gluon emission (2.56) in QCD has the form[28,29]

$$\frac{d\sigma(e^+e^- \to q\bar{q}g)}{dx_1\, dx_2} = \frac{2\alpha_S \sum e_{q_i}^2}{\pi} \sigma(e^+e^- \to \mu^+\mu^-) \frac{x_1^2 + x_2^2}{(1-x_1)(1-x_2)}, \quad (2.57)$$

where $x_i = 2E_{q_i}/W$, and is proportional to $\alpha_S(Q^2)$. The separation of the events (2.56) is, however, linked with the model assumptions about the fragmentation of quarks and gluons into hadrons (see Secs. 3 and 5) and for this reason the quantity $\alpha_S(Q^2 \sim 10^3$ GeV$^2)$, extracted from the experimental data, is highly uncertain. We shall return to this question in our discussion of the fragmentation of quarks and gluons (see Sec. 5).

We have presented the basic formulas of the parton model, which describes both soft and hard processes at high energies. Their modification, taking into account the interaction of the partons (QCD), reduces to the simple recipe

$$F_h^{q,g}(x) \to F_h^{q,g}(x, Q^2), \quad D_{q,g}^h(z) \to D_{q,g}^h(z, Q^2).$$

To find more detailed characteristics specific Feynman diagrams, which are best discussed in an analysis of the experimental data (see Secs. 4 and 5), must be studied.

3. FORMATION OF HADRON JETS

In the parton model a hadron jet has the quantum numbers of the parent parton and $\mathbf{p}_q(g) \approx \mathbf{p}(J)$ (see Sec. 2). In QCD it is also assumed that partons are decolorized without significant changes in these relations (the hypothesis of soft decolorization). Because of the absence of a complete theory of strong interactions the degree to which the parton-jet correspondence holds is unclear, and here experiment is the final arbiter. As a result, questions regarding the formation of jets become fundamental, because on the basis of these jets we attempt to study the dynamics of the development and fragmentation of partons, which do not occur in the free state.[24)]

The qualitative definition of a jet as a collection of particles moving in one direction with $p_{\perp i} \ll p_{\parallel i}$ relative to their total momentum ($\mathbf{p}(J) = \Sigma \mathbf{p}_i$) conceals numerous questions associated with the absence of quantitative criteria for referring hadrons to one or another jet. These criteria are determined based on an analysis of the experimental data on hard processes, in which jets are formed with different reliabilities. They are recorded most clearly in e^+e^- annihilation and in hard $p\bar{p}$ interactions ($s^{1/2} = 540$ GeV). In this section we shall briefly study the methodological problems of the formation of jets in hard processes, which determine our possibilities for studying the dynamics of parton interactions.

3.1. e^+e^- annihilation into hadrons

Hadron jets are most clearly recorded in e^+e^- annihilation processes, in which all the collision energy ($s^{1/2}$) goes into the energy of the hadron jets (W). The method for separating them has been under development for ten years, and we shall therefore summarize the basic results regarding this question.[28–31] At the energies now accessible ($s^{1/2} \lesssim 45$ GeV) primarily two hadron jets are formed in these reactions.

$$e^+ + e^- \to q_l + \bar{q}_l \to J_{q_l}(h) + J_{\bar{q}_l}(h), \quad (2.29')$$

and a three-jet pattern of hard gluon emission is observed only in approximately 10% of the events with $s^{1/2} \gtrsim 30$ GeV:

$$e^+ + e^- \to \bar{q}_l + \bar{q}_l + g \to J_{q_l}(h) + J_{\bar{q}_l}(h) + J_g(h). \quad (2.56')$$

In QCD these jets are actually a manifestation of the production of many jets in the quark-gluon cascade (see Sec. 5.1). The formation of a third hadron jet (2.56) is also linked with the quark-gluon cascade, caused by hard gluon emission. The ratio of the cross sections of the processes (2.56) and (2.29) is proportional to $\alpha_S(Q^2)$.

In the first case, different quantities characterizing the jet nature of the events are used to find the axes of separation of the jets.[28,31] They all give approximately the same results.[31] The so-called sphericity is often used.

$$S = \frac{3}{2} \frac{\min \sum_i p_{\perp i}^2}{\sum_i p_i^2}, \quad (3.1)$$

where $p_{\perp i}$ are the transverse momenta of the secondary hadrons relative to the selected orientation of the jet axis. Minimization of S over all possible directions enables finding the axis of separation of the jets in the reaction (2.29). The physical meaning of S is obvious: for thin jets ($p_{\perp i} \ll p_{\parallel i}$) $S \to 0$ and in their absence ($p_{\perp i} \sim p_{\parallel i}$) $S \to 1$. The value of $\langle S(W) \rangle$ decreases rapidly with increasing energy ($\sim 0.8\, W^{-1/2}$) and for $W \gtrsim 25$ GeV is equal to ≈ 0.1.[28 25)] For this reason, in this case, the two-jet picture of the processes (2.29) is already clearly determined when $W \gtrsim 10$ GeV, confirming the basic

kinematic representations of the parton model and QCD. The situation with the correspondence of the quantum numbers of the partons and of the jet is more complicated; this is attributable, in particular, to the wide angular distribution of the slow particles ($p_\perp \lesssim 0.5$ GeV).[28,30] They cannot, therefore, be referred to one or another jet. They probably do not in principle belong to them, and are formed as a result of fluctuations of the QCD vacuum accompanying the decolorization of the partons.[26] They can nevertheless substantially alter the quantum numbers (charge, baryon numbers, strangeness, etc.) of the jet, if such hadrons are linked to it. Since there is no clear boundary between the "vacuum" hadrons and the products of parton fragmentation, the determination of the quantum numbers of jets is a complicated methodological problem, which can be solved only by analyzing and comparing the data from different experiments (see Secs. 4 and 5).[27]

Three-jet events (2.56) are separated in an analogous manner. For example, the triplicity is used for this:

$$T_3 = \frac{\max\left(\left|\sum_{c_1} p_{\parallel i}\right| + \left|\sum_{c_2} p_{\parallel i}\right| + \left|\sum_{c_3} p_{\parallel i}\right|\right)}{\sum_i p_i}, \qquad (3.2)$$

where the maximization is performed with respect to all possible allocations of the particles in the event into three groups—C_1, C_2, and C_3, which is what enables the determination of the separation axes of the quarks and gluons. For ideally thin jets ($p_{\perp i} \to 0$) $T_3 \to 1$. An example of events of the type (2.56) is shown in Fig. 7.[30] Their separation, however, presents great methodological difficulties because of the large background ($\approx 90\%$) of the two-jet processes (2.29) and the unknown characteristics of parton hadronization. This is what leads to the uncertainties ($\approx 40\%$) in the measurement of the strong interaction constants $\alpha_s(Q^2)$ (see Sec. 5).

On the whole e^+e^- annihilation processes are a perfect example of hard collisions in which hadron jets are well separated and there is no interference from background soft interactions, which greatly complicate the analysis of l N and hadron collisions. For this reason, data on jets in e^+e^- annihilation occupy a central place in the study of the dynamics of parton production and fragmentation.[28-31]

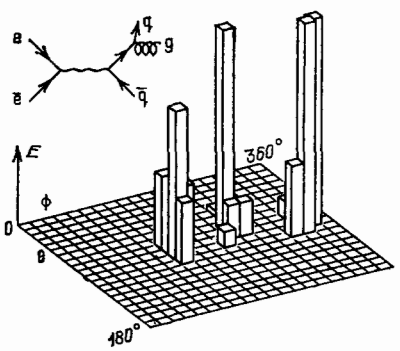

FIG. 7. Example of a three-jet event in e^+e^- annihilation. ϕ and θ are the azimuthal and polar emergence angles of the hadrons relative to the axis of the e^+e^- collision and E is the energy.

3.2. Hard hadron collisions

The formation of jets in hadron interactions

$$a + b \to J_{q_i}(h) + J_{q_j}(h) + J_S^a(h_S) + J_S^b(h_S) \qquad (2.42)$$

is complicated by the formation of spectator jets, which have small emergence angles ($\vartheta_J \lesssim 10°$) in the center of mass system of (a, b) and $\langle p_\perp(h_S)\rangle \approx 0.5$ GeV (see Fig. 4). Hadrons from hard scattering of partons (2.43) can therefore be recorded only at large angles ($\vartheta \gtrsim 10°$) and with high transverse momenta (or energies) $p_\perp(h) \gtrsim 0.5$ GeV. Attempts to separate $J_{q_i}(h)$ with $E_\perp(J) \lesssim 10$ GeV for $s^{1/2} \lesssim 30$ GeV were unsuccessful because of the large background formed by the spectator hadrons.[28] For this reason at energies $s^{1/2} \leqslant 62$ GeV hard scattering of partons (2.43) is, as a rule, studied by recording the trigger particles with $p_\perp^{tr} \gtrsim 4$ GeV:

$$a + b \to J_{c_{tr}}(h) + J_{q_j}(h) + J_S^a(h_S) + J_S^b(h_S), \qquad (3.3)$$

in which the interference from spectator hadrons is small. The angular and momentum characteristics of the jets in these processes are discussed in detail in the reviews Refs. 5, 10, 13, and 32. In this case, because of the sample of events ($p_\perp^{tr} \gtrsim 4$ GeV) the trigger hadron jet $J_{c_{tr}}(h)$ gives only limited information about parton fragmentation ($z \gtrsim 0.8$) and serves primarily as an indicator of hard scattering. Because of the internal motion of the partons in the hadrons the second jet $J_{q_j}(h)$ has a wide angular distribution and its separation presents great methodological difficulties.[5] As a result, in order to separate them better a so-called pseudotrigger is introduced, i.e., events, in which aside from c_{tr} there occurs another particle (c'_{tr}) with a high transverse momentum moving in a direction opposite to $\mathbf{p}_{c_{tr}}$, are separated. A careful study of the four-jet picture (3.3) in pp interactions ($s^{1/2} = 62$ GeV) with a large statistical sample ($\approx 10^5$ events) was performed in Ref. 33. Events with $p_\perp^{tr} \geqslant 2$; 4, and 6 GeV at $\vartheta_{tr} \approx 50°$ ($\langle y_{tr}\rangle \approx 0.7$) were selected. It was shown that all four hadron jets are separated when $p_\perp^{tr}(c_{tr}) \geqslant 4$ GeV and $\vartheta'(c'_{tr}) = 280 - 310°$ in the scattering plane. In addition, the jet picture is characteristic for the accompanying particles (excluding c_{tr} and c'_{tr}). In this case the "dimensions" of these jets for particles with $p_\perp \geqslant 1$ GeV are $\Delta y \approx 1.0$ and $\Delta\varphi \approx 50°$ (φ is the azimuthal emergence angle of the hadrons[28]). These values of Δy and $\Delta\varphi$ are in agreement with the results of the modeling of the scattering and fragmentation of partons in pp interactions.[33] Thus with the help of trigger particles and model calculations it is possible to separate hadron jets with $p_\perp(h) \gtrsim 1$ GeV.

An analogous situation also occurs in the separation of jets with respect to the transverse energy ($E_\perp(J)$) with $s^{1/2} = 45$ and 62 GeV in the reaction

$$p + p \to J_q(E_\perp) + X, \qquad (2.45')$$

with $|y_J| \lesssim 0.9$ and $E_\perp(J) = 8 - 12$ GeV.[34,35] To evaluate the cross section of (2.45) complex modeling of soft and hard pp interactions employing the structure $F_N(x, Q^2)$ and fragmentation $D(z, Q^2)$ functions obtained in l N interactions and e^+e^- annihilation was performed.[34,35] The comparison of the results of modeling with experiment

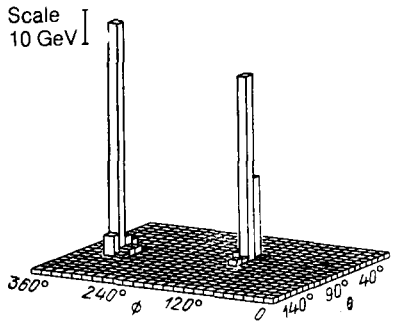

FIG. 8. Example of an event with the formation of two jets with high transverse energies in $p\bar{p}$ interactions at $s^{1/2} = 540$ GeV. UA2 installation ϕ and θ are the azimuthal and polar emergence angles of the hadrons.

yielded the cross section of the reaction (2.45) with $x_\perp = 2E_\perp(J)/s^{1/2} = 0.2 - 0.5$ with an accuracy of ~20–30%. Here it is necessary to take into account the fact that the uncertainty of the model representations is unknown. Because of this data on jets with $s^{1/2} \lesssim 60$ GeV in hadronic collisions are "semiquantitative" and are studied only in order to compare them with other results.

A clear picture of jet production of hadrons at high energies ($s^{1/2} = 540$ GeV) was already obtained in the first experiments on the CERN collider (Fig. 8).[36–38] Here the jets can be seen with the naked eye and for $E_\perp(J) \gtrsim 35$ GeV they are recorded with an efficiency of nearly 100%. Hadron jets were studied with the help of two enormous experimental installations (UA1 and UA2), on which large groups of physicists (135 and 65 people!) worked.[36,37] These installations have the same general structure. They consist of a vertex detector, surrounded by electromagnetic and hadron calorimeters with a high degree of segmentation (Fig. 9). The vertex detector consists of a system of cylindrical drift and proportional chambers, surrounding the collision region of the colliding beams in the collider. In these installations the number of secondary charged particles, their momenta (UA1) and emergence angles (φ, ϑ) (UA1, UA2) are measured in the intervals $\Delta\vartheta = 5 - 175°$, $\Delta\varphi = 360°$ (UA1) and $\Delta\vartheta = 20 - 160°$, $\Delta\varphi = 360°$ (UA2).[29] This corresponds to

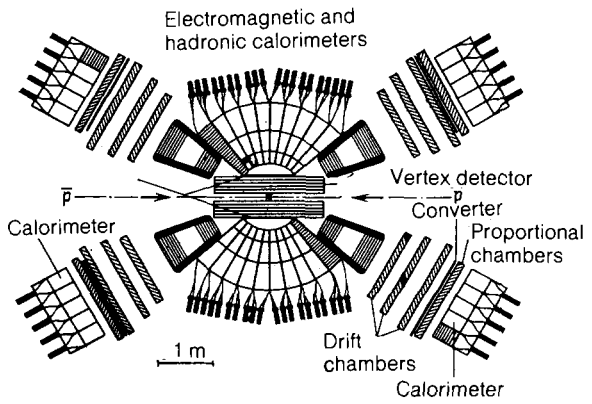

FIG. 9. Vertical section of the UA2 installation along the direction of the beam.

the following change in the pseudorapidity of the particles.:

$$\eta = -\ln \operatorname{tg}\frac{\vartheta}{2} \approx y, \qquad (3.4)$$

$$|\eta| \leqslant 3 \text{ (UA1)}, \quad |\eta| \lesssim 2.5 \text{ (UA2)}.$$

In the electromagnetic calorimeter, consisting of scintillation counters made of lead glass (UA2) or lead plates and a scintillator, the energy of the electrons and gamma rays produced in the decay of secondary hadrons is measured. The energy of the electromagnetic component of the interaction is measured with an accuracy of $\Delta E(\gamma, e^{\pm})/E \sim 0.14(E, \text{GeV})^{-1/2}$. The energy of the hadronic component is measured in the hadronic calorimeter (iron plates and a scintillator): $\Delta E(h)/E(h) \sim E^{-1/4}$ (GeV) (32% with $E = 1$ GeV and 11% with 70 GeV). The high degree of segmentation of the calorimeters makes it possible to measure these characteristics of groups of particles with a step of $\Delta\varphi = 15°$ and $\Delta\vartheta = 10°$.

Thus these gigantic installations have practically a 4π geometry, record all charged secondary particles and their momenta and emergence angles, and measure the total energy of all secondary particles with a step of $\Delta\varphi = 15°$ and $\Delta\vartheta = 10°$.[36–38] The computer complex controls the corresponding operating modes of these installations and performs the primary analysis of the information entering the computer during the session. The famous intermediate bosons ($W^{\pm}$, Z°) were discovered on these installations in 1983.[36–38]

In the study of the formation of hadron jets in $p\bar{p}$ interactions events with $E_\perp \gtrsim 25$ GeV were selected.[36,37] This condition enabled lowering substantially the background formed by the soft $p\bar{p}$ collisions. The recorded events were analyzed for the purpose of separating hadron jets with the help of a simple cluster algorithm (UA2)[37]: measurements of $E_\perp^i$ in segments of the calorimeter with a common side were combined into clusters (or jets) if $E_\perp^i \geqslant 0.4$ GeV. Clusters with two and more local maxima in $E_\perp$ were regarded as separate jets, if energies $E_\perp^i \lesssim 5$ GeV appeared between them. Further, the rank of a cluster (or jet) was introduced: $E_\perp^{(1)} > E_\perp^{(2)} > E_\perp^{(3)} > \ldots$ A typical cluster with $E_\perp = 2$ GeV incorporates measurements of $E_\perp^i$ in three segments, and a cluster with $E_\perp = 40$ GeV combines ten segments. The angular characteristics (ϑ_J, φ_J) of the jets were determined from the values of ϑ_i and φ_i of the corresponding segments.

Events from the UA1 installation were analyzed using a different algorithm[36]: measurements of $E_\perp^i$ in those segments in which $E_\perp^i > 2.5$ GeV and $\Delta = [(\Delta\varphi)_{ik}^2 + (\Delta\eta_{ik})^2]^{1/2} \leqslant 1$ were combined into jets. Clusters with $E_\perp^i < 2.5$ GeV were linked to a jet with respect to which they formed an angle $\vartheta \leqslant 45°$ and their transverse momentum relative to the axis of the jet $P_\perp^i(J) < 1$ GeV. In spite of some difference in the algorithms for separating the jets, basically the same results are obtained on both installations.

The accuracies with which the different characteristics of the hadron jets are determined depend on $E_\perp(J)$. Figure 10 shows $\langle E_\perp \rangle$, $\langle P_\perp \rangle$ and $\langle n_{ch} \rangle$ as a function of $\Delta\eta$ relative to the axis of the jet ($\eta(J) = 0$).[36] The values of $\langle E_\perp \rangle$ were determined from the calorimeter data, and the values of

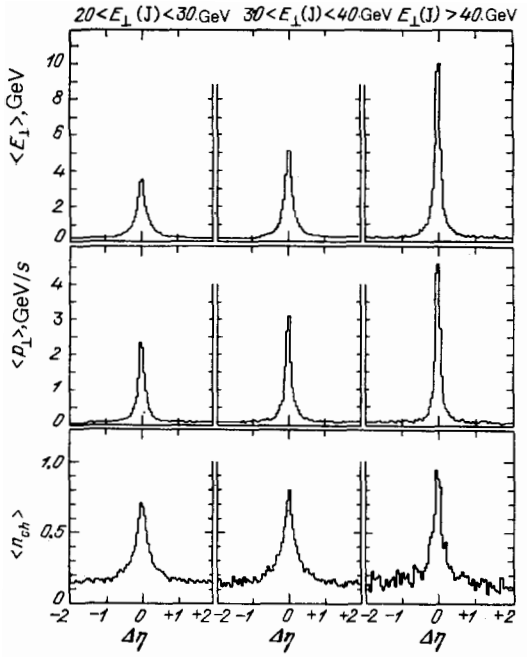

FIG. 10. $\langle E_\perp \rangle$, $\langle p_\perp \rangle$, and $\langle n_{ch} \rangle$ as functions of $\Delta\eta$ for different values of $E_\perp(J)$ ($\eta(J) = 0$) (UA1).

$\langle P_\perp \rangle$ and $\langle c_{ch} \rangle$ were determined more accurately from the indications of the vertex detector of UA1.[36] Figure 10 clearly shows a hadron jet whose "dimensions" with respect to $\Delta\eta$ decrease with increasing $E_\perp(J)$ for $\langle E_\perp \rangle$ and $\langle P_\perp \rangle$ and constitute $\Delta\eta \lesssim 0.5$ at the base of the peak with $E_\perp(J) \gtrsim 40$ GeV. The background events contribute $\lesssim 5\%$ to $E_\perp(J)$ and $\langle P_\perp(J) \rangle$. The situation is worse in the measurement of $\langle n_{ch}(J) \rangle$. In this case the background constitutes ≈ 20–30%, and $\langle n_{ch}(J) \rangle$ cannot be determined directly without the corresponding modeling of the parton hadronization and soft $p\bar{p}$ collisions.[36–38] These results indicate that as $E_\perp(J)$ increases particles with $E_\perp(h) \gtrsim 1$ GeV carry away an increasingly higher relative fraction of the energy of the jet than hadrons with $E_\perp(h) \lesssim 0.5$ GeV. For this reason they have virtually no effect on the measurement of the kinematic characteristics of the jet ($E_\perp$, $P_\perp$, ϑ, φ), but are important for determining their quantum numbers and $\langle \eta_{ch}(J) \rangle$.[30] We discussed an analogous problem in e^+e^- annihilation in Sec. 3.1. In this case the problem is complicated further by the background formed by the spectator hadrons, which cannot be taken into account without model calculations.[36,37]

Thus in $p\bar{p}$ interactions with $s^{1/2} = 540$ GeV hadron jets with $E_\perp \gtrsim 30$–35 GeV are well separated and their kinematic characteristics are easily measured. This is additionally confirmed by the separation of two- and three-jet events:

$$\bar{p} + p \to J^{(1)}_{q(g)}(h) + J^{(2)}_{q(g)}(h) + X, \quad (3.5)$$

$$\bar{p} + p \to J^{(1)}_{q(g)}(h) + J^{(2)}_{q(g)}(h) + J^{(3)}_{g}(h) + X, \quad (3.6)$$

which give direct information about the hard scattering of partons (3.5) and gluon bremsstrahlung (3.6).[36,37] The events (3.6) comprise about 15% of the events (3.5), which corresponds to $\alpha_s(Q^2) \sim 0.2$.[36,38] The distribution of the events (3.5) over the difference of azimuthal angles ($\Delta\varphi_{12}$) of the jets with $E^{(1)}_\perp(J)$, $E^{2}_\perp(J) \geqslant 20$ GeV has a sharp peak at $\Delta\varphi_{12} = 180°$ with a half-width of 10°![37] This strong correlation between the jets in the azimuthal plane is linked with the limited transverse momenta of the partons in the hadrons (see Sec. 2).

We shall examine some other methodological questions associated with the separation of jets in hard hadronic collisions when we discuss the data collected (see Secs. 4 and 5).

3.3. Deep-inelastic lN interactions

Data on the hadronic component, i.e., on parton fragmentation, in lN interactions were obtained only in individual studies, performed primarily with the help of the chamber method for relatively low values $\langle W \rangle \lesssim 15$ GeV and $\langle Q^2 \rangle \lesssim 20\,\text{GeV}^2$ (see, for example, Refs. 39 and 40). The jets were not quantitatively separated in these experiments. The jet nature of the events was, however, noted.[39,40] In addition, as we have already pointed out (see Sec. 2), deep inelastic $\nu(\bar{\nu})$N interactions enable the separation of the fragmentation of quarks with definite flavor, which is difficult to do in e^+e^- annihilation processes and in hadron collisions. In discussing the results on quark and gluon fragmentation (see Secs. 4 and 5) we shall therefore use the data on lN interactions, keeping in mind their limited nature.

4. QUANTUM NUMBERS AND INTERACTION OF PARTONS

The experiments on the formation of hadron jets in hard processes as a whole yield direct information about the interactions of partons at small distances and about the quantum numbers of partons (see Sec. 2). It is precisely this stage of hard processes that QCD purports to explain. However, the fact that the mechanism of parton hadronization is unknown makes it impossible to determine all characteristics of the jets. It has been shown experimentally that the cross sections $\sigma(J)$ for jet formation, $E(J)$, and $\vartheta_J(\eta_J)$ are measured relatively accurately (see Sec. 3). For this reason, only those quantum numbers (flavor, color, charge, and spin) of the partons on which these characteristics depend substantially are determined from these data. To measure other quantum numbers of the partons (for example, the baryon number, isospin, and strangeness) it is necessary to study the mechanism of parton hadronization (see Sec. 5).

The interaction of partons at short distances is determined by the "running" strong interaction constant $\alpha_s(Q^2)$ (2.52). The measurement of this constant is the main goal of the study of hard processes. At the present time $\alpha_s(Q^2)$ is determined most accurately in e^+e^- annihilation into hadrons both from the total cross sections and from the gluon bremsstrahlung (see Secs. 5).

4.1. Quark flavors and colors

Six quark flavors (u, d, s, c, b, t), each of which can have three different colors ($n_c = 3$), are now known. The available experimental data are well described by these quark states.[1–4] One of the important confirmations of these concepts was the measurement of the cross section of e^+e^- anni-

hilation into two hadron jets in the interval $s^{1/2} = W = 10 - 45.2$ GeV. Indeed, in the parton model the normalized total cross section of this process has the form

$$R_0(W) = \frac{\sigma(e^+e^- \to q_i\bar{q}_i)}{\sigma(e^+e^- \to \mu^+\mu^-)} = 3\sum_i e_{q_i}^2, \qquad (2.30)$$

where $\Sigma_i e_{q_i}^2 = 11/9$ for the known quarks and $n_c = 3$.[31] Taking into account the gluon bremsstrahlung in QCD:

$$R(\mathrm{QCD}) = R_0\left(1 + \frac{\alpha_S(Q^2)}{\pi} + C_2\frac{\alpha_S^2(Q^2)}{\pi^2}\right), \qquad (4.1)$$

where $C_2 = 1.39$.[43] This relation was carefully studied above the threshold for the creation of the b quark ($W \geqslant 10$ GeV).[42-43] As a result, it was found that $R_{\mathrm{exp}}(W) = 3.97 \pm 0.05 \pm 0.10$, is independent of W, and is in agreement with (4.1).[32] The following conclusions were drawn from this:

1. The number of quark colors is $n_c = 3$.
2. Quarks have fractional charges and $\Sigma_i e_{q_i}^2 = 11/9$.
3. There are no new quarks with $m_q \lesssim 22$ GeV.[43]

In addition, the formulas (2.30) and (4.1) are valid for the formation of point particles. Therefore the fact that they do not break down makes it possible to estimate the spatial dimensions of quarks: $r_q \lesssim 10^{-16}$ cm.[28] Data from $p\bar{p}$ interactions indicate that $r_q \lesssim 0.5 \cdot 10^{-16}$ cm.[38]

4.2. Quark and gluon spins

Quark spins were measured in the processes of e^+e^- annihilation into two hadron jets (2.29). In this case the angular distribution of the jets has the form

$$\frac{d\sigma(e^+e^- \to J_q J_{\bar{q}})}{\sigma_{\mathrm{tot}} d|\cos\vartheta_J|} = \frac{3}{4}(1 + \cos^2\vartheta_J), \qquad (2.33')$$

if $S_q = 1/2$. For scalar quarks ($S_q = 0$) it is proportional to $\sim\sin^2\vartheta_J$. Figure 11 shows the distribution $(1/N)dN/d|\cos\vartheta_J|$ with $W = 34$ GeV relative to the axis of the e^+e^- collision.[31] It is well described by (2.33) and is incompatible with the dependence $\sim\sin^2\vartheta_J$. Analogous results were also obtained for other energies (see the review of Ref. 31). Thus there is no doubt that $S_q = 1/2$.

The gluon spin ($S_g = 1$) was first determined from an analysis of three-jet events $e^+e^- \to q\bar{q}g$ (2.56) employing models of parton hadronization.[28] Convincing data on S_g in hard $p\bar{p}$ interactions ($s^{1/2} = 540$ GeV) with $\langle Q^2\rangle \approx 2000$ GeV^2 have now been obtained.[36,38] For this purpose the events

$$\bar{p} + p \to J^{(1)}(h) + J^{(2)}(h) + X \qquad (3.5)$$

with $E_\perp(J) \geqslant 35$ GeV, $|\eta| \leqslant 1.0$ and $|\Delta\varphi| \leqslant 45°$ relative to the axis of the jet (2432 events) were selected on the UA1 installation.[36] The angular distribution of these jets is determined by the expression:

$$\frac{d^3\sigma}{dx_1\,dx_2\,d\cos\hat{\vartheta}} = \frac{F(x_1)}{x_1}\frac{F(x_2)}{x_2}\frac{d\hat{\sigma}}{d\cos\hat{\vartheta}}, \qquad (4.2)$$

where $F(x_1)/x_1$ and $F(x_2)/x_2$ is the number density of partons with $x_1(x_2)$, $d\hat{\sigma}/d\cos\hat{\theta}$ is the cross section, and $\hat{\vartheta}$ is the angle at which the partons are scattered in their center of mass system.[33] The absolute magnitude of the parton scattering cross section depends on the type of "elementary" process:

$$q\bar{q} \to q\bar{q}, \qquad (4.3)$$
$$gq \to gq, \qquad (4.4)$$
$$g\bar{q} \to g\bar{q}, \qquad (4.5)$$
$$gg \to gg, \qquad (4.6)$$

but they all have a similar angular dependence. For example, for gluon scattering (4.6)

$$\frac{d\sigma}{d\cos\hat{\vartheta}} = \frac{9}{8}\frac{\pi\alpha_S^2(Q^2)}{2x_1x_2s}(3 + \cos^2\hat{\vartheta})^3(1 - \cos\hat{\vartheta})^{-2}, \qquad (4.7)$$

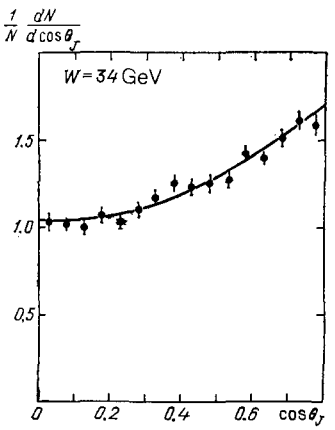

FIG. 11. Distribution of hadron jets in e^+e^- annihilation over $\cos\theta_J$ at $s^{1/2} = 34$ GeV. The solid curve is the approximation of the data by the function $\sim(1 + \cos^2\vartheta_J)$ (2.38).

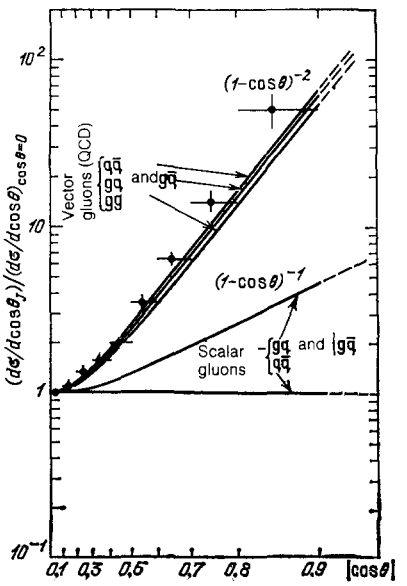

FIG. 12. Distribution of hadron jets formed in $p\bar{p}$ interactions at $s^{1/2} = 540$ GeV as a function of $|\cos\vartheta_J|$. The solid curves show the predictions of QCD for vector and scalar gluons.

and the leading angular dependence

$$\frac{d\sigma}{d\cos\hat{\vartheta}} \sim \frac{1}{(1-\cos\hat{\vartheta})^2} \sim \frac{1}{\sin^4(\hat{\vartheta}/2)} \tag{4.8}$$

is the same for all processes and is associated with the exchange of a vector gluon.[34] For scalar gluons $\sigma(\hat{\vartheta}) \sim [\sin^2(\hat{\vartheta}/2)]^{-1}$.[36] Figure 12 shows the distribution of jets in (3.5) over $|\cos\vartheta|$, normalized to $\sigma(\vartheta)$ at $\cos\vartheta = 0$. The figure also shows the expected jet distributions in the reactions (4.3)–(4.6) with the exchange of vector and scalar gluons. It is evident that the experiment is consistent with $S_g = 1$ and excludes $S_g = 0$.

Analogous experiments were performed at $s^{1/2} = 63$ GeV (pp interaction) with the detection of trigger particles (2.44) with $p_\perp^{tr} \geqslant 4$ GeV.[34] The results of their analysis using complex modeling in order to eliminate the soft background are consistent with $S_g = 1$. Thus the spins of quarks and gluons have been reliably determined and correspond to the predictions of QCD.

4.3. Quark charges

We have already pointed out that the fractional charges of quarks are determined indirectly from data on the cross sections of hard processes (see Sec. 4.1).[1–4] In the parton model the quantum numbers of the hadron jets are those of the parent parton. It is here that the possibility of direct measurement of the charge, strangeness, baryon number, and other quantum numbers of quarks and gluons arises. In an experiment this equality can break down because of the unknown origin of the "slow" hadrons (see Sec. 3). As was proposed back in the original version of the model,[8] however, the fast hadrons probably store the genetic information about the properties of the parent parton. In this case the problem of slow hadrons vanishes (see Sec. 5). Another reason for the breakdown of the correspondence between the parton and the hadron jet is linked with the mechanism of their hadronization. For example, when quarks transform into meson jets their average charge is $\langle Q_J^{(M)} \rangle = e_q + \langle e_{\bar{q}} \rangle$, where $\langle e_{\bar{q}} \rangle$ is the average charge of the light antiquarks ($\bar{u}$, $\bar{d}$, $\bar{s}$), which form mesons by combining with a quark. If all light quarks were to appear with the same probability, then $\langle Q_J^{(M)} \rangle = e_q$ and $\langle e_{\bar{q}} \rangle = 0$. Because of the well-known suppression of the production of the strange antiquark (see Sec. 5) $\langle Q_J^{(M)} \rangle \neq e_q$. This effect is not large numerically,[40,44] but it must be taken into account when studying specific processes.

Here we shall merely point out the first attempts to measure the charge of quarks from jets. It is simplest to measure e_q in $\nu(\bar{\nu})N$ interactions (see Sec. 2.2). In this case the hadron jets are formed with the fragmentation of "knocked out" quarks:

$$\nu + p \to W^+ + d \to u \to J\,(u) + X, \tag{4.7'}$$
$$\bar{\nu} + p \to W^- + u \to \bar{d} \to J\,(\bar{d}) + X, \tag{4.8'}$$

and for this reason their charges are $\langle Q_J^{\nu}(u) \rangle \approx 2/3$ and $\langle Q_J^{\bar{\nu}}(d) \rangle \approx -1/3$ ($\Delta Q = \langle Q_J^{\nu}(u) \rangle - \langle Q_J^{\bar{\nu}}(d) \rangle = 1$). In several experiments on $\nu(\bar{\nu})p$ interactions estimates of $\langle Q_J \rangle$ were made with $W \gtrsim 3$ GeV and $x_q \gtrsim 0.1$ (see, for example, Ref. 44).[35] As a result it was found that $\langle Q_J^{\nu}(u) \rangle = 0.80 \pm 0.11$ and $\langle Q_J^{\bar{\nu}}(d) \rangle = -0.33 \pm 0.15$.[44] The difference between the charges of the jets $\Delta Q = 1.13 \pm 0.19$ is virtually free of methodological and theoretical uncertainties and within the limits of error coincides with the expected value $\Delta Q = 1$ (see also the work in Ref. 40 on μp interactions).

An attempt to measure e_q was also made in the study of hard pp interactions ($s^{1/2} = 52$ GeV) with the trigger particles c_{tr} ($p_\perp^{tr} \geqslant 2$ GeV).[45] In this case the hadron jet $J_b(h)$, propagating in a direction opposite to $\mathbf{p}_\perp^{tr}(c_{tr})$ forms in the scattering of u or d quarks and the average charge is $\langle Q_J \rangle = \Sigma\, q_i/3 = 1/3$. In the experiment the dependence of $\langle Q_J \rangle$ on x_J, where x_J is the relative fraction of the momentum of the jet carried away by the leading charged hadrons, was studied. It turned out that for $x_J \gtrsim 0.6$, $\langle Q_J \rangle = 0.35 \pm 0.04$.[45,36]

Thus the first measurements of e_q show that probably the fast hadrons remember the fractional charge of the light quarks as an average over the events. Of course, to resolve this question quantitatively it is necessary to study the nature of the hadronization of partons (see Sec. 5).

4.4. Cross section for the formation of hadron jets and QCD

The basic hypotheses of QCD on the existence of colored quarks and gluons and the weakening of their interaction at short distances have been verified experimentally. To make quantitative calculations on the basis of QCD, however, the instantaneous strong interaction constants $\alpha_s(Q^2)$ or the parameter Λ (2.52) must be measured. We have already discussed the possibility of determining Λ in deep-inelastic processes from the evolution of the structure functions $F(x, Q^2)$ with $Q^2 \lesssim 200$ GeV^2 (see Sec. 2). In this case the corrections associated with the unknown physics at large distances have turned out to be significant, and for this reason the measured value of Λ falls in the range 50–150 MeV. From the QCD description of the physics of heavy mesons and low-lying hadron states it has been found that $\Lambda \approx 100$ MeV and $\alpha_s(m_\psi^2) = \alpha_s(10\text{ GeV})^2 \approx 0.2$ (references in Ref. 11). The data from the CERN collider on jets in $p\bar{p}$ interactions also enable checking the basic QCD representations of $F(x, Q^2)$ and $\alpha_s(Q^2)$ with record values of Q^2. Here we shall briefly study the results of the latest investigations of these questions in e^+e^- annihilation and $p\bar{p}$ interactions.

The total cross section of e^+e^- annihilation into hadron jets is determined by the expression (4.1), where the contribution of the terms $\sim\alpha_s$ and $\sim\alpha_s^2$ is only $\approx 8\%$. Nevertheless, the high accuracy of the measurement of R(4.1), which is equal to 3–5% and is determined entirely by systematic errors, enables finding the value of $\alpha_s(Q^2)$ (Table I).[29] The weighted average value determined from the data in Table I is

$$\langle \alpha_s(1170\text{ GeV}^2) \rangle = 0.19 \pm 0.06, \tag{4.9}$$

the error in which ($\approx 30\%$) does not exceed the uncertainty in $\alpha_s(Q^2)$, obtained from an analysis of three-jet events (see Sec. 5). This is attributable to the high accuracy of the measurement of $R(W)$ achieved in recent years and the absence

TABLE I. Summary of data on the measurement of $R(W)$.

Type of installation	W, GeV	$R \pm \Delta R_{ran} \pm \Delta R_{syst}$	$\alpha_S \pm \Delta\alpha_{ran} \pm \Delta\alpha_{syst}$
TASSO	30—36,7	4,05±0,06±0,19	0,24±0,04±0,13
JADE	30—36,7	3,99±0,04±0,10	0,20±0,03±0,08
MARK-I	30—36,7	3,95±0,05±0,22	0,18±0,03±0,15
MARK-II	29,0	3,90±0,05±0,25	0,17±0,03±0,17
MAC	29,0	3,87±0,10±0,10	0,15±0,06±0,08

of significant theoretical uncertainties in the calculation of the total cross sections (4.1). The value $\alpha_S < 1$ obtained with $s^{1/2} \gtrsim 10$ GeV can also be used in the perturbation theory to calculate the characteristics of the initial stage of hard processes. In this case it is difficult to extract from (4.9) the parameter Λ(2.52), because, strictly speaking, it is not known whether Q^2 is equal to s or the square of the mass of the quark emitting the gluon ($M_q^2 \sim s/8$).[28,29 and 37]

Experiments on the study of the formation of hadron jets in $\bar{p}p$ interactions with $s^{1/2} = 540$ GeV open up new possibilities for checking QCD.[36–38] Here record momentum transfers in hard processes ($Q^2 \approx 5000$ GeV^2), in which the problems of taking into account the physics at large distances are no longer important (see Sec. 2), have been achieved. In spite of the fact that a technique for separating jets and determining their numbers has still not been perfected (see Sec. 3), increasing Q^2 by almost two orders of magnitude makes it possible to exclude reliably the background processes and to study parton-parton scattering. We have already demonstrated the advantage of high energies on the example of the precise determination of the gluon spin (Fig. 12). We shall now discuss the data on the cross sections for the production of jets (see below, Figs. 13 and 14) in the following processes[36,37]:

$$\bar{p} + p \to J\,(h) + X, \qquad (4.10)$$

$$\bar{p} + p \to J^{(1)}\,(h) + J^{(2)}\,(h) + X, \qquad (3.5')$$

$$\bar{p} + p \to J^{(1)}\,(h) + J^{(2)}\,(h) + J^{(3)}\,(h) + X. \qquad (3.6')$$

The general picture of jet phenomena at these energies was studied even before the collider was put into operation on the basis of the available data on $F(x, Q^2)$ for $Q^2 \lesssim 200$ GeV^2 and trigger jets (3.3) in pp interactions with $s^{1/2} \leqslant 62$ GeV (see Sec. 2).[10] The extrapolation by an order of magnitude in the total energy in the center of mass system (63→540 GeV) was done on the basis of QCD taking into account the evolution of $F(x, Q^2)$ (2.53). A large increase (by three to four orders of magnitude!) in the cross section $\sigma(J_{tr})$ for comparable values of $p_\perp^{tr}$ ($\lesssim 10$ GeV) in the transition from 63 GeV to the collider energies was predicted. This phenomenon is determined by the fact that at $s^{1/2} = 540$ GeV these values of $p_\perp^{tr}$ correspond to small values of $x \lesssim 2p_\perp/s^{1/2} \approx 0.05$, where $F(x)$ increases sharply [see (2.25)] owing to the gluon component of the nucleons (2.46).[10] Data from the collider in general confirm this picture (Fig. 13).[32] Scattering of gluons by quarks and gluons plays the main role here.

The cross sections for the production of hadron jets in $\bar{p}p$ interactions with large $E_\perp$ (J) or $p_\perp$ (J) ($\gtrsim 30$ GeV) were measured with the help of the UA1 and UA2 installations (see Sec. 3).[36–38] The absolute values obtained for the cross sections of the reaction (4.10) in these experiments differ by a factor of 1.5–2. The systematic errors, however, in both experiments are still large [$\pm 65\%$ (UA1) and $\pm 45\%$ (UA2)] and it is therefore assumed for the time being that the data are consistent with respect to one another. The systematic errors in the determination of the cross sections are basically linked with the uncertainties in the measurement of the luminosity of the accelerator ($\pm 20\%$), the determination of the acceptance of the installation ($\pm 35\%$), and the calibration of the calorimeters ($\pm 20\%$).[37 and 38] Their dependence on $E_\perp$ (J) does not exceed 10%.

The largest statistical sample of events was obtained on the UA2 installation with a total accelerator luminosity of $L = 112$ nbn^{-1}.[37] In this case, events in which for the hadron jets $E_\perp$ (J) $\geqslant 30$ GeV, $|\eta(J)| \leqslant 1$ and $\varphi(J) \leqslant 360°$ were selected. The measured cross sections of the processes (4.10) and (3.5) are presented in Fig. 14 ($P_\perp$ (J) $\leqslant 150$ GeV and $m_{JJ} \leqslant 300$ GeV).[37] The results of QCD calculations are shown in the figures as shaded regions.[46–48] The uncertainty in the QCD predictions is basically attributable to two factors: the uncertainty in the determination of Q^2 in these processes ($Q^2 \sim p_\perp^2$ (J) or $4p_\perp^2$ (J)) and the errors in the measurement of the parton distributions in nucleons with $\langle Q^2 \rangle = 5 - 10$ GeV^2 (see Sec. 2). The effect of these uncertainties on the QCD predictions of the cross sections of the

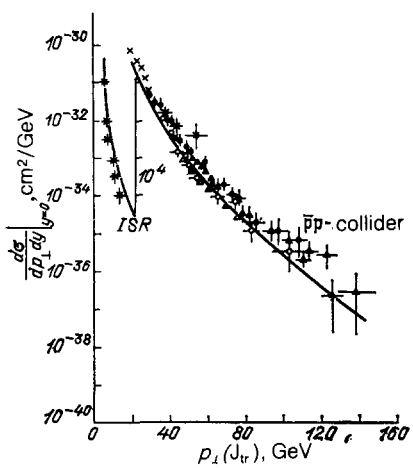

FIG. 13. Cross section for the formation of hadron jets in ISR and Sp$\bar{p}$S as a function of $P_\perp$ (J). The solid curves show the QCD calculations,[10] performed before the collider data were obtained.

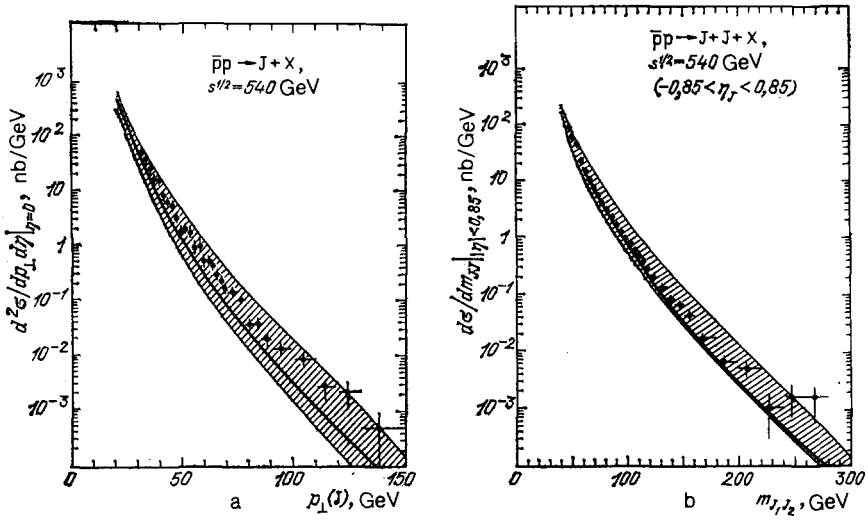

FIG. 14. a) Cross sections for the production of hadron jets (4.10) as a function of $P_\perp(J)$ at $s^{1/2} = 540$ GeV (UA2). b) Cross section for the production of two hadron jets (3.5) as a function of their effective mass ($m_{J_1J_2}$) at $s^{1/2} = 540$ GeV (UA2). The shaded regions show the results of QCD calculations.[46-49]

processes (4.10) and (3.5) was analyzed in Refs. 47 and 48. As a result the upper and lower limits of the cross sections were obtained (Fig. 14). The upper limit of the cross sections corresponds to QCD calculations with $\Lambda = 0.5$ GeV and $Q^2 = P_\perp^2(J)$, and the lower limit corresponds to calculations with $\Lambda = 0.5$ GeV and $Q^2 = 4P_\perp^2(J)$. The solid curves show the predictions from Ref. 10 with $Q^2 = P_\perp^2(J)$ and $\Lambda = 0.5$ GeV (see Sec. 2). As is evident from Figs. 13 and 14, QCD describes the inclusive cross sections for the production of hadron jets in the entire range of values of the variables studied: $s^{1/2}, P_\perp(J)$ and $m_{J_1J_2}$ ($s^{1/2} = 52 - 540$ GeV, $P_\perp(J) = 5 - 150$ GeV and $m_{JJ} = 30 - 300$ GeV), with an uncertainty factor $\lesssim 5$ for the largest values of these parameters. At the same time the cross sections themselves decrease by 11 orders of magnitude! This is undoubtedly a success of QCD, though as before it is not possible to draw definite conclusions about the value of Λ.

As we have already pointed out (Sec. 3), for $E_\perp(J) \geqslant 60$ GeV two-jet processes (3.5) dominate in $p\bar{p}$ interactions, and the relative fraction of the three-jet processes (3.6) drops to 10%.[36,37] In addition, these jets carry away more than 90% of the transverse energy of the $p\bar{p}$ collisions and in the azimuthal plane $\Delta\varphi_{12} \approx 180°$ with a half-width of $\lesssim 10°$! All this makes it possible to assume that in this case hard parton scattering processes of the type (4.3)–(4.6) are well separated and, therefore, direct data on $F(x, Q^2)$ with $\langle Q^2 \rangle \approx 2000$ GeV^2 can be obtained. Such an attempt was made by the UA1 group.[36] For this purpose the relation (4.2) integrated over $\cos\vartheta$ was used:

$$F(x_1)\,F(x_2) = x_1 x_2 \frac{d^2\sigma}{dx_1\,dx_2}\left(\int_0^{\cos\vartheta_{max}} K\frac{d\sigma}{d\cos\vartheta}\,d\cos\vartheta\right)^{-1}, \tag{4.11}$$

where $K \approx 2$ takes into account the effects of the higher orders of QCD.[36] The cross section $\sigma(\vartheta)$ in the form (4.7) with $\lambda = 0.2$ GeV and $Q^2 = P_\perp^2(J)$ was employed.

The factorization of the structure functions in (4.11) was checked experimentally for $x = 0.1$–0.8. As a result $F(x)$ with a systematic error of $\pm 30\%$ with $\langle Q^2 \rangle = 2000$ GeV^2 was obtained (Fig. 15).[39] Its values differ substantially from the data obtained at $Q^2 = 20$ GeV^2. This difference graphically demonstrates the scale of the breakdown of scaling when Q^2 is increased by two orders of magnitude. The number of partons with $x \gtrsim 0.3$ decreases substantially (by a factor of four to five!) and increases for $x \lesssim 0.1$ (compare with Fig. 6). The contribution of the quark component of the nucleons dominates for $x \gtrsim 0.4$ (see Fig. 15). These data can also be represented in an analytic form:

$$F(x) \approx 6{,}2\ e^{-9{,}5x} \tag{4.12}$$

or

$$F(x) \approx 8\,(1-x)^{13} + 1{,}1\,(1-x)^6. \tag{4.13}$$

The first term in (4.13) is linked with the behavior of the gluon and the second term can be linked with the quark com-

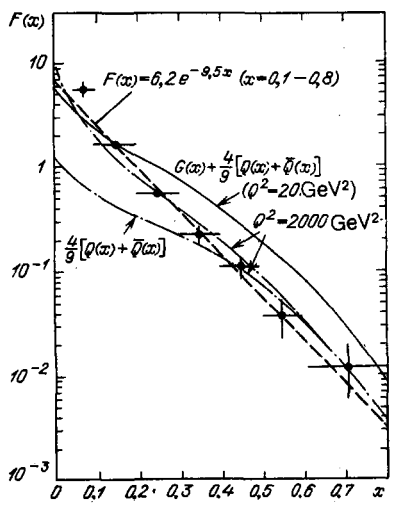

FIG. 15. Structure function $F(x)$ of a proton, obtained from data on $p\bar{p}$ interactions at $s^{1/2} = 540$ GeV (UA1). The broken straight line shows the dependence (4.12). The solid curve shows $F(x)$ at $Q^2 = 20$ GeV^2, the dot-dash curves are the QCD predictions for $F(x)$ at $Q^2 = 2000$ GeV^2 and the contribution of the quark component.

ponent of the nucleon with $Q^2 = 2000\ \text{GeV}^2$. In this case the scale of the breakdown of scaling when Q^2 varies from 20 to 2000 GeV^2 is manifested as a change in the exponents in (4.13) from the analogous approximations of $F(x)$ with $\langle Q^2 \rangle \approx 20\ \text{GeV}^2$ [see (2.25) and (2.26)] (6→13 and 3→4).

Figure 15 also shows the results of the QCD calculations of $F(x)$ with $\Lambda = 0.2$ GeV ($Q^2 = P_\perp^2(\text{J})$) and

$$F(x, Q_0^2) = G(x) + \frac{4}{9}[Q(x) + \bar{Q}(x)], \tag{4.14}$$

where $G(x)$, $Q(x)$ and $\bar{Q}(x)$ are the structure functions of the gluons, quarks, and antiquarks in the nucleon, and the factor of 4/9 takes into account the difference in the interactions of the quarks and gluons. A parametrization of these functions with $\langle Q_0^2 \rangle = 20\ \text{GeV}^2$ was used.[36] It is evident that the calculations describe the experimental data quite well.

Thus the data on the cross sections for the formation of jets at the highest achieved energies have confirmed the general QCD picture of the interactions of partons and their hadronization into jets. QCD successfully describes the dependences of the cross sections of the processes (4.10) and (3.5) on $P_\perp$ and m_{jj} with the cross sections decreasing by 11 orders of magnitude! The errors in the measurements of $F(x)$ in deep-inelastic lN interactions with $Q^2 \lesssim 200\ \text{GeV}^2$ and the uncertainty in the selection of Q^2 for hard hadron collisions, which give an uncertainty factor of $\lesssim 5$ in the cross sections of the processes (4.10) and (3.5), will decrease as a reuslt of new and more accurate experiments which are being planned. This will enable measuring $\alpha_s(Q^2)$ or Λ with $Q^2 \approx 2000\ \text{GeV}^2$.

Investigations of the formation of intermediate vector bosons ($W^\pm$, Z^0) in $p\bar{p}$ interactions at $\sqrt{s} \geqslant 540$ GeV open up new possibilities for checking QCD at short distances ($\lesssim 10^{-16}$ cm).[36,38] Because of their large mass (80 and 94 GeV) and the relatively high values of $\langle P_\perp(W, Z) \rangle = 4 - 7$ GeV they serve as an indicator of hard processes of the Drell-Yan type ($q\bar{q} \to W(Z)$) with $p_q \gtrsim 40$ GeV! In this case, both the characteristics of the production of W (Z) bosons and their accompanying jets are well calculated in QCD PT.[38] The first comparisons of these calculations with the available data on events in which $W^\pm$ bosons were produced show that they are well described by the theoretical curves.[38] The number of events in the statistical sample (≈ 100) is still small, however, so that values of Λ from 0.2 to 0.6 GeV are in agreement with experiment. A significant increase in the number of events in which W (Z) bosons are produced with $s^{1/2} \geqslant 540$ GeV is planned in the near future, which will enable a more precise check of QCD.

On the whole, studies of the hard stage of the formation of partons based on hadron jets have enabled measuring experimentally the quantum numbers of quarks and gluons and checking the basic ideas of QCD for $Q^2 \lesssim 2000\ \text{GeV}^2$. Quantitative measurements of the single parameter of the theory $\alpha_s(Q^2)$ show that $\alpha_s(Q^2) \lesssim 0.2$ for $Q^2 \gtrsim 200\ \text{GeV}^2$ and that perturbation theory can be used to calculate the characteristics of the initial stage of hard processes.

5. HADRONIZATION OF QUARKS AND GLUONS

After the successful verification of the basic postulates of QCD at short distances (see Sec. 4) the main unsolved problem of the theory is the description of the transformation of partons into hadrons. This occurs at large distances ($r \gtrsim R$) with small momentum transfer ($Q \sim p_\perp \sim 0.5$ GeV/c), which precludes the direct application of QCD PT. The experimental study of parton hadronization is therefore at the present time the main source of information both for solving the problem of confinement and for measuring some basic characteristics of hard processes with $\alpha_s \ll 1$ (see Secs. 3 and 4).

The model description of parton hadronization is given either on the basis of QCD PT, including the principle of correspondence of the parton and hadron spectra, or with the help of phenomenological models based on the known properties of soft hadron collisions (see Sec. 2) and some elements of QCD, which take into account the characteristics of the hard stage of the process (see Sec. 5.1). This establishes the general mechanisms of parton hadronization processes, required for constructing a theory of strong interactions.

Quark jets of hadrons have been studied in greatest detail in e^+e^- annihilation processes at $s^{1/2} = 3 - 43$ GeV (see Sec. 5.2).[28–31,50,57] Data on the fragmentation of quarks and diquarks have now been obtained from deep-inelastic interactions.[26,39,40,44,51] The hadronization of heavy quarks (c, b) was studied in e^+e^- annihilation.[50]

The fragmentation of gluons was first studied in e^+e^- annihilation into three hadron jets and in the decays $\Upsilon \to 3g$ (see Sec. 5.3).[28–31] Data on the hadronization of gluons in $p\bar{p}$ interactions at $s^{1/2} = 540$ GeV have now been obtained.[36–38] Thus the experimental information on parton hadronization encompasses a wide range of energies and different types of processes, which makes it possible to establish the basic mechanisms of hadronization.

The unity of the physics of hard and soft collisions of particles is manifested in the universality of the characteristics of the hadrons in the jets produced in these different interactions (see Sec. 5.4). This feature has not yet been satisfactorily explained theoretically.

5.1. QCD and phenomenological models

5.1.1. Quark-gluon cascades in QCD

The possibility of employing QCD PT to study the hadronization of partons is based on the space-time picture of the development of a parton cascade (see Secs. 1 and 2).[11] It follows from the general principles of quantum mechanics that the characteristic time for the production of colored partons, for example, in e^+e^- annihilation, decreases as W increases:

$$\tau \sim \frac{1}{E_q} \sim \frac{1}{W}. \tag{5.1}$$

On the other hand, the characteristic quark hadronization time (see Secs. 1 and 2) is[14,20]

$$t \sim \frac{E_q}{M_q^2} \sim WR^2, \tag{5.2}$$

where M_q is the effective (constituent) mass of the quark and $R \sim 1/M_q$. For light quarks (u, d, s) $R \sim 1$ fm. It is evident from a comparison of (5.1) and (5.2) that as the energy increases the time interval $\Delta t = t - \tau$, comprising the "lifetime" of a colored quark in accordance with the laws of QCD PT, increases. In this case, bremsstrahlung gluons, which form new gluons and $(q\bar{q})$ pairs, are emitted, i.e., the so-called quark-gluon cascade develops. Its development can be calculated using perturbation theory up to $Q^2 \gtrsim Q$.[11,52 40)] Parton multiplication proceeds via successive decays[11]

$$q \to q + g, \tag{5.3}$$

$$g \to g + g, \tag{5.4}$$

$$g \to q + \bar{q}, \tag{5.5}$$

whose differential probabilities have the form

$$dW(q \to qg) = \frac{4}{3}\frac{\alpha_s}{\pi}\frac{dk_\perp^2}{k_\perp^2}dz\,\frac{1+(1-z)^2}{2z}, \tag{5.6}$$

$$dW(g \to gg) = 3\frac{\alpha_s}{\pi}\frac{dk_\perp^2}{k_\perp^2}dz\left[z(1-z) + \frac{z}{1-z} + \frac{1-z}{z}\right], \tag{5.7}$$

$$dW(g \to q\bar{q}) = \frac{1}{2}\frac{\alpha_s}{\pi}\frac{dk_\perp^2}{k_\perp^2}dz\,\frac{z^2+(1-z)^2}{2}, \tag{5.8}$$

where $k_\perp$ is the transverse momentum of a gluon (quark) relative to the momentum of the parent parton and z is the corresponding relative fraction of the energy. These "elementary" processes essentially determine the jet nature of the quark-gluon cascade up to the moment at which the partons are hadronized.[41)] It is evident from these formulas that fast partons primarily emit soft gluons (quarks) with $z \ll 1$ and $x_\perp = k_\perp/p \ll 1$, which move in the same direction ($\vartheta \ll 1$) as the parent partons. The total probability of these processes increases with energy:

$$W^{(g)} \sim \frac{\alpha_s}{\pi}\int_{R^{-1}}^{E}\frac{dE_g}{E_g}\int_{R^{-2}}^{E^2}\frac{dk_\perp^2}{k_\perp^2} \approx \frac{\alpha_s}{\pi}\ln^2(ER), \tag{5.9}$$

$$W^{(q\bar{q})} \sim \frac{\alpha_s}{\pi}\int_{R^{-2}}^{E^2}\frac{dk_\perp^2}{k_\perp^2} \approx \frac{\alpha_s}{\pi}\ln(ER)^2, \tag{5.10}$$

where $k_\perp^2 \gtrsim R^{-2}$ and R is the distance at which QCD PT can still be used. Its value is unknown and can be determined from the experimental data. The value of R can be estimated roughly by using the value $\langle p_\perp \rangle \approx 0.5$ GeV for direct hadrons (see Sec. 2). In this case $k_\perp > 0.5$ GeV and $R < 1/\langle p_\perp \rangle \approx 0.4$ fm. In any case, it follows from (5.9) and (5.10) that as the energy increases $W^{(g)}$ and $W^{(q\bar{q})} \to 1$, i.e., a quark-gluon cascade develops, and hard bremsstrahlung gluons ($z \sim 1, \vartheta \sim 1$), which give rise to the hadron jets separated experimentally, are already produced with an appreciable probability. For example, in e^+e^- annihilation these processes constitute $\approx 10\%$ of the events with $W \geqslant 30$ GeV, i.e., for $E_q \geqslant 15$ GeV.

Thus in this approach fast colored partons by the moment of hadronization shed their coat of collinear and relatively soft ($k_\perp \gtrsim 0.5$ GeV) gluons and quarks, whose number increases with E_q (Fig. 16a). The decolorization of this multiparton configuration already occurs at large distances ($\sim R$), owing to $(q\bar{q})$ pairs created by the bremsstrahlung gluons.

Perturbative QCD can be used to calculate the characteristics of the quark-gluon cascade. The question of the hadronization of the cascade naturally arises next. The local correspondence between the parton and hadron spectra (local parton-hadron duality) has been proposed as a working hypothesis.[52 42)] This enables comparing the model with experiment and determining the region of its applicability. Specific calculations of the quark-gluon cascade in different approximations of QCD PT and the first comparisons with experimental data are carried out in Refs. 11 and 52. In particular, it is shown that the $\pi^\pm$ meson spectra in e^+e^- annihilation at $W \gtrsim 20$ GeV are described satisfactorily.[52]

This model of parton hadronization, however, is based on quite strong assumptions, which must be verified experimentally (such a program is proposed in Refs. 11 and 52). It therefore makes sense to study at the present time only its general predictions, associated with the structure of the quark-gluon cascade, rather than with specific calculations of the hadron spectra.

The average multiplicity of the hadrons in this model increases rapidly with energy[11]:

$$\langle n(s) \rangle = a + b\exp\left[c\left(\ln\frac{s}{Q_0^2}\right)^{1/2}\right], \tag{5.11}$$

where a, b, and Q_0^2 are experimentally determined param-

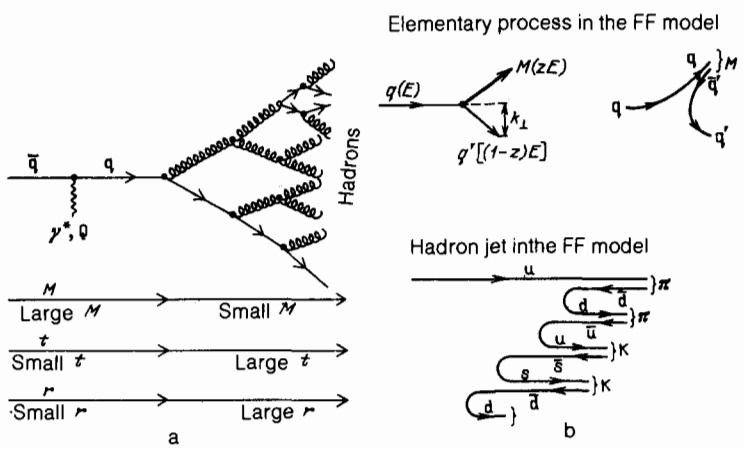

FIG. 16. a) Illustration of a quark-gluon shower formed by fast quarks (q), the nature of the change in the invariant masses (M), the time (t) and the distance (r) with the development of the cascade are indicated at the bottom of the figure. b) Scheme of quark hadronization in the FF model.

eters, $c = [72/(33 - 2N_q)]^{1/2}$, and N_q is the number of quark flavors. This behavior of $\langle n(s)\rangle$ is linked with the rapid increase in the number of soft bremsstrahlung gluons and $(q\bar{q})$ pairs with E_q and the assumption of their independent hadronization.

Another important consequence of the appearance of quark-gluon cascades is the breakdown of scaling in quark fragmentation processes (see Sec. 2). The values of the functions $D_q^h(z, s)$ increase as $z \to 0$ and decrease as $z \to 1$ with increasing s.[43)]

A characteristic feature of this model is the hadron rapidity distribution:

$$\frac{1}{\sigma}\frac{d\sigma}{dy} = \rho(y). \tag{5.12}$$

As is well known, in the parton model $\rho(y) = \text{const}$, and therefore $\langle n(s)\rangle \sim \ln(W/m)$ because of the increase in the admissible range of rapidities $(0 \leqslant y \leqslant \ln(W/m))$ (see Sec. 2). The development of the quark-gluon cascades gives rise not only to a rapid growth of $\langle n(s)\rangle$ (5.11), but also to a characteristic dependence $\rho(y)$. In this case it has turned out that it is important to study the quantum-mechanical picture of the emission of soft gluons, in contrast to the classical scheme of the branching process.[11,52–53] Indeed, a beam of partons with an aperture angle $\vartheta_1 \ll 1$ emits soft gluons with $\vartheta > \vartheta_1$ coherently with the "color charge" of their common parent. For this reason, instead of a large number of new gluons (according to the number of partons in the beam) only one will be emitted.[44)] Because of this the number of soft gluons decreases as $\xi = y/y_{max} \to 0$, which is what causes the corresponding decrease in the number of hadrons in this region. As $\xi \to 1$ the number of hadrons also decreases with the development of the cascade because of the law of energy-momentum conservation. For this reason, in this model $\rho(\xi)$ will have the characteristic bell-shaped form, reaching a maximum as $\xi \to 1/2$. For finite energies ($W \lesssim 50$ GeV) the maximum in $\rho(\xi)$ is located at $\xi = 0.3$–0.4.[52] Thus cascading of gluons causes $\rho(\xi)$ to grow rapidly with W at $\xi \sim 1/2$ and gives rise to a finite number of hadrons as $\xi \to 0$ and $\xi \to 1$. It is undoubtedly of interest to check this unusual behavior of $\rho(\xi)$ (see Sec. 5.2).

The behavior of jets of hadrons, formed by gluons, in QCD PT has some peculiarities associated both with the quantum numbers of the gluon and with their interaction with partons. Gluons emit gluons more intensively (5.7) than do quarks (5.8). For this reason, the cascade begins to develop earlier in a gluon jet than in a quark jet, that is, all phenomena noted above must be observed in gluon jets at lower energies than in quark jets. It is expected that at high energies the ratio between the multiplicities of the hadrons in these jets will approach

$$\langle n^{(g)}(s)\rangle \approx \frac{9}{4}\langle n^{(q)}(s)\rangle. \tag{5.13}$$

Because of the universality of the interaction of a gluon with quarks of all flavors there should be more heavy quarks (c, b) in a gluon jet. Finally, entirely new objects, for example, bound states of gluons—glueballs—should also appear in gluon jets.[56]

The attractiveness of the model studied lies in the systematic application of QCD PT up to $Q_0 \sim m_h$. Its extension to the region of confinement is, of course, a working hypothesis, which is required in order to make comparisons with experiment (see Secs. 5.2 and 5.3).

5.1.2. Phenomenological models

During the last few years numerous phenomenological models for describing hadronization of partons in hard collisions of particles have been developed (see the reviews Refs. 50 and 57). The two most popular models among them are the Field-Feynman model (FFM)[58–60] and the Lund model (LM),[61,62] which are widely used in the analysis of experimental data.[63 45)] We should also call attention to an entirely new class of so-called cluster models,[64–67] in which parton hadronization is described without the introduction of the fragmentation function ($D_q^h(z)$) and the limitation of parton transverse momenta.

The FF model was the first parametrization of the hadron distribution in jets.[58] The well-known theoretical physicist R. Feynman thought that experimenters should have a simple description of hadron jets, based on the properties of soft and hard hadronic interactions ("standard jets"), in order to find new phenomena.[58] This goal was rapidly achieved and in 1979–1980 there appeared modifications of this model which took into account the emission of hard gluons ($q \to qg$) and the formation of heavy quarks (c, b).[59,60]

The scheme of quark hadronization in the FF model is analogous to the formation of hadrons in the parton model (see Sec. 2.1). Hadrons are formed as a result of successive and independent decays of the type (Fig. 16b):

$$q_a \to M(q_a, \bar{q}_b) + q_b, \tag{5.14}$$

in which the starting quark (q_a) fragments into a meson (M), while the remaining quark (q_b) decays according to the scheme (5.14). This process continues until the remaining quark has an energy $W_q > W_0$ ($W_0 = E + P_z \approx 1$ GeV). The parameter W_0 is determined from experiment.[63]

The FF model takes into account two experimental results: the approximate scaling of the $D_q^h(z)$ functions and the limitation on the transverse momenta of the hadrons ($p_\perp$). To reproduce the scaling in z it is postulated in the model that the probability (P) for the fragmentation of q into $M(z)$ is independent of E_q:

$$\frac{dP}{dz} = f(z), \tag{5.15}$$

where

$$z = \frac{(E + p_\parallel)M}{(E+p)q_a}, \tag{5.16}$$

$$\int_0^1 f(z)\,dz = 1. \tag{5.17}$$

The relationship between $D(z)$ and $f(z)$ is given by the integral equation

$$D(z) = f_1(z) + \int_z^1 \frac{d\eta}{\eta} f(1-\eta) D\left(\frac{z}{\eta}\right), \tag{5.18}$$

where $\eta = 1 - z$. The first term in (5.18) gives the probability for the formation of the first hadron (5.14) and the second term takes into account the remaining cascade (see Fig. 16). If $f(z)$ is expressed in a simple polynomial form

$$f(z) = (d+1)(1-z)^d, \tag{5.19}$$

then from (5.18) we obtain

$$D(z) = (d+1)\frac{(1-z)^d}{z}, \tag{5.20}$$

which corresponds to experiment.[50,57] From here it follows that the average multiplicity of the hadrons

$$\langle n(W)\rangle = \int D(z)\,dz = A + B\ln W, \tag{5.21}$$

grows logarithmically with energy, as in the parton model (see Sec. 2.1). The function $f(z)$ is usually parametrized in the following form:

$$f(z) = 1 - a_F + 3a_F(1-z)^2, \tag{5.22}$$

where a_F is a parameter of the model.

The limitation on the transverse momenta of the hadrons in the model is associated with the assumption that $k_\perp$ of the associated quarks is limited (see Fig. 16b):

$$\frac{dN}{dk_\perp^2} \sim e^{-k_\perp^2/2\sigma_q^2}, \tag{5.23}$$

which gives

$$\langle p_\perp(h)\rangle = \pi^{1/2}\sigma_q. \tag{5.24}$$

Two additional parameters are introduced into the model:

$$a_V = \frac{N(V)}{N(V)+N(P)}, \tag{5.25}$$

$$\gamma_S = \frac{N(s\bar{s})}{N(u\bar{u})+N(d\bar{d})+N(s\bar{s})}, \tag{5.26}$$

which determine the relative fraction (a_V) of vector mesons and the suppression factor (γ_S) of the strange pairs ($s\bar{s}$). A detailed comparison of the FF model with experiment was made in 1979–1980.[28–31,50,57,63] We shall therefore present only the results of this analysis. The parameters of the model were determined from the data obtained by the TASSO group at $W = 12$ and 30 GeV for two-jet e^+e^- annihilation events ($S \leqslant 0.25$)[57,63 46]:

$$\left.\begin{aligned} a_F &= 0.57 \pm 0.20,\\ \sigma_q &= 0.32 \pm 0.04\ \text{GeV},\\ a_V &= 0.56 \pm 0.15. \end{aligned}\right\} \tag{5.27}$$

With these values of the parameters the FF model describes well the hadronization of quarks in hard $\nu(\bar{\nu})N$-, $e(\mu)N$-, and hN interactions and in e^+e^- annihilation.[28–32,50,57,63]

Deviations from the model were observed for $W \gtrsim 30$ GeV, for example, in the hadron distributions over $\langle p_\perp^2\rangle$ in the event plane ($\langle p_{\perp in}^2\rangle$) and outside it ($\langle p_{\perp out}^2\rangle$) (Fig. 17a).[57,63] They are associated with hard bremsstrahlung from hard gluons (2.56), which is taken into account in modifications of the model with an accuracy of $O(\alpha_S)$[59] and $O(\alpha_S^2)$[60] in QCD PT (Fig. 17b). In this case the quark and gluons formed ($e^+e^- \to q\bar{q}g$) fragment independently. The gluon decays into q and $\bar{q}$:

$$g(E) \to q(zE) + \bar{q}[(1-z)E], \tag{5.28}$$

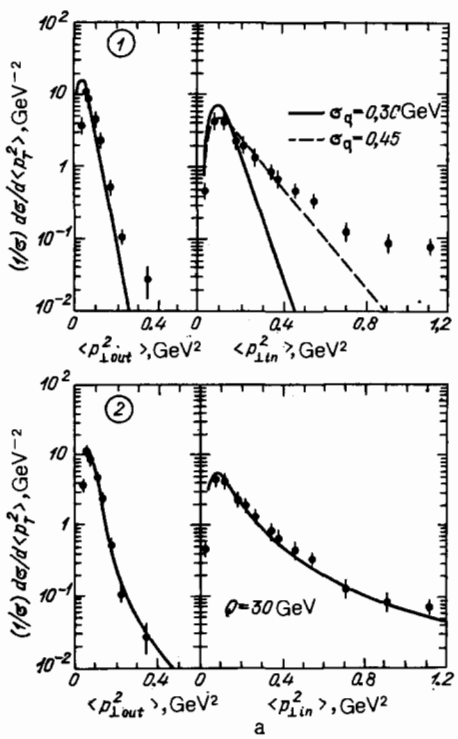

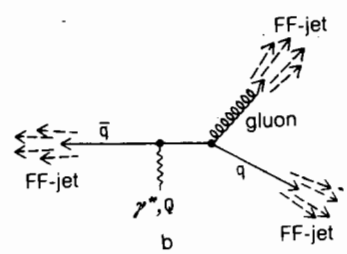

FIG. 17. a) Hadron distributions in e^+e^- annihilation at $s^{1/2} = 30$ GeV over $\langle p_{\perp out}^2\rangle$ and $\langle p_{\perp in}^2\rangle$; the curves show the results of calculations using the FFM model without (1) and with (2) emission of hard gluons (2.56).[59,60] b) Scheme of the FF model taking into account hard gluon emission.

which further fragment according to the FF scheme. The energy of the gluon is divided between the quarks or in accordance with[59]

$$f(z) = 1, \tag{5.29}$$

or according to the law[60]

$$f_g(z) = z^2 + (1-z)^2. \tag{5.30}$$

These modifications of the model are widely used to analyze three-jet events in e^+e^- annihilation and to measure the strong interaction constants of partons (α_s) in QCD (see Sec. 5.3).

The fragmentation of heavy quarks (Q≡b, c) in the FF model proceeds according to the same scheme:

$$Q \to H(Q\bar{q}) + q, \tag{5.31}$$

where the heavy mesons H ($Q\bar{q}$) carries most of the energy of the Q quark. This follows from simple kinematic considerations. Indeed, the probability of the transition (5.31)[50,57] is

$$P(i \to f) \sim \frac{1}{\Delta E^2}, \tag{5.32}$$

where

$$\Delta E \sim E(Q\bar{q}) + E(q) - E(Q) \sim 1 - \frac{1}{z} - \frac{\varepsilon}{1-z} \tag{5.33}$$

and $\varepsilon = (m_q/m_Q)^2$. From here it is found that

$$D_Q^H(z) = \frac{1}{z} \frac{k}{\{1-(1/z)-[\varepsilon/(1-z)]\}^2} \tag{5.34}$$

has a peak at large values of z (see Sec. 5.2).

To complete the total scheme of the FF model, employed for describing experimental data, it is necessary to examine the formation of baryons. In this case it is assumed that the starting quarks pick up diquarks (qq) from the QCD vacuum

$$q_a \to (q_a qq) + \bar{q}\bar{q} \tag{5.35}$$

with a probability of ~0.1, which corresponds to the observed relative fraction of protons in e^+e^- annihilation for $W \gtrsim 30$ GeV.[60] In this scheme short-range correlations between baryons in different variables and local compensation of their quantum numbers should be expected.

This exhausts the basic elements of the FF model of the hadronization of partons.[58–60] Before proceeding to other models we shall draw a number of general conclusions.

In the FF model[58–60] the fragmentation of quarks proceeds independently of the fragmentation of gluons. In this respect it differs substantially from the LM.[61,62] For this reason the FF model is also often called the model of independent fragmentation. The term "fragmentation" itself is associated with a specific scheme for the transformation of partons into hadrons (see Fig. 16b). Its widespread use is, of course, unjustified. It is better to use a more general term—"hadronization," since the mechanism of confinement is unknown.

The FF model does not take into account the laws of conservation of the energy and quantum numbers (charge, color, flavor) of the partons. The space-time evolution of partons into hadrons occurs in a manner opposite to that expected in QCD PT (see Sec. 5.1.1). Indeed, in the FF scheme in the center of mass system of (e^+e^-) the fast quarks hadronize first, after which the slow quarks hadronize (see Fig. 16b). Nevertheless, the success of this model in describing the experimental data[50,57] for $E_q \lesssim 15$ GeV shows that the model correctly reproduces the basic mechanisms of parton hadronization.

In the Lund model[61,62] unlike the FFM the evolution of ($q\bar{q}$) systems as a whole is studied taking into account the nature of the forces acting between colored quarks. At large distances ($R \gtrsim 1/\Lambda$), because of the strong nonlinear interaction of the gluons, the lines of force between q and $\bar{q}$ form a string tube with a radius of $\sim 1/\Lambda$. At the same time the force of interaction of the quarks is independent of the distance (d) between them and the potential energy of the string[1,50,57] is

$$E \sim kd, \tag{5.36}$$

where the tension in the string is

$$k \sim 1 \text{ GeV/fm} \approx 0.2 \text{ GeV}^2 \tag{5.37}$$

As the quarks fly apart their energy transforms into the potential energy of the string, and for $E > E_0$ (~ 1 GeV) pairs of light quarks ($q\bar{q}$) can form from the QCD vacuum owing to the tunneling effect. As a result the string begins to divide up into shorter strings with the formation first of slow ($q\bar{q}$) systems and then faster systems, which corresponds to the ideas of QCD (Fig. 18a).[11,57] The study of the evolution of the entire system of ($q\bar{q}$) pairs enables taking into account the laws of conservation of the energy and quantum numbers of the partons transforming into hadrons. In this respect the

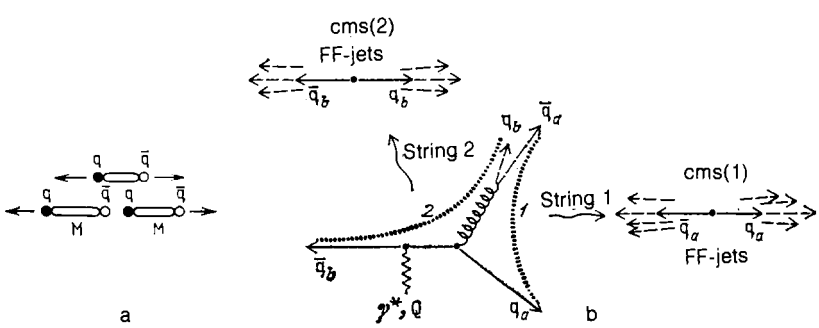

FIG. 18. a) Diagram of the formation of mesons in the Lund model. b) Scheme of the formation of gluons in the Lund model. The strings 1 ($\bar{q}_a q_a$) and 2 ($\bar{q}_b q_b$) decay according to the FF model in their rest system.

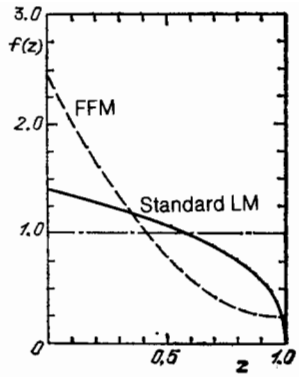

FIG. 19. The function $f(z)$ for the FF and Lund models. The broken straight line corresponds to $f(z) = 1$.

Lund model is more systematic than the FFM. Nevertheless, the transformation of $(q\bar{q})$ pairs into hadrons is studied in the LM following the same scheme as in the FFM (Fig. 18b).

In the simplest variant of the LM

$$f(z) = 1, \tag{5.38}$$

and for the so-called standard LM

$$f(z) = (1 + c)(1 - z), \tag{5.39}$$

where $c \approx 0.3 - 0.5$ (Fig. 19),[57,62] that is, the distribution of hadrons over z has a scaling character, just as in the FFM, but their spectrum is harder because of the choice of a different form for $f(z)$. However, the function $f(z)$ (5.22) is often used in the LM, especially for comparing the results obtained with both models in analyzing experimental data.

The distribution of the hadrons over $p_\perp^2$ relative to the axis of the colored tube in the LM is believed to be the result of the tunneling formation of $(q\bar{q})$ pairs from the vacuum[61,62]:

$$dN \sim dp_\perp^2 \exp\left[-\frac{\pi(m^2+p_\perp^2)}{k}\right], \tag{5.40}$$

which leads to scaling of the hadron distributions over $m_\perp^2 + m^2 + p_\perp^2$. From (5.40) there also follow relations between the probabilities for the formation of different types of $(q\bar{q})$ pairs from the vacuum:

$$u : d : s : c = 1 : 1 : 0.3 : 10^{-11}, \tag{5.41}$$

which gives the strong suppression of the formation of $(c\bar{c})$ pairs. All remaining elements of the LM—a_V, $D_Q^H(z)$, formation of baryons, etc., are analogous to the corresponding assumptions in the FFM.

The most significant difference between these models appears in the study of the bremsstrahlung of hard gluons (2.56).[50,57] In the FFM the formation and fragmentation of gluons occurs independently of the evolution of the remaining system. In the LM the string "is stretched" between the quarks, gluons, and antiquarks, which is what couples their further development (see Fig. 18b). For sufficiently high E_g this string separates into two strings $(q_a\bar{q}_a)$ and $(q_b\bar{q}_b)$, which fragment into hadrons independently in their rest systems, for example, according to the FF scheme. As a result, part of the gluon energy is transferred to the hadrons in quark jets. This is what leads to the fact that the same relative fraction of three-jet events (2.56), distinguished experimentally, requires higher values of α_S in the LM than in the FFM (see Sec. 5.3).

Monte Carlo algorithms for modeling events on the basis of these models were developed in Refs. 58–62, which made it possible to compare these models in detail with experiment for $W \lesssim 40$ GeV (see Secs. 5.2 and 5.3).

A new point of view of the parton hadronization stage has been under development in recent years in the so-called cluster models (CM).[64–67] These models do not contain two of the principal assumptions of the LM and FFM: the existence of a fragmentation function $D_q^h(z)$ and the limitation on the transverse momenta of the partons. At the same time they successfully describe the experimental data.

The first stage of a hard process—the development of a parton shower—is studied in the CM, as in all other models, on the basis of QCD PT (Fig. 20). The development of the shower proceeds until $M^2(q\bar{q}) \gtrsim t_{cl}$ where t_{cl} is a parameter of the model. The new feature occurs at the hadronization stage. Because of the color forces acting at large distances the quarks and antiquarks combine into white clusters with

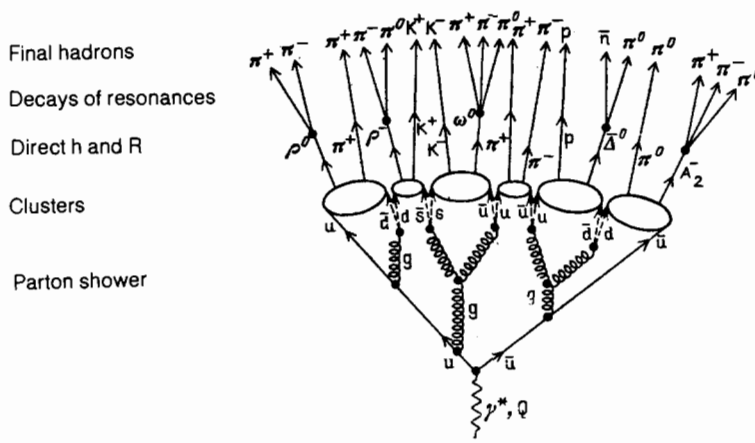

FIG. 20. Scheme of parton hadronization in cluster models (CM).

$$M_{\rm cl}(q_i\bar{q}_j) \geqslant m(q_i) + m(\bar{q}_j) + W_{\min}, \quad (5.42)$$

where $W_{\min}$ is the minimum energy required for a cluster to decay into hadrons. Thus in the CM a virtual photon with $M = Q$ forms many white clusters with $M_{\rm cl} \leqslant Q$. It is further assumed that they decay independently according to the scheme

$$M_{\rm cl}(q_i\bar{q}_j) \to h_1(q_i\bar{q}_a) + h_2(q_a\bar{q}_j), \quad (5.43)$$

isotropically in their rest systems. The probability of the decay (5.43) is determined by the usual factors:

$$P(M \to h_1h_2) = p_f p_s p_k, \quad (5.44)$$

where p_f characterizes the relative probabilities of the formation of $(u\bar{u})$, $(d\bar{d})$, $(s\bar{s})$, and $(c\bar{c})$ vacuum pairs, p_s is the spin factor of the hadrons, and p_k is a kinematic factor corresponding to the phase volume of the decay (5.43):

$$p_k = \sqrt{\lambda}(M_{\rm cl}^2, M_1^2, M_2^2) M_{\rm cl}^{-2}, \quad (5.45)$$

$$\lambda(a, b, c) = a^2 + b^2 + c^2 - 2ab - 2ac - 2bc. \quad (5.46)$$

The value of p_f is determined from formulas of the type (5.45) and (5.46) for the decay:

$$M_{\rm cl} \to q_a\bar{q}_a. \quad (5.47)$$

The formation of baryons in the model is viewed as being the result of the attachment of $(q_a q_a)$ and $(\bar{q}_a\bar{q}_a)$ pairs. The spin factor is

$$p_s = (2J_1 + 1)(2J_2 + 1), \quad (5.48)$$

where J_1 and J_2 are the spins of the hadrons in (5.43). The algorithms of cluster models are described in greater detail in Refs. 64–67. Here we point out only that the number of parameters in them is small (Λ, $t_{\rm cl}$, $W_{\min}$) and with the values

$$\left.\begin{aligned} \Lambda &= 0.2 \text{ Gev}, \\ t_{\rm cl} &= 1{,}5 \text{ GeV}^2, \\ W_{\min} &= 1.25 \text{ GeV}, \end{aligned}\right\} \quad (5.49)$$

the characteristics of hadrons in e^+e^- annihilation can be described for $W \lesssim 40$ GeV.[65,67] The CM take into account the effect of the coherence of soft gluon emission on the energy spectra and the angular correlations of hadrons in QCD PT.[66,67] In this respect the CM are close to the quark-gluon cascade model.[11,52]

The absence of a theory of strong interactions of partons at large distances led to the rapid development of phenomenological models, whose basic features we have examined above. In all models the first stage of the process is studied in QCD PT up to $Q^2 \gtrsim Q_0^2$, where $Q_0^2 \approx 10$ GeV^2 in the FFM and $Q^2 \sim 1$ GeV^2 in the CM and LM. In the quark-gluon cascade models $Q_0^2 \sim M_h^2$![52] The value $Q_0^2 \approx 10$ GeV^2 basically distinguishes FFM from other approaches, which evolve in the direction $Q_0^2 \to m_h^2$.[11,66,67] Because of this the region of applicability of the FFM is limited to $E_q \lesssim 10$–15 GeV, when the parton cascade has not yet developed, and coherent effects are therefore unimportant (see Secs. 5.2 and 5.3).

5.2. Hadronization of quarks

As we have already noted, by the moment of hadronization high-energy quarks comprise a quark-gluon shower, and for this reason their transformation into hadrons is determined by both quarks and gluons (see Sec. 5.1). An analogous situation also occurs for high-energy gluons. At the same time, some characteristics of hadron jets depend on their origin. It is therefore of interest to study quark and gluon jets separately.

The basic results on the hadronization of quarks were obtained in e^+e^- annihilation with $W \leqslant 43$ GeV.[28–31,50,57] In deep-inelastic $\nu(\bar{\nu})p$ and μp interactions the jet characteristics of hadrons were studied in the regions of fragmentation of quarks and diquarks with $W \lesssim 15$ GeV.[39,44,57,68,69] A comparison of these data with models makes it possible to establish the general laws governing the transitions of quarks into hadrons.

5.2.1. Momentum distributions of hadrons in jets

a) Transverse evolution of a hadron jet. In e^+e^- annihilation into two jets (2.29) the distribution of the so-called direct hadrons (h_d) over $p_\perp^2$ relative to the axis of the jet is described by the FFM (5.24) with $\sigma_q = 0.32 \pm 0.04$ GeV and $W = 12$–30 GeV, which corresponds to $\langle p_\perp(h_d)\rangle = 0.57 \pm 0.07$ GeV.[57] As a result of the decays of resonances the transverse momenta of the recorded long-lived hadrons (π, K, N, ...) decrease and are equal to $\langle p_\perp(h)\rangle = 0.343 \pm 0.007 + 0.010$ GeV with $W = 12$–17 GeV.[47]

In the analysis of all cases of e^+e^- annihilation there occurs an appreciable broadening of the hadron distributions over $p_\perp^2$ with increasing W ($\gtrsim 30$ GeV), associated with the hard gluon bremsstrahlung, and

$$\langle p_\perp^2(h)\rangle = a + bW, \quad (5.50)$$

where $a = 0.072 \pm 0.008$ GeV^2 and $b = 0.0070 \pm 0.0003$ GeV (Fig. 21).[31] It is interesting that for $p_\perp^2 \lesssim 0.3$ GeV^2 the distributions are practically independent of W and the properties of these hadrons are probably determined by the characteristics of the QCD vacuum. It is in this connection that the well-known problems of "associating" them with one or another jet appear, which makes it difficult to determine their quantum numbers (see Secs. 3 and 4). The increase in the "width" of the jet is not isotropic in the azimuthal plane relative to the axis of the jet, which is what causes the different distributions over $\langle p_{\perp\rm in}^2\rangle$ and $\langle p_{\perp\rm out}^2\rangle$ (see Fig. 17a). They are described well by the FFM and LM if the processes (2.56) are taken into account.

The hadron distributions over the dimensionless variable $x_\perp = 2p_\perp/W$ exhibit the characteristic breakdown of scaling predicted by QCD PT: the increase in the number of hadrons for $x_\perp \lesssim 0.05$ and their decrease for $x_\perp \gtrsim 0.1$ with increasing W.[28–31 48]

Analogous effects have also been observed in μp interactions for $E_\mu = 280$ GeV, $Q^2 \geqslant 4$ GeV^2 and $W^2 = 40$–400 GeV^2.[40–68,69] The experimental installation for studying deep inelastic μp interactions consists of a double magnetic spectrometer with a vertex detector—a two-meter streamer

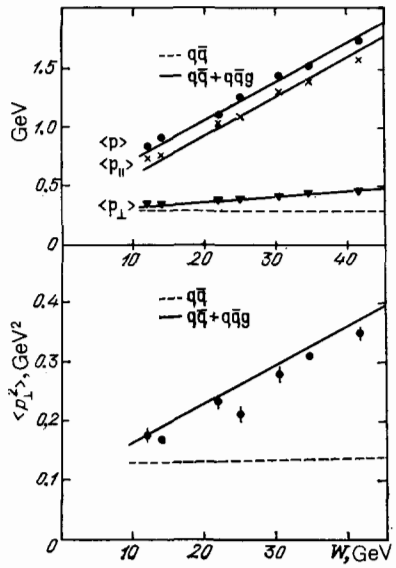

FIG. 21. $\langle p\rangle$, $\langle p_\parallel\rangle$, $\langle p_\perp\rangle$, and $\langle p_\perp^2\rangle$ as functions of W for e^+e^- annihilation. The straight lines show the QCD calculations for e^+e^-–$q\bar{q}$ processes (broken lines) and taking into account the hard gluon bremsstrahlung (solid lines).

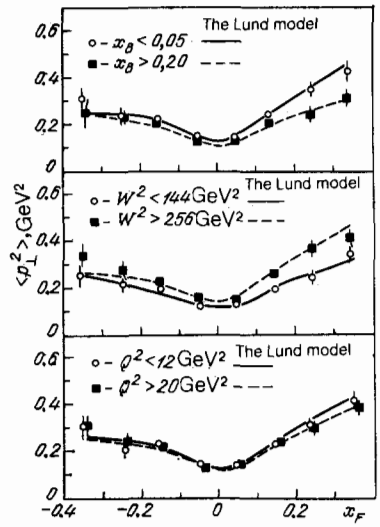

FIG. 22. $\langle p_\perp^2\rangle$ as a function of x_F for hadrons formed in μp interactions at $E_\mu = 280$ GeV. The curves in the figures show the calculations employing the Lund model.

chamber, containing a 1-m liquid-hydrogen target. It detects all secondary charged particles with momenta from 280 GeV to 200 MeV in a 4π geometry. This is the first electronic installation with whose help the hadron component in the μp interactions at high energies was measured. A total of about 11 000 μp interactions were selected and the momentum distributions of the secondary hadrons in their rest system over $x_F = 2p_\parallel^*/W$ were constructed.[68] In this case the forward-propagating hadrons ($x_F \geqslant 0$) can be linked with the fragmentation of the knocked out u quark, while hadrons with $x_F < 0$ can be linked with the hadronization of the diquark (ud) (see Sec. 2). The dependence $\langle p_\perp^2\rangle = f(x_F)$ has a characteristic form similar to the "seagull effect" in soft hadron interactions[5,6] and the value of $\langle p_\perp^2\rangle$ increases with W^2 (especially for $x_F > 0$), just as in e^+e^- annihilation (Fig. 22). Here we present the calculations based on LM taking into account the emission of soft and hard gluons and the limitation on the transverse momentum of the partons inside the nucleon ($\langle k_\perp^2\rangle = 0.44$ GeV^2). As can be seen from the figure, this variant of LM describes the experimental data well. The correlation between the transverse momenta of the secondary particles is an argument in favor of taking into account the soft gluon emission. Figures 23a and 23b show the y^* distributions of the fluxes of the transverse momenta of fast hadrons ($x_F^{tr} = 0.5$–1.0) and the particles accompanying them, for which $p_\perp' = p_\perp \cos\varphi_\perp$, where $\varphi_\perp$ is the azimuthal angle relative to $\mathbf{p}_\perp^{tr}$. It is evident from these figures that $p_\perp^{tr}$ is compensated by the hadrons in the central region, and not in the region of fragmentation of the diquark ($y^* \approx -2$), as would have happened if $\langle k_\perp^2\rangle$ increased (dashed curve).[49] An obvious explanation of this phenomenon is the emission of soft gluons (solid curve).

Thus the evolution of the quark jet of hadrons $D_q^h(p_\perp^2, W)$ for $E_q \lesssim 20$ GeV over $p_\perp^2$ is satisfactorily described by the phenomenological models (FFM and LM) with the parameters (5.27) and taking into account the emission of soft and hard gluons in QCD PT (see Sec. 5.1).[28–31] We also note that these distributions are described well by the CM also, where it is not assumed that the transverse momenta of the partons are limited and only three parameters are employed (Fig. 24).[65,67]

b) Longitudinal evolution of a jet. Hadron distributions over $x_p = 2p/W$, normalized to σ_{tot}, are shown in Fig. 25 for different values of W.[31,50] They have a characteristic form: as W increases the number of hadrons decreases if $x_p \gtrsim 0.2$ and increases if $x_p \lesssim 0.1$. This behavior is anticipated in QCD because of the logarithmic increase in the probability

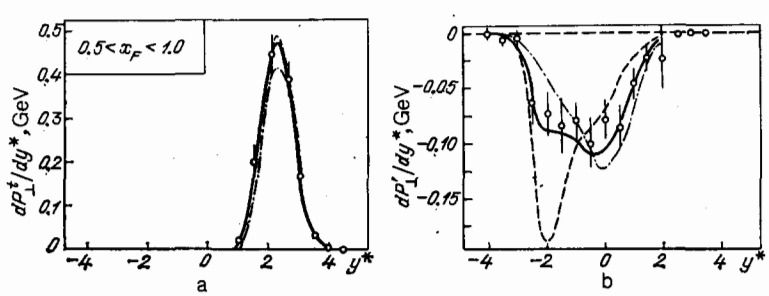

FIG. 23. Rapidity distributions of transverse momentum fluxes of fast hadrons (a) and the particles accompanying them (b) in the center of mass system of the hadrons. The curves were calculated using the Lund model: for the dashed curve ($\langle k_\perp^2\rangle = (0.88\text{ GeV})^2$) the soft gluon emission was neglected; for the solid curve ($\langle k_\perp^2\rangle = (0.44\text{ GeV})^2$) and the dot-dash curve ($\langle k_2\rangle_\perp = 0$) soft gluon emission is included.

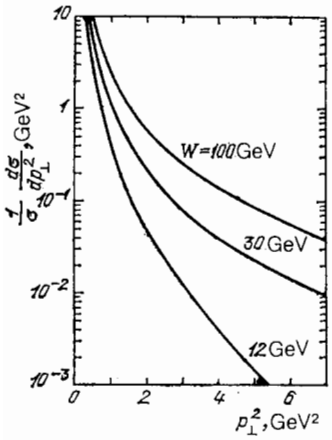

FIG. 24. Distribution of hadrons over $p_\perp^2$ in e^+e^- annihilation, calculated in the CM with $\Lambda = 0.2$ GeV, $t_{cl} = 1.5$ GeV^2, and $W_{min} = 1.25$ GeV for $W = 12$, 30, and 100 GeV.

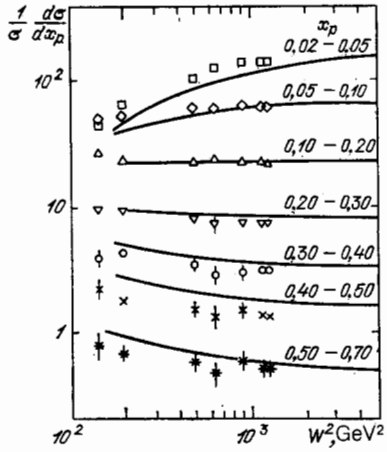

FIG. 26. The curves $(1/\sigma)\, d\sigma/dx_p$ as functions of W in e^+e^- annihilation for different intervals of x_p. The curves were computed using the FF model.

for gluon emission with increasing W (see Sec. 5.1). This effect is more clearly seen in Fig. 26, where the dependences $\langle n(x_p)\rangle = f(W^2)$ are shown for different intervals of x_p. The breakdown of scaling can be expressed quantitatively in the form

$$\frac{1}{\sigma_{tot}}\frac{d\sigma}{dx_p} = c_1\left(1 + c_2 \ln\frac{s}{s_0}\right), \qquad (5.51)$$

where $s_0 = 1$ GeV^2 and c_2 varies from 0.30 ± 0.08 for $x_p = 0.05 - 0.10$ up to 0.84 ± 0.008 for $x_p = 0.4$–0.5.[31] The drop in the cross section for $x_p > 0.3$ is equal to $\approx 25\%$ in the measured interval $W^2 = 144 - 1350$ GeV^2, and is determined primarily by the region of small values $W^2 \lesssim 200$ GeV^2 (see Fig. 26).

An analogous effect was also observed in μp interactions (Fig. 27).[30] The fragmentation function of the u quark decreases with increasing W for $x_F = 0.3$–1.0 and increases for $|x_F| \leqslant 0.3$. The fragmentation of the diquark is independent of the energy for $W \leqslant 20$ GeV. As in the case of $\nu(\bar{\nu})p$ interactions the diquark behaves at the attained energies more passively with respect to gluon emission than the quark.

The phenomenological models satisfactorily describe the longitudinal evolution of the quark jet taking into account the processes $q \to qg$ in QCD PT.[28–31] Here part of the breakdown of scaling (from 5% to 15%) is associated with the masses of the heavy quarks (c, b) and the transverse masses of the hadrons ($m_\perp^2$), especially for $W^2 \lesssim 200$ GeV^2. Hard gluon emission contributes from 5% to 10% for $W^2 \gtrsim 400$ GeV^2. The combination of all these effects explains the observed s dependence in (5.51). The complexity of the pattern of the breakdown of scaling precludes the use of the dependence $D_q^h(x_p, x_\perp, s)$ for making a quantitative check of QCD at existing energies. The situation is analogous to that which also occurs for the structure functions $F(x, Q^2)$ (see Sec. 2.2). Figure 28 shows the values of $s\,d\sigma/dz$ for $s^{1/2} = 12$, 30, and 100 GeV, calculated on the basis of the CM, which also describe well the experimental data.[65,67] It is evident from here that even on the next-generation accelerators (LEP, $s^{1/2} = 100$ GeV) the breakdown of scaling is not

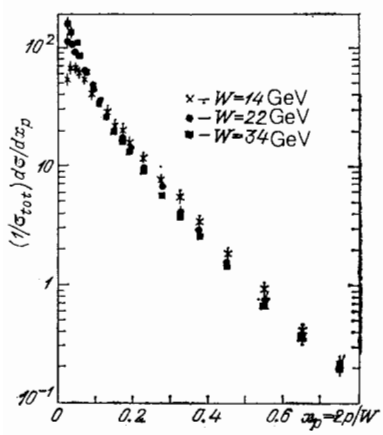

FIG. 25. Distribution of hadrons in e^+e^- annihilation over $x_p = 2p/W$ at $W = 14$, 22, and 34 GeV.

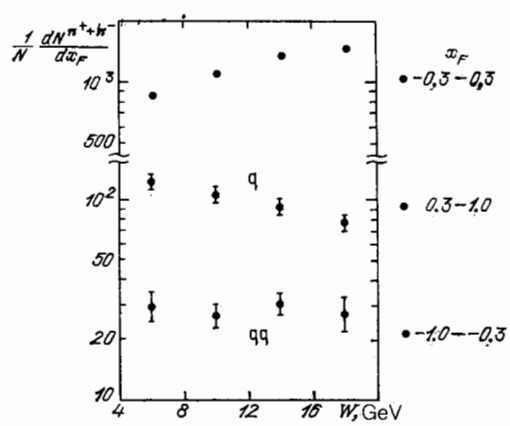

FIG. 27. The dependence of $(1/N)\, dN(\pi^\pm)/dx_F$ on W in μp interactions at $E_\mu = 280$ GeV for different intervals of values of x_F.

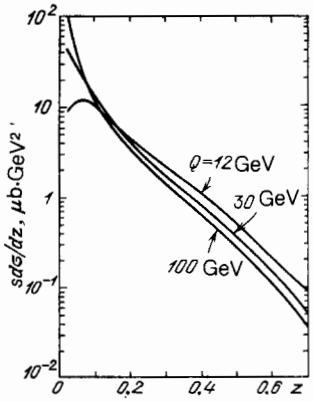

FIG. 28. $sd\sigma/dz$ as a function of z in e^+e^- annihilation at $W = 12$, 30, and 100 GeV. The calculations were carried out in the CM with $\Lambda = 0.2$ GeV, $t_{cl} = 1.5$ GeV^2, and $W_{min} = 1.25$ GeV.

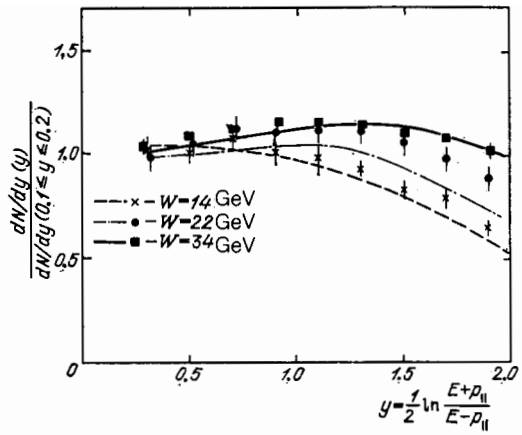

FIG. 30. Rapidity distribution of hadrons in e^+e^- annihilation, normalized to the region $\Delta y = 0.1$–0.2. The curves show the calculations employing the Lund model at $W = 14$, 22, and 34 GeV.

large ($<20\%$) compared with $s^{1/2} = 30$ GeV, where mass effects are no longer important.

The normalized hadron rapidity distributions $(1/\sigma_{tot})(d\sigma/dy)$ relative to the axis of the jet in e^+e^- annihilation are presented in Fig. 29.[31] The width and height of these distributions increase with W ($\sim \ln s$). This is what leads to the growth of the average multiplicity of the hadrons.

In connection with the QCD PT predictions of the unusual form of the hadron spectra as a function of y owing to the interference effect in the emission of soft gluons (see Sec. 5.1), these distributions were carefully studied in Ref. 31. The possible errors in the determination of the axis of the hadron jet and in the identification of the type of particle were taken into account. Figure 30 shows these distributions normalized to the region $y = 0.1$–0.2. The region $y < 0.1$ is excluded from the analysis because of the relatively large systematic errors. From Fig. 30 it is evident that the position of the maximum in the distributions shifts toward larger values of y as W increases. At $W = 34$ GeV $y_{max} \approx 1$ and the hadron yield is $16 \pm 2\%$ higher than in the region $0.1 \leqslant y \leqslant 0.2$, as QCD PT predicts (see Sec. 5.1). However, the LM, taking into account the processes $q \to qg$, but without the interference of soft gluons, gives a qualitative description of the results obtained (solid curve in Fig. 30). The increase in the hadron yield with increasing y is partially associated with the formation and decay of heavy quarks (c, b), which carry most of the energy of the jet (see below). For this reason, the question of the manifestation of interference effects in soft gluon emission (see Sec. 5.1) requires further experimental investigation.[51)]

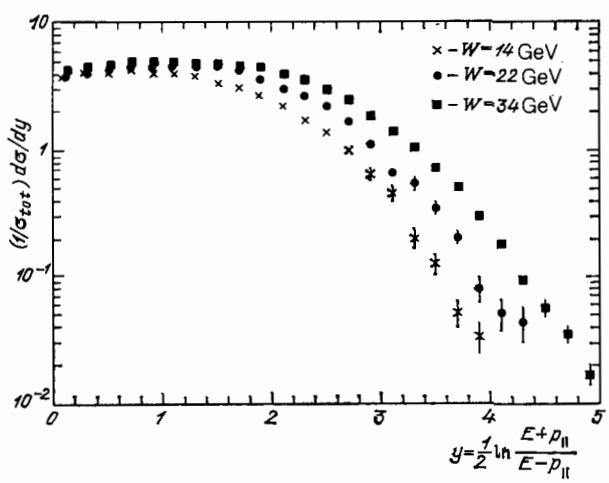

FIG. 29. Rapidity distribution of hadrons in e^+e^- annihilation of $W = 14$, 22, and 24 GeV.

Thus the longitudinal evolution of quark jets, depends not only on the scaling variables, but also on the energy ($D(z, s)$). The scaling breakdown effects are not large, especially in the region $s \gtrsim 400$ GeV^2, and are mainly described by the hard gluon emission (5–10%).

The growth in the number of particles with increasing s is linked with the increase in the yield of slow particles and $\langle n \rangle \sim \ln^2 s$. The functions $D_q^h(s, z)$ for hadrons of a definite type exhibit an analogous behavior.[28–31]

c) Hadronization of light quarks (u, d). As we have already pointed out (formulas (2.40)′ and (2.41)′), neutron experiments enable studying the hadronization of light quarks with a definite flavor. Neglecting the sea quarks (for large $x_B = Q^2/2M\nu$) νp interactions give information on the transformations of u quarks ($x_F > 0$) and (uu) diquarks ($x_F < 0$) into hadrons, while $\bar{\nu}p$ collisions give information on d-quarks and (ud)-diquarks (Fig. 31).[39] As is evident from the figure, at $W = 3$–10 GeV the isotopic equalities

$$D_{u\to\pi^+}^{(\nu p)}(x_F) = D_{d\to\pi^-}^{(\bar{\nu}p)}(x_F); \quad D_{u\to\pi^-}^{(\nu p)}(x_F) = D_{d\to\pi^+}^{(\bar{\nu}p)}(x_F) \qquad (5.52)$$

hold well. The difference between $D_{u\to\pi^+}^{(\nu p)}(x_F)$ and $D_{u\to\pi^-}^{(\nu p)}(x_F)$ yields an estimate of the probability that the leading meson ($x_F(\pi^+) \gtrsim 0.5$) has as a constituent the starting quark $u(\pi^+(\bar{u}d), \pi^-(\bar{u}d))$. This probability turns out to be high ($\approx 0.7 - 0.8$), but the relative fraction of such events is small. Analogous estimates were also made for e^+e^- annihilation processes.[30,31] It was found that a hadron with $y \sim y_{max}$ has with a probability exceeding 60% the charge of the initial quark. Thus fast hadrons in the jet carry

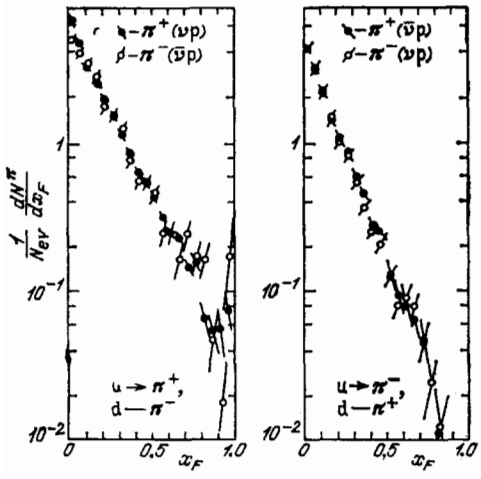

FIG. 31. Distributions of $\pi^{\pm}$ mesons in $\nu(\bar{\nu})$p interactions as functions of x_F.

information about the parent quark, which is what makes it possible to measure its quantum numbers (see Sec. 4).

Data on the fragmentation of diquarks were obtained in the same experiments.[39] They turned out to be different from $D_q(x_F)$:

$$D(uu) \neq 2D(u),$$
$$D(ud) \neq D(u) + D(d), \tag{5.53}$$

i.e., the fragmentation of diquarks is not an incoherent sum of the fragmentation of their constituent quarks. Actually $D(ud) < D(u)$ and $D(d)$. Thus at existing energies the diquark forms fewer hadrons than a quark, which is what gives rise to the scaling behavior of $D^h_{(qq)}(x_\perp, x_F)$ (see Figs. 22 and 27). This probably occurs because of its large mass ($M(qq) \approx M_N$), as also in the case of heavy quarks.

In conclusion we note that the results presented were obtained at relatively low energies ($W \lesssim 10$ GeV), where the separation of jets from q and (qq) is not distinct. It is therefore of great interest to perform analogous experiments with quasimonochromatic $\nu(\bar{\nu})$ beams with $W \geqslant 10$ GeV.

d) Hadronization of heavy quarks (c, b). The observation of decays of heavy c and b quarks in e^+e^- annihilation makes it possible to identify the starting quark, since the formation of sea $(c\bar{c})$ and $(b\bar{b})$ pairs is negligibly small. The following methods for the separation of the production of c and b quarks were employed in experiments of Refs. 28, 30, 70:

1) detection of the decays of charmed mesons:

$$D^+ \to K^-\pi^+\pi^+;\ D^0 \to K^-\pi^+; \tag{5.54}$$
$$D^{*\pm} \to D^0\pi^\pm,\ D^0 \to K^-\pi^+,\ K^-\rho^+; \tag{5.55}$$

by means of the observation of peaks in the spectra of the effective masses in $(K-\pi^+)$, $(K-\pi^+\pi^+)$ and $(K-\rho^+\pi^\pm)$ systems;

2) detection of weak semileptonic decays:

$$c \to qe\nu,\quad q\mu\nu; \tag{5.56}$$
$$b \to qe\nu,\quad q\mu\nu. \tag{5.57}$$

In this case the large masses of the quarks gives rise to larger values of $p_\perp(l)$ ($\gtrsim 1$ GeV) relative to the axis of the jet than that for the background decays of light quarks ($p_\perp(l) \lesssim 0.5$ GeV), which is what makes it possible to obtain data on $D_c(z)$ and $D_b(z)$.[52] The main result of these experiments lies in the fact that in the fragmentation of heavy quarks the main fraction of their energy ($z = 2E_h/s^{1/2}$) is transferred to the hadrons containing c and b quarks[30,70]:

$$\langle z_c \rangle = 0{,}57 \pm 0.02, \tag{5.58}$$
$$\langle z_b \rangle = 0{,}75 \pm 0.03. \tag{5.59}$$

Within the limits of experimental error ($\lesssim 20\%$) the data on $D^h_{c,b}(z)$ are described by the expression (5.34) with $\varepsilon_c \sim 0.20$ and $\varepsilon_b \sim 0.02(\varepsilon_b \sim \varepsilon_c\, m_c^2/m_b^2)$. As a result c and b mesons for $z \gtrsim 0.4$ are indicators of the flavors of the primary (c, b) quarks in e^+e^- annihilation, which makes it possible to study their hadronization.

The distributions of $D^{*\pm}$ mesons over $p_\perp^2$ relative to the axis of the jet were studied in experiments on the JADE and TASSO installations.[70-72] They are satisfactorily described by a Gaussian distribution with $\sigma_c = 0.36 \pm 0.2 \pm 0.04$ GeV, which coincides with the analogous results for all charged particles and with the description of the hadron $p_\perp^2$ distributions in the FFM (5.24).[53]

In addition, the separated $D^{*\pm}$ mesons were used as a "trigger" for hadron jets from the c quarks in the opposite hemisphere. The study of their distributions over y, $p_\perp^2$, z, S, and T showed that there are no significant differences from hadron jets formed in e^+e^- annihilation by all quarks with the same energy ($W = 34.4$ GeV). Of course, the number of events in the statistical sample (~ 100) is still too small to draw definite conclusions, but the general characteristics of the jets of long-lived hadrons (π, K, N) are apparently virtually independent of the quark flavors.

On the whole the hadronization of heavy quarks occurs differently than that of the light quarks because of their large mass. For example, the energy lost by a c(b) quark to gluon emission is lower than for u(d) quarks. It is for this reason that the distinct effect of leading of c(b) mesons, kinematically reminiscent of the leading of baryons in hN collisions, appears. An analogous effect also occurs in the hadronization of diquarks. Because of this jets of quarks and antiquarks and jets of gluons and quarks can be separated on the basis of the c(b) particles. All this opens up new experimental possibilities for checking QCD and the structure of the theory of electroweak interactions for heavy quarks.[11,70-72] This, however, requires that the size of the statistical sample of events with c(b) particles be substantially increased.

5.2.2. Correlation and compensation of the quantum numbers of secondary hadrons

The study of the usual correlations of the type (2.13) for long-lived charged hadrons (π, K) in the rapidities, transverse momenta, and azimuthal angles relative to the axis of the jets in e^+e^- annihilation showed that they are of short range, as in the case of soft hadronic collisions (see Sec. 2.1).[28] This is largely explained by the copious production of resonances, decaying into π and K mesons.[5,6] The parton

model (FFM) successfully describes these phenomena.[28,50]

The Δy (or Δx_F) intervals of compensation of the charge, strangeness, baryon number, and other quantum numbers of hadrons are of great interest. This is associated both with the dynamics of hadronization and the possibility of determining the quantum numbers of primary quarks (see Sec. 4). In models the compensation of the quantum numbers of hadrons is assumed to be local because of the formation of sea ($q_{Ns}\,q_s$) pairs with zero quantum numbers, with the exception of the leading hadrons.[58,62,67]

The charge correlations of secondary hadrons with respect to rapidities have been studied in detail in e^+e^- annihilation at $W = 34$ GeV.[28,31,50] In addition to the short-range correlations with $L(\Delta y) \approx 1.5$, associated with the creation of resonances, long-range correlations between the leading hadrons ($y_1 < -2.5$ and $y_2 > 1$; $y_{max} \approx 5$) have been observed. The probability that the charge of a particle with $y_1 < -2.5$ is compensated by the charge of a particle with $y_2 > 1$ in the opposite jet is equal to $15.4 \pm 2.6\%$. These results are described by the FFM.[50] Thus the leading hadrons "remember" the charge of the parent quark. Analogous data were obtained in νp and μp interactions; this is what enabled the evaluation of the charges of quarks (see Sec. 4).

The observation of the copious production of (BB) pairs in e^+e^- annihilation shows that the transitions $q \to B$ are a significant feature of their hadronization. For example, at $W = 34$ GeV on the average 0.8 ± 0.1 ($p\bar{p}$) pairs form per event.[31] The production of ($B\bar{B}$) pairs is usually linked with the formation of sea diquarks: ($q_s\,q_s$) and ($\bar{q}_s\,\bar{q}_s$), which are "attached" to the quark (antiquark).[28–31,58,62] In this case short-range correlations between baryons and antibaryons with $L(\Delta y) \lesssim 2$ should be expected. At the present time we have only the first estimates of the number of ($p\bar{p}$) pairs (15.5 ± 4.5) formed in the same jet and the number of pairs formed (1.2 ± 2.6) when p and $\bar{p}$ occur in different jets.[31,54] They support the adopted scheme for the formation of baryons. Analogous results were obtained in μp interactions.[68,69] The fragmentation of the u quark into p and $\bar{p}$ was studied. It turned out that the average rapidity interval between them is $\langle |y_p - y_{\bar{p}}| \rangle \approx 0.7$.

The correlation and intervals of compensation of the quantum numbers of secondary hadrons have been intensively studied in hard pp collisions:

$$p + p \to c_{tr}\,(p_\perp) + X \qquad (2.44')$$

at $s^{1/2} = 45$ and 63 GeV.[32,73,74] In this case the parton scheme of these processes (see Fig. 4) predicts the formation of two hadron jets with $\vartheta \sim 90°$ as a result of the hadronization of strongly scattered partons. Separation of the process (2.44') on the basis of c_{tr} ($p_\perp$) yields a sample of events in which a leading particle (c_{tr}) occurs. As a result of the study of the processes (2.44) with different types of trigger particles ($\pi^\pm$, π^0, $K^\pm$, η^0) it was established that

1) for $x_\perp = \frac{2p_\perp}{s^{1/2}} \gtrsim 0.3$ we have the ratio $\frac{N(\pi^+_{tr})}{N(\pi^-_{tr})} = 2.0 \pm 0.3$, which corresponds to the ratio u/d = 2 in the starting protons and

2) for $x_\perp$ in the interval 0.1–0.3 the ratios assume the following values:

$$\frac{N(K^+_{tr})}{N(\pi^+_{tr})} = 0.45 \pm 0.03, \qquad (5.60)$$

$$\frac{N(\eta^0_{tr})}{N(\pi^0_{tr})} = 0.46 \pm 0.02\,. \qquad (5.61)$$

They are independent of $s^{1/2}$, $x_\perp$ and ϑ. From here is may be concluded that the leading (trigger) particles ($x_\perp \gtrsim 0.3$), which have as constituents the same quarks as the starting hadrons (p(uud), $\pi^+(u\bar{d})$, $\pi^-(\bar{u}d)$), reflect the quark composition of the latter (u/d = 2).[55] The constancy of the ratios (5.60) and (5.61) indicates that the "attachment" of a sea antiquark ($\bar{u}, \bar{d}, \bar{s}$) to the scattered u or d quark does not depend on the variables indicated above. The charge of the leading particles is compensated in small intervals $y(L(\Delta y) \approx 2)$.[73,74] Other features of the correlation phenomena in hard hadronic collisions are similar to those which have already been studied in soft interactions of hadrons (see Sec. 2.1) and e^+e^- annihilation.[5,32,73,74] They are well described by the phenomenological models (FFM and LM). Thus the first results on correlation phenomena in hard collisions of particles at high energies have confirmed the two basic assumptions of the parton picture of these interactions:

1) The short-range correlations are linked primarily either with the formation and decay of resonances for the long-lived particles (π, K, p) or with the formation of sea pairs of quarks ($q_s\bar{q}_s$) and diquarks ($q_s\bar{q}_s$, $\bar{q}_s\bar{q}_s$) for the primary hadrons.

2) The leading particles retain the quantum numbers of the parent quark. These features of the hadronization of quarks are similar to those already established in soft collisions of hadrons and employed in the construction of the models (see Sec. 2.1).

5.2.3. Multiplicity and composition of hadrons

The average multiplicity of charged hadrons ($\langle n_{ch} \rangle$) in jets increases with the energy as $\sim \ln^2 s$. This is associated with the growth in the height ($\sim \ln s$) and width ($\sim \ln s$) of the plateau in the distribution $(1/\sigma)(d\sigma/dy)$ (see Fig. 29). As can be seen from the hadron momentum distributions (see Figs. 25, 26, 27, and 29), this growth of $\langle n_{ch} \rangle$ is associated with the increase in the number of relatively slow hadrons with $x_F \lesssim 0.2$–0.3, which is the cause of the difficulty in determining $\langle n_{ch} \rangle$ in $p\bar{p}$ interactions (see Sec. 3, Fig. 10).

In principle, $\langle n_{ch} \rangle$ is measured most accurately in e^+e^- annihilation, where there is no soft background. Even in this case, however, the disagreement between $\langle n_{ch} \rangle$ at $W = 30$–40 GeV, measured by different groups, reaches 5–10%.[31,75] This is attributable primarily to the inadequacies of the method and the detection of all secondary hadrons. The total correction for this is equal to $\approx 10\%$ and is determined with the help of the phenomenological models (LM and FFM). In addition, in some of the articles corrections for the decays $K^0_S \to \pi^+\pi^-$ and $\Lambda^0 \to \pi^-p$ were not introduced, which precludes a direct comparison of these data with the results obtained in lN and hN interactions.[76] For this reason the analysis of the dependence of $\langle n_{ch} \rangle$ on s must

TABLE II. Values of the parameters a, b, and c for various approximations to $\langle n_{ch}\rangle(s)\rangle$.

Type of approximation	a	b	c	$\chi^2/N_{d.o.f.}$
(5.62)	1,4±0.1	1,18±0,03	—	260/80
(5.63)	3,33±0,11	−0,40±0,08	0.26±0,11	85/79
(5.64)	2.71±0.08	0,058±0,010	1.97±0,06	81/79

take into account these circumstances, allowing for possible systematic errors of 5–10%.

The usual analytical approximations of $\langle n_{ch}\rangle$ have the form[31,75]:

$$\langle n_{ch}\rangle = a + b\ln s, \tag{5.62}$$

$$\langle n_{ch}\rangle = a + b\ln s + c\ln^2 s, \tag{5.63}$$

$$\langle n_{ch}\rangle = a + b\exp\left[c\left(\ln\frac{s}{Q_0^2}\right)^{1/4}\right], \tag{5.64}$$

where a, b, and c are free parameters and $Q_0 = 1$ GeV. The results of the approximations (5.62)–(5.64) of the existing data on e^+e^- annihilation are presented in Table II (Fig. 32).[56] It is evident from here that the FFM (5.62) does not describe $\langle n(s)\rangle$ in the interval $s^{1/2} = W = 2 - 41.5$ GeV.[31] For $W \gtrsim 8$–10 GeV, however, the dependence (5.62) is in agreement with experiment. We also point out that the LM and CM describe $\langle n(s)\rangle$ well in the entire energy interval. Because of this it is still early to talk about the rapid growth of $\langle n(s)\rangle$ in accordance with the predictions of QCD PT (5.64).[76,57] Figure 32 also shows measurements of $\langle n_{ch}(W)\rangle$ for soft pp and $p\bar{p}$ interactions, where $W = s_{pp}^{1/2}$. As we shall see below (see Sec. 5.4), taking into account the effect of the leading particles gives $\langle n_{ch}(W)\rangle$ which is in agreement with the data on e^+e^- annihilation.

It is of interest to compare $\langle n_{ch}(s)\rangle$ obtained in e^+e^- annihilation ($s^{1/2} \leqslant 41.5$ GeV) and in hadron jets from $p\bar{p}$ interactions ($s^{1/2} = 540$ GeV). As we have already pointed out, the background of soft collisions in $p\bar{p}$ interactions is significant in determining $\langle n_{ch}(J)\rangle$ (Fig. 10). If it is assumed that this background has an isotropic distribution in the azimuthal plane relative to the axis of the jet, then the values obtained for $\langle n_{ch}(J)\rangle$ continue one another quite well (Fig. 3a).[36–38,66] If the background is taken into account with the help of the fragmentation models, then the data from the UA1 and UA2 experiments contradict one another.[30] Figure 33b presents data on $\langle n_{ch}(J)\rangle$ obtained in e^+e^- annihilation and on the UA2 installation.[37] The theoretical curves for the quark and gluon hadron jets, calculated on the basis of CM, are also presented here.[66] As is evident from the figure, they are consistent with experiment, if it is assumed that gluon jets form in $p\bar{p}$ interactions, while quark jets are primarily formed in e^+e^- annihilation. It can be expected that more accurate data for $s^{1/2} \gtrsim 50$–100 GeV will be obtained on the new generation of accelerators (1986–1990).

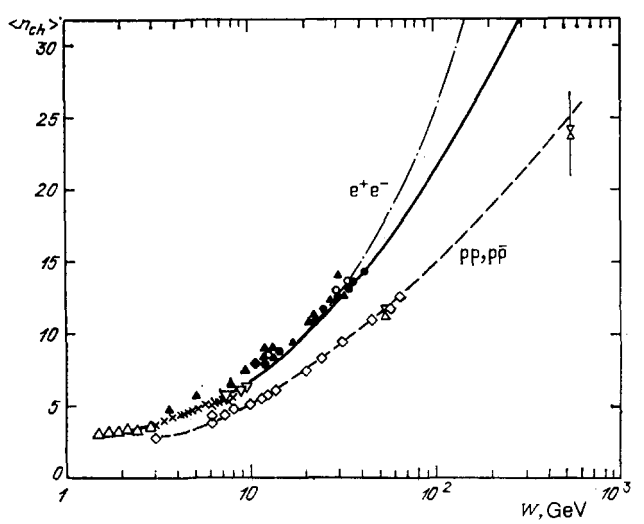

FIG. 32. $\langle n_{ch}\rangle$ as a function of W in e^+e^- annihilation and in $pp(\bar{p}p)$ interactions (dashed curve). The solid curve shows the dependence (5.63) and the dot-dashed curve shows the dependence (5.64).

The variance

$$D = (\langle n_{ch}^2\rangle - \langle n_{ch}\rangle^2)^{1/2} \approx \frac{1}{3}\langle n_{ch}\rangle \tag{5.65}$$

of the multiplicity distribution of charged hadrons ($P(n_{ch})$) in e^+e^- annihilation differs from the Poisson distribution ($D = a\langle n_{ch}\rangle^{1/2}$), which indicates the existence of long-range correlations.[31,75] The distribution $P(n_{ch})$ itself satisfies KNO scaling[77]:

$$P(n_{ch})\langle n_{ch}\rangle = \psi\left(\frac{n_{ch}}{\langle n_{ch}\rangle}\right), \tag{5.66}$$

with $W = 7.5$–34 GeV, for both the full multiplicity in the event and the multiplicity $n_{ch}(J)$ in one hemisphere relative to the axis of the jet (Fig. 34).[30,31,75] Moreover there is virtually no correlation of the multiplicities between the particles from different hemispheres.[28–31] Therefore the long-range multiplicity correlations in jets are explained by the fluctuation of the small numbers n_g (the numbers of hard gluons), giving rise to fluctuations of large numbers n_{ch}.[78] This is a general property of branching processes, which probably explains the mechanism of KNO scaling.

The composition of the long-lived hadrons ($\pi^\pm$, $K^\pm$, $p,\bar{p}$) in e^+e^- annihilation at $W = 34$ GeV is shown in Fig. 35 as a function of the momentum.[30] As is evident from the figure, the relative fraction of $\pi^\pm$ mesons decreases from $\approx 100\%$ at $p = 0.3$ GeV to $\approx 50\%$ at $p = 10$ GeV. Analogous behavior of the composition of hadron jets was also observed in hard pp interactions. Most pions are products of the decay of resonances. The average multiplic-

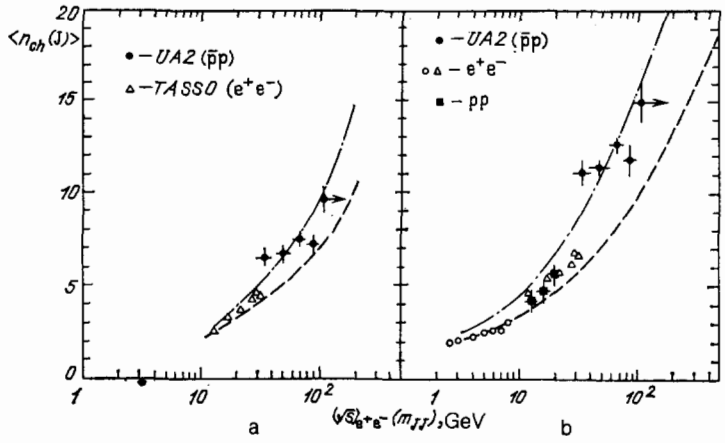

FIG. 33. $\langle n_{ch}(J)\rangle$ as a function of $s^{1/2}_{e^+e^-}$ (or m_{jj}). The dashed curves show the calculations using the CM for quark jets and the dot-dashed curves show the calculations for gluon jets. a) Isotropic background, b) background included according to the LM.

ities $\langle n_i\rangle$ grow with the energy, but their ratios remain virtually constant in the interval $W = 10$–35 GeV (Fig. 36). The average number of particles $\langle n_i\rangle$ of different type at $W = 34$ GeV is presented in Table III.[30] Under the assumption that $\langle n(\rho^0)\rangle = \langle n(\rho^+)\rangle = \langle n(\rho^-)\rangle = \langle n(\omega^0)\rangle$, several conclusions can be drawn from Table III.

1. The total number of secondary hadrons is $\langle n_{tot}\rangle \approx 21$, from which $\langle n_{ch}\rangle \approx 13$.

2. About 90% of all pions are the products of the decays of resonances or weak decays of particles.

3. About 9–10 hadrons are primary hadrons, i.e., ~ 1.3 hadrons per unit rapidity interval. The remaining hadrons are formed as a result of their decays.

4. Approximately eight to nine sea $(q_s\bar{q}_s)$ pairs are required in order to produce these primary hadrons.

5. The suppression factor (γ_s) for the formation of sea $(s\bar{s})$ pairs is equal to $\gamma_s \approx 0.3$–0.4.

6. The ratio of the number of primary pseudoscalar mesons to vector mesons is $N(PS)/N(V) \approx 0.7$.

These conclusions correspond to the parameters of the phenomenological models which describe the composition and multiplicity of hadrons in hard processes.[5,58,62,64–67] More detailed data on $\langle n_i\rangle$ are given in Refs. 31, 70, and 75. The characteristics presented are practically identical for different types of hard processes with the same energies $E(J)$.[5,13]

In concluding this section on the hadronization of quarks we point out the most important results.

1. The evolution of a quark jet of hadrons along $x_\perp$ and x_F with increasing energy is in agreement with QCD PT and occurs owing to the gluon bremsstrahlung.

2. Hard gluon bremsstrahlung from quarks has been observed in e^+e^- annihilation processes at $W \gtrsim 30$ GeV and is equal to 5 to 10%.

3. The first indications of effects associated with the emission of soft gluons were obtained in deep-inelastic μp interactions.

4. The fragmentation functions for light (u, d) quarks were studied in $\nu(\bar{\nu})p$ interactions and the isotopic ratios between them were verified.

5. The first data on $D^h_{c,b}(z)$ for heavy quarks have been obtained and the effect of their leading has been observed.

6. The correlations of the quantum numbers of secondary hadrons are primarily of a short-range nature $(L(\Delta y) \approx 1.5$–$2)$. Long-range correlations associated with the charges of the initial quarks have also been observed.

7. It has been established in hard processes that the leading hadrons with $x_F \gtrsim 0.3$–0.4 retain the initial quark, which enables the measurement of its quantum numbers.

8. The average multiplicity of the secondary hadrons increases and is practically the same for different types of hard processes (μp, $\nu(\bar{\nu})p$, pp and e^+e^-).

9. The composition of primary particles is also approximately the same in hard processes. Pions and K mesons are primarily the products of the decays of primary hadrons.

10. The parton model (FFM) and the Lund model on

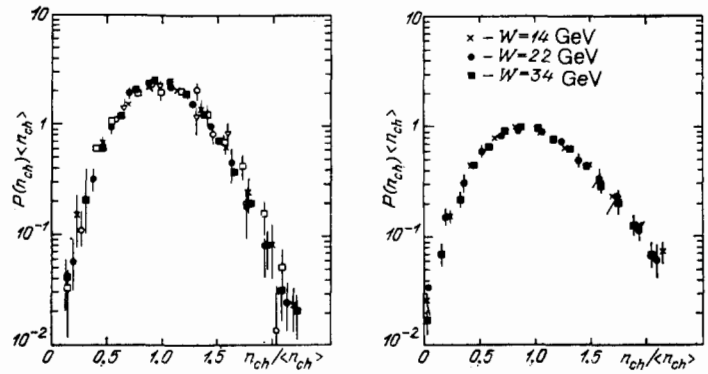

FIG. 34. a) KNO distribution for e^+e^- annihilation processes at $W = 7.4$–34 GeV. b) KNO distribution for one hadron jet in e^+e^- annihilation at $W = 14$, 22, and 34 GeV.

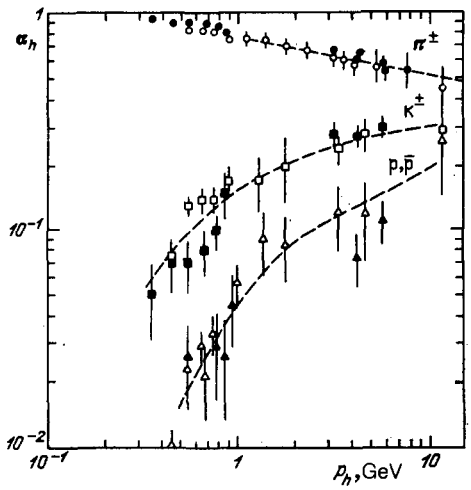

FIG. 35. Relative fraction (α_h) of hadrons ($\pi^\pm$, $K^\pm$, p, $\bar{p}$) as a function of their momentum in e^+e^- annihilation at $W = 34$ GeV. The curves were drawn in by hand.

the whole satisfactorily describe the studied characteristics of hard processes.[58] A new class of models (CM) also describe these data well without the introduction of the parton transverse momentum limitation and fragmentation functions. All these models employ QCD PT to describe the initial stage of the hard processes.

5.3. Gluon hadron jets

The basic characteristics of gluon hadron jets (compared with quark jets) are associated with the quantum numbers of the gluons ($Q = B = S = C = 0$) and their high color charge (see Sec. 5.1).[11,66,78-80] For this reason, a large number of isoscalar neutral particles (η, η', φ), $B\bar{B}$ pairs, and strange and charmed particles should be expected in gluon jets. Because of the large color charge of gluons the

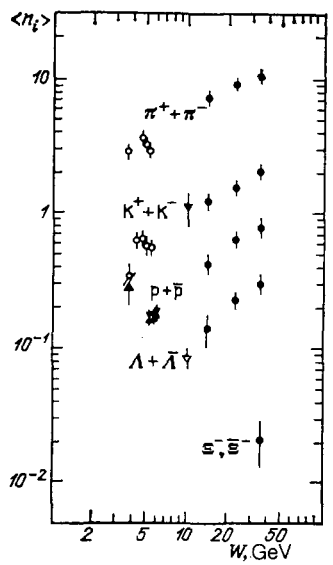

FIG. 36. Average multiplicities $\langle n_i \rangle$ of secondary hadrons in e^+e^- annihilation as a function of W.

TABLE III. Values of $\langle n_i \rangle$ in e^+e^- annihilation at $W = 34$ GeV.

Type of particle	$\langle n_i \rangle$	Type of particle	$\langle n_i \rangle$
π^+	10,3±0,4	ω	—
π^0	6,0±0,5	φ	$\sim 0{,}08$
K±	2,0±0,2	Δ^{++}	$\lesssim 0{,}1$
K^0, $\bar{K}^0$	1,48±0,10	$\Sigma^{*\pm}$	$\lesssim 0.09$
η^0	0,72±0,20	$D^{*\pm}$	~ 0.3
$\rho^\pm$		p, $\bar{p}$	0.8±0.1
ρ^0	0,98±0,10	Λ, $\bar{\Lambda}$	0.31±0,03
$K^{*\pm}$	0,87±0.20	Ξ^-, $\bar{\Xi}^-$	0,026±0.008
K^{*0}, $\bar{K}^{*0}$	0,8±0,1		

ratio of the probabilities of the processes is

$$\frac{W(g \to gg)}{W(q \to qg)} = \frac{9}{4}, \tag{5.67}$$

and this is responsible for the fact that the parton shower appears in gluonic jets earlier than in quark jets and for the asymptotic ratio of their multiplicities is 9/4 (5.13).

At finite energies ($s^{1/2} \lesssim 540$ GeV) the characteristics of gluon jets were obtained on the basis of CM using only three parameters:

$$\Lambda = 0.25 \text{ GeV}, \; Q_0 = 0.6 \text{ GeV}, \; M_f = 4 \text{ GeV}, \tag{5.68}$$

where M_f is the maximum mass of the colorless cluster.[66] These parameters were determined from an analysis of quark jets in e^+e^- annihilation. An attractive feature of these calculations is that new parameters were not introduced. The largest difference between the quark and gluon jets occurs because of (5.67) and is reflected in the hadron distributions over the multiplicity, rapidity, and transverse momentum, as well as in characteristics of the jets such as S and T (see Sec. 3).[66]

The data on $\langle n_{ch}(s) \rangle$ are consistent with the large contribution of gluon jets at $\bar{p}p$-collider energies (see Fig. 33). The ratio of the average multiplicities at $s^{1/2} = 100$ GeV constitutes

$$\frac{\langle n_g \rangle}{\langle n_q \rangle} \approx 1.8, \tag{5.69}$$

which is associated with the large preasymptotic corrections. The asymptotic limit (5.13) is reached slowly[66]:

$$\frac{\langle n_g \rangle}{\langle n_q \rangle} = \frac{9}{4} - 1.28 \left(\ln \frac{E_J}{\Lambda} \right)^{-1/2}. \tag{5.70}$$

Distributions of the KNO-scaling type (see Fig. 34) for gluon jets are expected to be narrower than for quark jets:

$$\left(\frac{\langle n \rangle}{D} \right)_{qq} \left(\frac{\langle n \rangle}{D} \right)_{gg}^{-1} \xrightarrow[s \to \infty]{} \frac{2}{3}, \tag{5.71}$$

because of their higher multiplicity.

Gluon jets of hadrons have higher average values $\langle S \rangle$ and $\langle 1 - T \rangle$, $\langle p_{lin} \rangle$ and $\langle p_{lout} \rangle$ than quark jets for the same values of $E(J)$, and this served as the basis for the separation of the processes q→qg (see Fig. 17). All this is determined by the intense emission of gluons (5.7) and, as a result, by the wider angular distribution of the hadrons in gluon jets than in quark jets.

5.3.1. Gluon jets in e^+e^- annihilation

Some characteristics of gluon jets have been studied experimentally and compared with quark jets for e^+e^- annihilation at $W = 14.22$ and 29–36.4 GeV.[30,81,82] At high energies ($W \geqslant 29$ GeV) three-jet events were separated with the help of the thrust (T) and triplicity (T_3):

$$e^+ + e^- \to q + \bar{q} + g \to J_1(E_1^J) + J_2(E_2^J) + J_3(E_3^J), \quad (2.56)$$

where $E_1^J > E_2^J > E_3^J$ (see Sec. 3).[81,82] With the help of the FFM and the LM it was found that for $E_J = 6 - 10$ GeV the percentage of gluon jets is equal to 25% for E_2^J and 50% for E_3^J. Data on e^+e^- annihilation for $W = 14$ and 22 GeV were used to obtain the characteristics of quark jets for $E_J = 7$ and 11 GeV under identical experimental conditions. The following results were obtained:

$$r_{32} = \frac{\langle p_\perp(h)\rangle_{J=3}}{\langle p_\perp(h)\rangle_{J=2}} = 1.16 \pm 0.02, \quad (5.72)$$

$$l_{32} = \frac{\langle p_{\perp\text{out}}(h)\rangle_{J=3}}{\langle p_{\perp\text{out}}(h)\rangle_{J=2}} = 1.16 \pm 0.02, \quad (5.73)$$

with $E^J = 6$–10 GeV.[82] Comparison of the average hadron multiplicities ($\langle n_i^J \rangle$) and hadron distributions over $x_\parallel^J$ in different jets (2.56) showed that for $E_3^J = 6$–10 GeV the values of $\langle n_3^J(h)\rangle$ are 5–10% higher and $\langle x_\parallel^J\rangle$ is somewhat lower than in quark jets with the same energy (E^J). The LM and CM describe these data better than the FFM; this is attributable to the effect of the gluon radiation on the momentum characteristics of the quarks (see Sec. 5). Taking into account the interference of gluons in the processes (2.56) reduces the multiplicity of the hadrons between the "quark" jets (E_1^J and E_2^J) below that of the two other extra-jet regions (E_1^J and E_3^J; E_2^J and E_3^J) (see Fig. 18b).[11] This effect is called the "string effect" and was discovered in experiments on the JADE and TPC installations.[81,82] It is described well by the LM and CM, in which the coherence of gluon radiation is taken into account, and contradicts the predictions of the FFM, where independent fragmentation of partons is assumed. On the whole these results confirm only qualitatively the expected features of gluon jets. This is attributable to the model-dependent methods employed to determine the gluon jet in the events (2.56) and the relatively low values of E_g^J, which are responsible for the low magnitudes of the observed effects. For $W \gtrsim 100$ GeV these problems will be less significant.

The composition of gluon jets of hadrons were studied in the decays

$$\Upsilon \to ggg, \quad (5.74)$$

and in events of the type (2.56).[28,30,31,50,83] Comparison of the average multiplicities of ($p\bar{p}$) and ($\Lambda\bar{\Lambda}$) pairs in the decays (5.74) and in the regions outside the resonance ($e^+e^- \to q\bar{q}$) shows that $\langle n(B\bar{B})\rangle$ is two times higher in gluon jets than in quark jets (Table IV). At the same time, within the limits of error of the experiment ($\pm$ 10%), $\langle n_{ch}\rangle$ and $\langle n(K^\pm)\rangle$ do not differ from one another.

To obtain indirect data on the composition of a gluon jet of hadrons the formation of ($\Lambda\bar{\Lambda}$) pairs in the events (2.56) at $W = 34$ GeV was studied.[30,31] It turned out that

TABLE IV. Values of $\langle n_i\rangle$ in the decays $\Upsilon \to 3g$.

Installation	Type of particle	$\frac{\Upsilon \to 3g}{\langle n_i\rangle}$	$\frac{\text{outside}}{\langle n_i\rangle}$
DASP-II	$p, \bar{p}$	0,64±0,16	0,10±0,06
CLEO	$p, \bar{p}$	0,55±0,05	0.27±0,02
CLEO	$\Lambda, \bar{\Lambda}$	0,19±0,01	0,080±0,008

$\langle n(\Lambda\bar{\Lambda})\rangle = 0.59 \pm 0.12$, while in two-jet events ($e^+e^- \to q\bar{q}$)—$\langle n(\Lambda\bar{\Lambda})\rangle = 0.32 \pm 0.04$. Analogous results on the yield of $p(\bar{p})$ were obtained in deep-inelastic μp interactions with $E_\mu = 280$ GeV ($W^2 \geqslant 200$ GeV^2).[69] Thus experiments at $W \leqslant 40$ GeV show that the yield of baryons in gluon jets is higher than in quark jets. So far there are no accurate data on the formation of K mesons and neutral isoscalar particles (η, η', φ).[30,31]

The characteristics of the events (2.56) have been analyzed in detail in the last three years in order to measure the strong interaction constant $\alpha_s(Q^2)$ (2.52). Indeed, the cross section of the process (2.56) is proportional to $\alpha_s(Q^2)$ and it is therefore in principle possible to measure $\alpha_s(Q^2)$ accurately. Because there is no theory of parton hadronization, however, phenomenological models must be used to separate and analyze the events (2.56) (see Sec. 5.1).[29,30,84]

Data on the processes (2.56) at $\langle W\rangle = 35$ GeV were obtained with the help of four large experimental installations: JADE, TASSO, CELLO, and MARK-J.[30] They were analyzed with the help of QCD PT taking into account second-order diagrams in $\alpha_s(O(\alpha_s^2))$. The parton hadronization stage was described by phenomenological models: FFM, LM, and CM (see Sec. 5.1). As a result the values of $\alpha_s(Q^2)$ obtained turned out to depend on the type of model (Table V). As we have already pointed out (see Sec. 5.1), the assumption of independent emission of gluons in the FFM gives rise to the fact that $\alpha_s(\text{FFM}) < \alpha_s(\text{LM})$, as is evident from Table V. The measured values of $\alpha_s(Q^2)$ vary from 0.12 ± 0.02 (MARK-J) up to 0.210 ± 0.051 (TASSO) depending on the type of hadronization model and the experimental data obtained. These data are consistent with the values of $\alpha_s(Q^2)$ obtained from an analysis of the evolution of the structure functions of nucleons and the total cross sections for e^+e^- annihilation ($\langle\alpha_s(Q^2)\rangle = 0.19 \pm 0.06$) (see Sec. 4.4).[29] At the same time the mea-

TABLE V. Values of $\alpha_s(Q^2)$ at $Q^2 \approx 1200$ GeV^2.*

Installation	FFM	LM
JADE	0,12±0,02	0,16±0,03
TASSO	0,160±0,015	0,21±0.015
CELLO	0,135±0,025	0,19±0.02
MARK-J	0,12±0,02	0.14±0,02

*The total error in the measurements (systematic plus random) is shown.

surement of the processes (2.56), whose cross section is $\sim\alpha_s(Q^2)$, motivates theoreticians and experimenters to obtain more accurate data on $\alpha_s(Q^2)$. In this connection we call attention to the work performed by the TASSO group, in which the most complete analysis of this process was performed.[84] A record statistical sample on e^+e^- annihilation at $\langle W\rangle = 34.6$ GeV ($\approx 16\,500$ events) was collected on this installation. In the analysis of the experimental data different variants of calculations based on QCD PT and the FFM, LM, and CM with different values of their free parameters were employed. To determine $\alpha_s(Q^2)$ three experimental hadron distributions in four variants were compared at the same time with the calculations. To this end 4000 events were modeled for each set of $\alpha_s(Q^2)$ and model parameters employed. A total of $4\times4\times4$ variants of the free parameters for the chosen model of parton hadronization was used. The following results were obtained by this analysis.[84]:

1. Fitting of hadron distributions over different kinematic variables yields values of α_s which differ by 15–20%.

2. The variation of $\alpha_s(Q^2)$ as a function of the hadronization model used (FFM and LM) reaches $\approx 30\%$.

3. Uncertainties in taking into account the emission of soft gluons by partons in QCD PT calculations lead to errors of 10–15%.

4. Taking these uncertainties in the data analysis into account, Althoff *et al.*[84] give values of $\alpha_s(Q^2)$ ranging from 0.12 to 0.23.

Thus at the present time data on processes of the type (2.56), in spite of the direct separation of hard gluon emission ($\sim\alpha_s$), do not permit measuring the value of $\alpha_s(Q^2)$ with higher accuracy than in other experiments. As the energy is raised ($W\gtrsim 100$ GeV) the uncertainties indicated above decrease, suggesting that more accurate measurements of α_s will be made on future accelerators.

5.3.2. Gluon jets in pjp interactions ($s^{1/2} = 540$ GeV)

Hadron jets with $E_\perp(J) = 25 - 50$ GeV in $p\bar{p}$ interactions at $s^{1/2} = 540$ GeV have small values of $x_\perp = \frac{2E_\perp}{s^{1/2}} = 0.1$–$0.2$, and the contribution of gluon jets to them is expected to be about 90–70% (see Sec. 2.4).[59] For this reason the study of their properties and comparison with the properties of quark jets obtained in e^+e^- annihilation and in hard pp (hp) interactions with $E_J^{(q)} = 5$–20 GeV is of interest for checking the predictions of QCD.

The average multiplicity of charged hadrons $\langle n_{ch}(J)\rangle$ in these jets in the interval $E_J^g = 25$–30 GeV is described satisfactorily by the hadronization of gluons on the basis of the CM (Fig. 33).[66] The composition of gluon jets formed in $p\bar{p}$ interactions has not yet been studied in detail. Only the first data on the strange particles (Λ^0, K^0, Ξ^-) and $D^{*\pm}$ mesons are available.[85–87] The formation of $D^{*\pm}$ mesons was studied with the help of the UA1 installation in jets with $P_J = 25$–45 GeV.[86] It was found that $\langle n(D^{*\pm})\rangle_J = 1.1 \pm 0.2 \pm 0.6$ with $z = \mathbf{p}_D\mathbf{p}_J/(p_J)^2 \gtrsim 0.1$. In spite of the large systematic errors (± 0.6), this value of $\langle n(D^{*\pm})\rangle_J$ is high. In addition, $\langle z_{D^*}\rangle \approx 0.2$ for $z\gtrsim 0.1$, while for quark jets $\langle z_c\rangle = 0.57 \pm 0.02$ (5.58). The probability that the recorded D^* mesons were formed as a result of the hadronization of a c quark is equal to 10^{-2}.[60] It is therefore natural to propose that in this case the hadronization of gluons into charmed mesons ($g\to c\bar{c}$) has been observed for the first time.

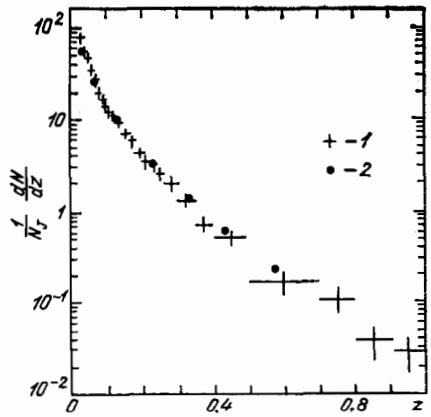

FIG. 37. z distribution of secondary hadrons in jets in $p\bar{p}$ interactions (1) and in e^+e^- annihilation (2). $s_{p\bar{p}}^{1/2} = 540$ GeV and $E_\perp^{(J)} > 30$ GeV; $E_J(e^+e^-) = 17$ GeV.

The momentum distribution of hadrons in jets were measured by the UA1 and UA2 groups.[36,37] The statistical samples of N_J consisted of 1435 events (UA1) with $E_\perp^{(J)} \geqslant 30$ GeV and $3\cdot10^4$ (UA2) with $E_\perp(J) \geqslant 20$ GeV. These data were compared with the TASSO results on the hadronization of quarks in e^+e^- annihilation ($W = 34$ GeV, $E_q = 17$ GeV) and with QCD PT calculations taking into account the interference of soft gluons.[66,88,89]

Figure 37 shows the distributions of charged hadrons over z in a jet with $E_\perp(J) \geqslant 30$ GeV and $\vartheta_h \leqslant 35°$ (UA1).[36] For $z\gtrsim 0.1$ for all hadrons in the jet $\vartheta_h \leqslant 35°$ relative to the axis of the jet.[61] For particles with $z\lesssim 0.1$ corrections amounting to 35% at $z = 0.02$–0.03 and 5% for $z = 0.07$ were introduced. The errors in the measurement of $E_\perp(J)$ are equal to about 15%. The same figure shows the TASSO data at $E_q = 17$ GeV. It is evident that there is no significant difference between the hadronization of the gluons and quarks for $z\gtrsim 0.02$. It should be noted, however, that the data on $D_g(z)$ were obtained with relatively large systematic ($\sim 50\%$) and random ($\sim 20\%$) errors, while the expected difference between the fragmentation of quarks and gluons is relatively small ($\sim 20\%$).[66,88,89] The approximation of these data for different intervals in z for $E_\perp(J) = 30$–60 GeV by the dependence

$$D_g(z, Q) = D_g(z, Q_0)\left[1 + c_1^g(z)\ln\frac{Q^2}{Q_0^2}\right], \qquad (5.74)$$

with $Q_0 = 1$ GeV and $Q = 2E_\perp(J)$ shows that $c_1^g(z) \geqslant c_1^q(z)$.[30] For this reason, new more accurate measurements of $D_g(z, Q)$ are required in order to determine the characteristic features of gluon hadronization.

Analogous conclusions also follow from a comparison of the hadron distributions in gluon and quark jets over $p_\perp(h)$ (Fig. 38). They are satisfactorily described by the formula

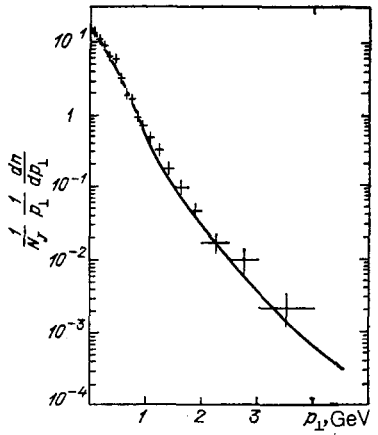

FIG. 38. $p_\perp$ distribution of hadrons in $p\bar{p}$ interactions for $E_\perp(J) = 10$–25 GeV ($\langle E_\perp(J)\rangle = 18$ GeV) and in e^+e^- annihilation (the solid curve) for $E(J) = 17$ GeV.

$$\frac{1}{p_\perp}\frac{dN}{dp_\perp} = \frac{A}{(p_\perp + p_{\perp 0})^N} \tag{5.75}$$

with $p_{\perp 0} = 4$ GeV and $N = 14.8$.[36]

The flux ($(2\pi/n)dE_\perp/d(\Delta\varphi)$) of the transverse energy relative to the axis of a jet for $p\bar{p}$ events with $E_\perp^{(1)}(J_1), E_\perp^{(2)}(J_2) \geqslant 15$ GeV and $\Delta\varphi(J_1, J_2) > 140°$ was measured on the UA2 installation (Fig. 39).[37] Comparison of these data with the results of calculations based on the FFM ($\langle p_\perp(h)\rangle = 0.35$ GeV) neglecting the hard gluon emission shows a significant difference in the region $\Delta\phi \leqslant \pi/4$. Cluster models taking into account the evolution of the parton shower in QCD PT and the interference of soft gluons are in agreement with experiment.[89 62)]

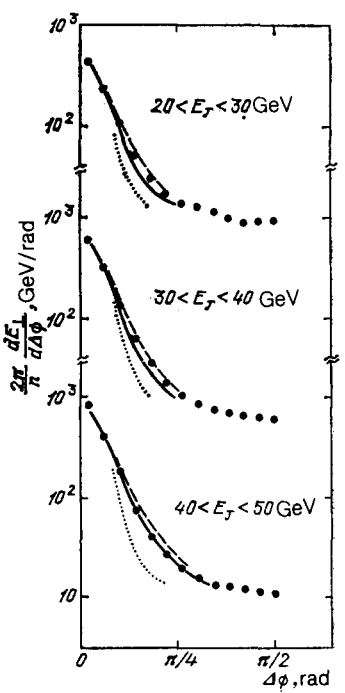

FIG. 39. The transverse energy flux relative to the axis of the jet as a function of $\Delta\varphi$ for $E_\perp(J) = 20$–30, 30–40, and 40–50 GeV in $p\bar{p}$ interactions at $s^{1/2} = 540$ GeV. The dots show the results of calculations in the FFM. The dotted and dashed curves show the results of calculations in the CM taking into account the interference of soft gluons.

The first data on the analysis of three-jet events (3.6) were obtained on the UA2 installation.[37] It turned out that in events with $E_\perp^{(1)}(J) > E_\perp^{(2)}(J) \geqslant 20$ GeV 25% of the events have a third hadron jet with $E_\perp^{(3)}(J) > 4$ GeV. It has a small angle with $E_\perp^{(2)}(J)$, which corresponds to the distribution ($\sim d\vartheta/\sin\vartheta$) of the gluon bremsstrahlung. The probability of these events and the ϑ distribution of the third jet are in agreement with $\alpha_s \sim 0.2$.

Thus the first data on gluon jets obtained on the $p\bar{p}$ collider are consistent with the expected characteristics of gluon hadronization. The systematic and random errors in the experiments are, however, still too large in order to observe the characteristic features of these processes.

The study of gluon hadronization has only just begun. Thus far it has been established that ($B\bar{B}$) pairs form more often in gluon jets than in quark jets. The first data on the development of jets as a function of energy along the longitudinal and transverse variables have been obtained. These results correspond to the expected properties of gluon hadronization, associated with the quantum numbers and high color charge of the gluons. New data for $E_g \gtrsim 50$ GeV are required in order to make a quantitative check of QCD.

5.4. Universality of hadron jets in soft and hard collisions of particles

The relative simplicity of the picture of hard particle collisions and the possibility of its interpretation on the basis of QCD PT distinguish this class of reactions in both the collection and analysis of the experimental data. At the same time the physics of strong interactions (soft and weak) is, of course, unified and requires that they be studied together. As is well known, the difficulties in the description of strong interactions are linked with the unknown mechanism of parton confinement, which are also important for hard collisions (see Sec. 5). Therefore, in order to construct a complete theory, all types of strong interactions must be studied jointly and their common mechanisms must be found. The first step in this direction was the parton model, in which the interaction of the partons was neglected (see Sec. 2). Taking this interaction into account on the basis of QCD for hard processes led to the development of phenomenological models, which describe the experimental data (see Sec. 5.1). It is more difficult to carry out an analogous program for soft hadron collisions, in which there are no large momentum transfers. The first attempts to describe them were undertaken on the basis of the LM and CM.[61–67]

On the other hand, phenomenological models of soft hadron collisions taking into account the quark-gluon structure of the strong interactions, which successfully describe the experimental data in a wide energy range $s^{1/2} = 5$–540 GeV, are being rapidly developed.[5–7,15–19,21,22] The unification of these directions is a problem for the future.

There now already exist experimental data showing

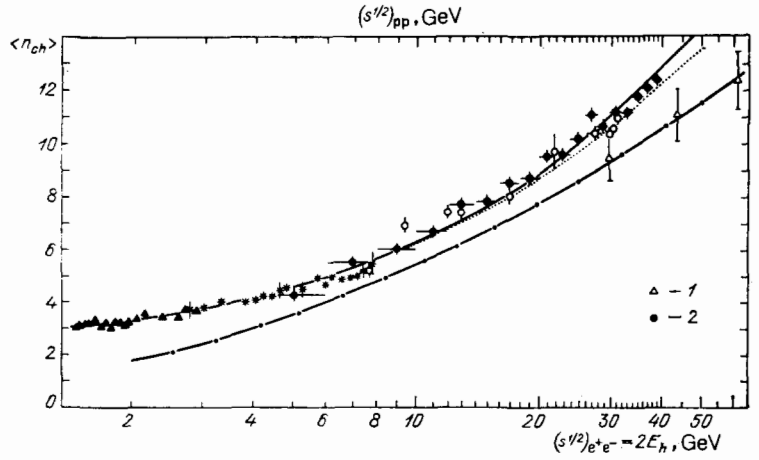

FIG. 40. $\langle n_{ch} \rangle$ as a function of $s_{e^+e^-}^{1/2} = 2E_h = W_h$ (pp) and of $s_{pp}^{1/2}$ (dot-dash curve). The solid and dashed curves show the approximation of the data by the dependences (5.64) and (5.63). The data from the pp experiment are presented as a function of $s_{pp}^{1/2}$ (1) and of W_{pp} (2).

that hadron jets in soft and hard collisions have much in common.[90–94 63)]

We first call attention to a series of articles (more than 40!) on the analysis of inelastic pp interactions with $s_{pp}^{1/2} = 30$, 44, and 62 GeV and their comparison with deep elastic $\nu(\mu)$p interactions and e^+e^- annihilation.[90,91 64)] It was pointed out in these articles that in processes of the type

$$p + p \to p + X \tag{5.76}$$

there occurs a distinct leading of protons, which carry away a large fraction (≈ 0.5) of the initial energy $s_{pp}^{1/2}$.[65)] Because of this only part of the total energy ($\langle W \rangle \approx 0.5 s_{pp}^{1/2}$), goes into the formation of new hadrons, in contrast, for example, to e^+e^- annihilation. In addition, the initial states of these processes also differ, which must be taken into account when comparing them. The characteristics of soft processes (5.76) and e^+e^- annihilation were therefore compared with

$$s_{e^+e^-}^{1/2} = W = [(s_{pp}^{1/2} - q_{1p} - q_{2p})^2]^{1/2} = [(q_{tot}^h)^2]^{1/2}, \tag{5.77}$$

where $q_{1,2}$ are the four-momenta of the leading protons. Exclusion of protons in the reaction (5.76) from the analysis yields $B = Q = 0$ for the system of hadrons formed, just as in the case of e^+e^- annihilation. Thus the initial differences between the soft and hard collisions were eliminated and the characteristics of the secondary hadrons in their rest system for the same values of W were compared. At the same time, the procedure for separating jets described in Sec. 3 was employed in order to determine the jet characteristics of the hadrons in pp interactions. In comparing the processes (5.76) with deep inelastic νp and μp interactions only one leading proton was excluded from the analysis, and therefore

$$W_{\nu(\mu)p} = W_{pp} = [(s_{pp}^{1/2} - q_{1p})^2]^{1/2} = [(q_{tot}^h)^2]^{1/2}. \tag{5.78}$$

The data on hard (e^+e^-, $\mu(\nu)$p) and soft (pp) collisions were compared in the energy range (W) from 3 to 40 GeV.[90] All available characteristics of the processes, beginning from $\langle n_{ch}(W) \rangle$ and ending with the correlations of hadrons in jets, were compared. As an illustration we shall present the results of this comparison for $\langle n_{ch}(W) \rangle$ and $R(y, y')$ (Figs. 40 and 41a). As is evident from the figures, the available data on hard and soft processes do not differ from one another for the same values of W. At the same time, if the variable $s_{pp}^{1/2}$ is used for the pp interactions (dot-dash curve in Fig. 40), then the behavior of $\langle n_{ch}^{pp}(s) \rangle$ differs substantially from that of $\langle n_{ch}^{e^+e^-}(s) \rangle$. An analogous result is also

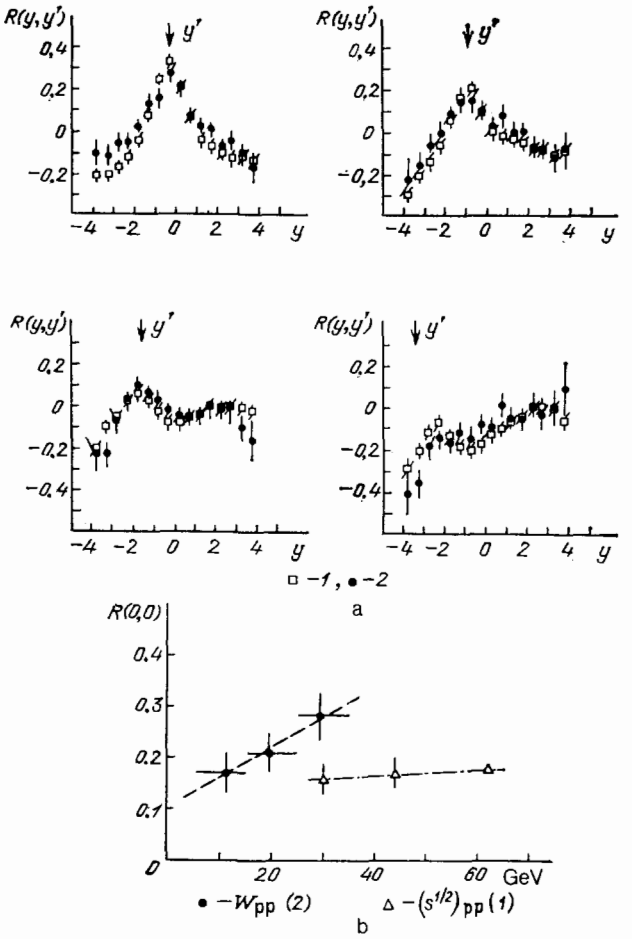

FIG. 41. a) Correlation functions of hadrons $R(y, y')$ in e^+e^- annihilation (1) and in pp interactions (2) at $s_{e^+e^-}^{1/2} \approx W_{pp} = 25$–36 GeV, in Fig. 41a the values of y' are marked by (↓). b) The values of $R(0,0)$ for pp interactions as a function of $s_{pp}^{1/2}$ (1) and of W_{pp} (2).

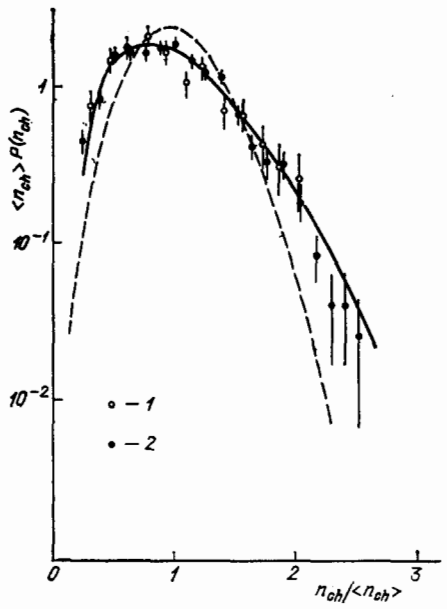

FIG. 42. KNO distribution for pp interactions ($s^{1/2} = 62$ GeV) at W_{pp} = 10–15 GeV (1) and 25–30 GeV (2). The solid curve shows the approximation of these data and the broken curve shows the results of the approximation of the data on e^+e^- annihilation.

obtained for the correlations: the value of $R(y, y')$ for pp interactions in the usual approach ($s_{pp}^{1/2}$) is approximately two times lower than in e^+e^- annihilation (see Fig. 41b). Extrapolation of the data on $\langle n_{ch}(W)\rangle$ using the formula (5.64) up to the energy of the collider ($s^{1/2} = 540$ GeV) describes well the data on the multiplicity in $p\bar{p}$ interactions.[91] Analyzing the entire collection of data, Basile *et al.*[90,91] arrive at the conclusion that all characteristics of hadron systems in soft and hard collisions of particles are the same, with the exception of the form of KNO scaling (5.66) (Fig. 42). The distribution $\langle n_{ch}\rangle P(n_{ch})$ is narrower in e^+e^- annihilation than in $p\bar{p}$ interactions.[91] It is possible that this is linked to the difference between the quark (e^+e^- annihilation) and gluon ($p\bar{p}$ interaction) hadron jets.

A relativistically invariant description of multiple processes in the space of relative four-dimensional velocities is proposed in Ref. 94. A new method for separating hadron jets, which was used in the analysis of π^-p and $\pi^{12}C$ interactions at $p = 40$ GeV/c is presented. It was found that in the new variables hadron distributions in jets have a universal character in the fragmentation of both pions and nuclei.

Thus the universality of the jet characteristics of hadrons in soft and hard particle collisions has been established experimentally.[90–94] The main difference between them lies only in the transverse momenta of the jets $P_\perp$ (J), which it is natural to attribute to the method used to separate the soft and hard processes. For this reason, the dynamics of parton hadronization in the first approximation is virtually independent of the transferred momenta (Q) and is determined primarily by the energy of the parton jet. Of course, these results are of a semiquantitative character and the specific features of soft processes will appear in more detailed studies (see, for example, Refs. 76, 92, 93). These effects are calculated in quark-gluon models of soft hadron collisions.[15,16]

6. CONCLUSIONS

The experimental study of hadron jets formed in hard processes has confirmed the basic ideas of QCD. The study of the characteristics of a jet has on the whole made it possible to measure the quantum numbers of quarks and gluons and to evaluate the quantity $\alpha_s(Q^2)$ in the interval $Q^2 = (5$–$2000)$ GeV^2 (Sec. 4). Data on jets, obtained at the highest energies ($s^{1/2} = 540$ GeV), have shown that as the energy is raised their "parton origin" is increasingly more clearly manifested (see Figs. 8, 12, 15). This has made it possible to demonstrate clearly the vector nature of gluons and obtain for the first time data on the structural functions of nucleons in strong $p\bar{p}$ interactions (see Secs. 4.2 and 4.3).

The verification of QCD is nevertheless still at a semiquantitative level. This primarily concerns the stage of parton hadronization, whose mechanism is unknown. This is what determines the systematic errors in the measurement of $\alpha_s(Q^2)$, which constitute 30–40% at $Q^2 \approx 1200$ GeV^2 (see Sec. 5, Table V). Because of this the hadronization of quarks and gluons has been intensively studied in recent years on all the largest accelerators in the world. As a result significant progress has been made in understanding the basic laws governing the interaction of partons at large distances.

It has been established that the characteristics of hadrons in a jet are virtually independent of the type of hard collisions, and are determined by the quantum numbers and energy of the starting parton (hypothesis of soft decolorization of partons). This result is based on the comparison of data on parton hadronization obtained in e^+e^- annihilation ($s^{1/2} = W \leqslant 45$ GeV), in deep inelastic lN interactions ($W \lesssim 15$ GeV) and in hard hN interactions ($W \lesssim 200$ GeV) (see Secs. 4 and 5). As a result, the combined analysis of all types of hard processes yields rich information on the mechanisms of the formation and hadronization of partons.

It has been shown experimentally that the development of the quark-gluon cascade (QCD PT) largely determines the evolution of the hadron jet with increasing energy (see Sec. 5). In this respect we should note the new important results obtained in μp interactions on the observation of effects associated with the emission of soft gluons and the first experimental indications of their interference in e^+e^- annihilation (see Sec. 5.2). The description itself of hadron jets on the basis of QCD PT is currently employed to quite low momentum transfers ($Q \sim 0.5$–1.0 GeV), which already makes it possible to apply it also to soft processes (see Secs. 5.1 and 5.2).

The first data on the hadronization of gluons in e^+e^- annihilation, confirming the predictions of QCD associated with their quantum numbers and the more intense emission of gluons than in quark jets, have been obtained (see Sec. 5.3). The longitudinal and transverse evolution of hadron jets with energy is consistent with the predictions of QCD PT. At the energies attained, however, the effects associated with the hadronization of partons are still important (see Secs. 2.2, 2.3, and 5.2). All these results refer to the first

stage of hard processes, where QCD PT is applicable.

Important results have also been obtained for the soft stage of these processes. It has been shown that in e^+e^- annihilation, pp interactions, and l N collisions the fast hadrons in the jet preserve information on the quantum numbers of the parent partons. This makes it possible to measure their charge, isotopic spin, strangeness, and other characteristics (see Secs. 4.3 and 5.2). The first evaluations of the charges of quarks were obtained in l N interactions and in hard pp collisions (Sec. 4.3). Data on the hadronization of light (u, d) quarks in $\nu(\bar{\nu})$p interactions show that they are an isotopic doublet (Sec. 5.2). The spectacular leading effect has been observed in the hadronization of heavy quarks (c, b), which makes it possible to "tag" them and to study the hadronization of quarks of a definite type (Sec. 5.2).

The correlations between the secondary hadrons in jets and the intervals of compensation of their quantum numbers in the main coincide with the analogous data for soft processes (see Secs. 2.1 and 5.2). They have a short-range character, which indicates the local nature of the hadronization of partons. In particular, this also refers to the creation of $(B\bar{B})$ pairs, which on the basis of the parton scheme are formed as a result of the attachment of sea diquarks ($q_s q_s$ or $\bar{q}_s \bar{q}_s$), which is now directly linked with the structure of the QCD vacuum.

The multiplicity and composition of secondary hadrons are practically identical in different types of hard collisions ($s^{1/2} = W \lesssim 50$ GeV) and largely depend on the energy of the jet. It is of great interest to obtain accurate data on this question at collider energies ($E(J) \lesssim 100$ GeV).

The results obtained are well described by the phenomenological models (LM and CM), which are being continuously modified as new experimental data becomes available.[66] When the emission and interference of soft gluons are included in them the stage of development of the quark-gluon cascade plays a determining role (QCD PT). An attractive feature of cluster models is the description of parton hadronization with three to four free parameters without the introduction of fragmentation functions and the limitation of parton transverse momenta (see Sec. 5.1).[64–67] In these models QCD PT is employed up to $Q_0 \sim 0.5$ GeV, which makes it possible to describe soft processes also,[65,66,11] especially since the observed universality of jets in soft and hard processes clearly indicates a single mechanism for parton hadronization (see Sec. 5.4). Much is promised by the successful description of the hadron momentum distributions on the basis of QCD PT, beginning with $p = 200$ MeV.[11,52] Such a correspondence between the parton and hadron distributions is unexpected, since one would think that confinement effects should already be observed at such low hadron momenta.

On the whole, however, the basic mechanisms of the formation and hadronization of partons in hard processes have now been established, and the characteristics of hadron jets have been confidently predicted for the future generation of accelerators ($s^{1/2} = W \gtrsim 100$ GeV). The main problem is to determine them within the framework of QCD in order to clarify their origins. The study of hadron jets at higher energies will make it possible to specify these characteristics and to perform quantitative measurements of the basic parameter of the theory of strong interactions—$\alpha_s(Q^2)$.

It is a pleasure for me to thank A. B. Kaĭdalov, E. M. Levin, Yu. M. Shabel'skiĭ, and the participants of the school of physicists in Bakuriani and of the seminars at the High Energy Physics Laboratory at the Joint Institute of Nuclear Research for numerous useful discussions of the questions touched upon in this review.

[1)]Here R is the "size" of a hadron (~ 1 fm).

[2)]In this review we shall, as a rule, use the system of units in which $\hbar = c = 1$.

[3)]In the literature this stage is often called fragmentation of partons into hadrons, which is associated with the first models of the fragmentation type (see Sec. 5).

[4)]These interactions are usually called multiple hadron creation processes (or simply multiple processes).[5–7] In these processes, as a rule, many secondary particles are created ($\langle n \rangle \gtrsim 10$). For example, at $s^{1/2} = 540$ GeV ($p\bar{p}$ collider CERN) $\langle n \rangle_{\pm} = 27.5 \pm 0.4$ and $\langle n \rangle \approx 40$.[14]

[5)]f_c^{ab} are also often called the structure functions of the process (2.1).

[6)]We shall study the interaction of unpolarized primary particles.

[7)]In what follows we shall omit the particle indices everywhere except in special cases.

[8)]For heavier resonances, consisting of c and b quarks, $\langle p_\perp(J)/\psi \rangle \approx 1$ GeV and $\langle p_\perp(\Upsilon) \rangle \approx 1.5$ GeV, and such resonances are formed as a result of hard collisions.

[9)]These values of the coefficients were obtained at $s^{1/2} = 23$–63 GeV for long-lived particles (π, K).[5] Unfortunately there are no analogous data for resonances.

[10)]The quasiplateau in y (2.10) corresponds to the distribution of dx/x (2.7) over x.

[11)]The function $R_2(y_1, y_2)$ is less sensitive to errors in measurements of σ_{in} than $C_2(y_1, y_2)$, which is very important for experiments performed with colliding beams.

[12)]Here it is necessary to take into account the effect of the energy-momentum conservation laws, especially at the boundaries of the phase volume of the processes (2.2).

[13)]$z = p_h/k = p_h/xp$ is the relative fraction of the momentum (or energy) of a parton carried away by the hadron.

[14)]Since the transverse momenta of the hadrons and partons are much smaller than the longitudinal momenta, in the first approximation they can be neglected. The dependence of F_h^q and D_q^h on the square of the transferred momentum (Q^2) is associated with the field picture of the interaction (QCD) and will be discussed below.

[15)]The square of the total energy of the secondary hadron is $W^2 = m^2 + 2m\nu - Q^2$.

[16)]The dependence of the cross section on $e_{q_i}^2$ is introduced under the summation sign because of the difference between the quark charges ($e_u = +2/3, e_d = -1/3, e_s = -1/3$).

[17)]The corresponding distributions $xq_i^n(x)$ in the neutron follow from $xq_i^p(x)$ and isotopic invariance: $u^p(x) = d^n(x)$ and $d^p(x) = u^n(x)$.

[18)]For nonrelativistic hadrons, having $\beta_h = p_h/E_h < 1$, a factor β (hadron velocity), taking into account the increase in the phase volume with the energy ($s^{1/2}$), must be included in (2.35).

[19)]Here the index $(qq)_i$ denotes the system of partons remaining after the q_i quark is knocked out. As a rule, this is a diquark.

[20)]Here we have approximately set the Cabibbo angle $\vartheta_C = 0$ and have neglected the creation of charmed particles. Because of the law of conservation of leptonic charge the d quarks in (2.40) and the u quarks in (2.41) transform correspondingly into u and d quarks before they fragment into hadrons.

[21)]Here $\Lambda \equiv \Lambda_{\overline{MS}}$.[4]

[22)]As the resolution increases ($\sim Q^2$), because of the interaction of the quarks and gluons the parton spectrum will soften. The data at $\langle Q_0^2 \rangle = 5$–$10$ GeV are usually used for $F_N^q(x', t_0)$.

[23)]The extreme point of view is that all breakdowns of scaling are caused by twists and $\Lambda = 0$.

[24)]A similar situation occurs in all of particle physics: the particles themselves cannot be seen, and their properties are judged based on their interactions with the macroscopic medium. For example, from the

tracks of particles in a bubble chamber. To this case the "free" partons interact with the QCD vacuum.

[25] This value of $\langle S \rangle$ corresponds to $\langle \delta \rangle \approx 17°$, where δ is one-half the angle of the emergence cone of the particles relative to the axis of the jet. For $W = 5$ GeV $\langle \delta \rangle \approx 30°$.

[26] In this case the total quantum numbers of these hadrons must be zero.

[27] In addition, the mechanism of the decolorization of the partons as they transform into hadrons also destroys the equality of the parton-jet quantum numbers (see Secs. 4 and 5).

[28] For events without a pseudotrigger the hadrons in the jet $J_{q_i}(h)$ have a wider angular distribution.[5]

[29] The vertex detector in the UA1 apparatus is located in a magnetic field of 0.7 T, and the particle momenta are measured with an accuracy of $\Delta p/p = 0.5\% p$ (GeV) per meter of track length.

[30] The "dimensions" of the jet in φ are equal to $\pm 30°$.[36,37]

[31] The t quark has a mass $m \gtrsim 40$ GeV and for this reason is not yet formed at $s^{1/2} \leqslant 45$ GeV.

[32] Here the random (0.05) and systematic (0.1) errors in the measurement of $R(W)$ are presented.

[33] The values of x_1 and x_2 were determined from the four-momenta of the jets $(P(J^1), P(J^2))$ in (3.5).

[34] Analogously to Rutherford scattering of point charged particles.

[35] $x_q \gtrsim 0.1$ is chosen in order to exclude sea quarks (see Sec. 2).

[36] The condition $x_J > 0.6$ selects the jets $J_b(h)$ with the leading charged hadrons.[45]

[37] In this case the value of Λ varies from 0.46 to 0.17 GeV, respectively.

[38] From here we obtain the total systematic error in the cross-section measurements of $\pm 45\%$ (UA2), if the separate contributions to this error are added quadratically $[\Delta\sigma = (\Sigma_i (\Delta\sigma_i)^2)^{1/2}]$.

[39] The statistical errors in the measurements of $F(x)$ are indicated in Fig. 15. A twofold change in Λ (increase or decrease) produces a 15% change in $F(x)$, which is less than the total error of the measurements.

[40] Detailed justification of this approach and references to the original works are given in the reviews[11] of the Schools held at the Leningrad Institute of Nuclear Physics (1980–1985).

[41] An important property of these cascades was discovered while they were being studied. It turned out that the emergence angles of the partons systematically decrease along the branch of the parton cascade with the number of the decay, i.e., the jets branch into converging angular cones.[53] Thus the "dimensions" of a jet are determined by the primary decays of the partons.

[42] An analogous assumption is also made in the parton model (see Sec. 2).

[43] This phenomenon is analogous to the breakdown of scaling in the structure functions of nucleons (see Secs. 2 and 4).

[44] An analog of the phenomenon under study in QED is the Chudakov effect.[54] In this effect the electron and positron from an ultrarelativistic pair ionize the medium as two independent charges only after a macroscopically long time, when they become separated in space by atomic distances.

[45] The Lund model is named after the city of Lund (Sweden). The physicists B. Andersson, G. Gustafson, G. Ingelman, and others at Lund University developed a detailed model for describing soft and hard processes, which is disseminated to scientific centers in the form of the corresponding computer programs.[61,62] This has made possible its rapid dissemination among experimenters.

[46] Here S is the sphericity of the event [see the formula (3.1)]. In the initial version of the model[58] it was assumed that $a_F = 0.77$, $\sigma_q = 0.32$ GeV, $a_V = 0.5$, and $\gamma_S = 0.4$. Naturally, the accuracy of the parameters will increase as more data are obtained.

[47] For $\langle p_\perp(h) \rangle$ the random (0.07) and systematic (0.010) errors, associated with the use of different variables for determining the axis of the jet (see Sec. 3), are indicated.

[48] This means that D_q^h depends on $p_\perp^2$ and W.

[49] This result covers the well-known problem of $\langle k_\perp^2 \rangle$ increasing with W^2 in hard hadron collisions.[5,13]

[50] At large W and not very small E_h ($> m_h$) the usually used variables $x_E = E_h/(W/2)$, $x_F = 2p_\parallel^*/W$, $x_p = 2p/W$ practically coincide, and we shall not discuss their differences.

[51] It is pointed out in Refs. 11 and 31 that hadron distributions over the "total" rapidity ($y = \ln[(E+p)/M]$) are more sensitive to interference effects than the distributions over $y_\parallel$.

[52] The first indications of a t quark with $M \sim 40$ GeV in $p\bar{p}$ interactions at $s^{1/2} = 540$ GeV were obtained precisely by this method from leptons with $p_\perp \gtrsim 12$ GeV.[38]

[53] In the same studies[71,72] the coupling constant α_S^c of the gluon and charmed quark was evaluated: $\alpha_S^c/\alpha_S = 1.00 \pm 0.20 \pm 0.20$. Within the limits of error ($\sim 20\%$) it is independent of the flavor of the quarks.

[54] The protons (antiprotons) were identified in the momentum interval from 1 to 5 GeV in the center of mass system.

[55] For $x_\perp \gtrsim 0.3$ the valence (u_V, d_V) quarks of the protons primarily participate in the hard scattering.

[56] It was assumed at the same time that the systematic errors are equal to 5%.

[57] As is evident from Fig. 32, (5.63) and (5.64) will differ significantly for $W \gtrsim 100$ GeV.

[58] The FF model does not describe effects associated with the emission of soft gluons.[68]

[59] In this case the percentage of gluon jets is significantly higher than in e^+e^- annihilation (5–10%).[30,31]

[60] An additional factor which reduces this probability is the smallness ($\lesssim 0.01$) of the probability of formation of a scattered charmed quark (see Sec. 2).

[61] In this case the background formed by the hadrons not belonging to the jet constitutes $\lesssim 1\%$. For $z < 0.1$ the hadron distribution is wider and the corrections were calculated with the help of the QCD model.[36]

[62] In the model the contribution of gluon jets varies from 75% ($E_J = 20$ GeV) to 35% ($E_J = 70$ GeV). It was determined from data on the structure functions $F_{q,g}(x, Q)$ at $s^{1/2} = 540$ GeV (see Fig. 15).[36,37]

[63] It is interesting to note that in the parton model the characteristics of hadrons in jets formed in hard collisions were taken from the data on soft hadron interactions (see Sec. 2).

[64] References to the original works on this question are given in the review article of Ref. 90.

[65] This effect was discovered in the 1950s in experiments with cosmic rays.[6]

[66] The FFM does not describe collective effects associated with the emission of gluons and their effect on the momentum distributions of the quarks (see Sec. 5).

[1] L. B. Okun', Leptony i kvarki, Nauka, M., 1981 (Engl. transl., Leptons and Quarks, North Holland, Amsterdam, 1982]; Fizika élementarnykh chastits (Physics of Elementary Particles), Nauka, M., 1984.

[2] F. E. Close, Introduction to Quarks and Partons, Academic Press, 1980 [Russ. transl., Mir, M., 1982].

[3] I. V. Andreev, Khromodinamika i zhestkie protsessy pri vysokikh énergiyakh (Chromodynamics and Hard Processes at High Energies), Nauka, M., 1981.

[4] B. L. Ioffe, L. I. Lipatov, and V. A. Khoze, Glubokoneuprugie protsessy (Deep-Inelastic Processes), Énergoizdat, M., 1983. M. B. Voloshin, and K. A. Ter-Martirosyan, Teoriya kalibrovochnykh vzaimodeĭstviĭ élementarnykh chastits (Theory of Gauge Interactions of Elementary Particles), Énergoatomizdat, M., 1984. P. S. Isaev, Kvantovaya élektrodinamika v oblasti vysokikh énergiĭ (Quantum Electrodynamics at High Energies), Énergoatomizdat, M., 1984.

[5] V.G. Grishin, Inklyuzivnye protsessy v adronnykh vzaimodeĭstviyakh pri vysokikh énergiyakh (Inclusive Processes in Hadronic Interactions at High Energies), Énergoizdat, Moscow (1982).

[6] V. S. Murzin and L. I. Sarycheva, Vzaimodeĭstviya adronov vysokikh énergiĭ (Interaction of Hadrons at High Energies), Nauka, M., 1983; Kosmicheskie luchi i ikh vzaimodeĭstvie (Cosmic Rays and Their Interaction), Atomizdat, M., 1968.

[7] Yu. P. Nikitin and I. L. Rozental', Teoriya mnozhestvennykh protsessov (Theory of Multiple Processes), Atomizdat, M., 1976.

[8] R. Feynman, Photon-Hadron Interaction, Benjamin, Reading, 1972 [Russ. transl., Mir, M., 1975]; Phys. Rev. Lett. 23, 1415 (1969). M. A. Markov, Neĭtrino (The Neutrino), Nauka, Moscow (1964). J. D. Bjorken and E. A. Paschos, Phys. Rev. **185**, 1975 (1969).

[9] V. N. Gribov in: Proceedings of the 8th Winter School at the Leningrad Institute of Nuclear Physics, Leningrad Institute of Nuclear Physics of the USSR Academy of Sciences, Leningrad, 1973, Vol. 2, p. 4.

[10] R. Horgan and M. Jacob, Physics at Collider Energy, CERN, Geneva, 1981 [Russ. transl., Usp. Fiz. Nauk **136**, 219 (1982)].

[11] Ya. I. Azimov, Yu. L. Dokshitser, and V. A. Khoze, Usp. Fiz. Nauk **132**, 443 (1980) [Sov. Phys. Usp. **23**, 732 (1980)]. Ya. I. Azimov, Yu. L. Dokshitser, S. I. Troyan, and V. A. Khoze in: Proceedings of the 15th Winter School of the Leningrad Institute of Nuclear Physics, LINP of the USSR Academy of Sciences, L., 1980, p. 3. Proceedings of the 16th Winter School of the Leningrad Institute of Nuclear Physics, LINP of the USSR Academy of Sciences, L., 1981, p. 26. Proceedings of the 17th Winter School of the Leningrad Institute of Nuclear Physics, LINP of the USSR Academy of Sciences, L., 1982, p. 162. Proceedings of the 18th Winter School of the Leningrad Institute of Nuclear Physics, LINP of the USSR Academy of Sciences, L., 1983, p. 18. Proceedings of the

20th Winter School of the Leningrad Institute of Nuclear Physics, LINP of the USSR Academy of Sciences, L., 1985, p. 82.
[12]V. A. Khoze and M. A. Shifman, Usp. Fiz. Nauk **140**, 3 (1983) [Sov. Phys. Usp. **26**, 387 (1983)].
[13]G. Ranft and I. Ranft, Fiz. Elem. Chastits At. Yadra **10**, 90 (1979); **15**, 555 (1984) [Sov. J. Part. Nucl. **10**, 35 (1979); **15**, 249 (1984)]; V. G. Grishin, *ibid.*, 178. [Sov. J. Part. Nucl. **15**, 80 (1984)].
[14]G. Matthiae, Preprint CERN-EP, 83-140, Geneva (1983). I. M. Dremin, Usp. Fiz. Nauk **141**, 517 (1983) [Sov. Phys. Usp. **26**, 993 (1983)].
[15]a) A. B. Kaĭdalov in: 10th Physics School at the Institute of Theoretical and Experimental Physics, Energoatomizdat, M., 1983, No. 2, p. 3. b) A. Capella, Acta Phys. Polon. B **15**, 1185 (1984).
[16]K. A. Ter-Mertirosyan in: Ref. **15**a, No. 2, p. 64.
[17]B. Andersson *et al.*, Z. Phys. C **20**, 317 (1983).
[18]V. V. Anisovich *et al.*, Usp. Fiz. Nauk **144**, 553 (1984) [Sov. Phys. Usp. **27**, 901 (1984)]; V. V. Anisovich and V. M. Shekhter, Nucl. Phys. B **55**, 455 (1973). V. V. Anisovich, M. N. Kobrinskiĭ, and Yu. Niri, Preprint No. 982, Leningrad Institute of Nuclear Physics of the USSR Academy of Sciences, L., 1981.
[19]S. J. Brodsky and J. F. Gunion, Phys. Rev. D **17**, 848 (1978).
[20]E. L. Feĭnberg in: Problemy teoreticheskoĭ fiziki (Problems in Theoretical Physics: Collection of Papers in Memory of E. I. Tamm), Nauka, M., 1972, p. 248.
[21]N. N. Nikolaev, Usp. Fiz. Nauk **134**, 369 (1981) [Sov. Phys. Usp. **24**, 531 (1981)].
[22]Yu. M. Shabel'skii, Fiz. Elem. Chastits At. Yadra **12**, 1070 (1981) [Sov. J. Part. Nucl. **12**, 430 (1981)].
[23]F. Eisele in: Proceedings of the XXI International Conference on High Energy Physics, Paris (1982), p. C3-337.
[24]I. A. Savin in: Proceedings of the XXII International Conference on High Energy Physics, Leipzig (1984), p. 251.
[25]K. Rith, Preprint THEP-83/5, Freiburg (1983).
[26]F. Dydak, Preprint CERN/EP 83-171, Geneva (1983).
[27]J. Badier *et al.*, Z. Phys. C **18**, 281 (1983).
[28]G. Wolf, Preprint DESY 80/85, Hamburg (1980); Preprint DESY 81/86, Hamburg (1981); Preprint DESY/82/077, Hamburg (1982).
[29]G. Wolf, Preprint DESY 83/096, Hamburg (1983).
[30]P. Soding, Preprint DESY 83/104, Hamburg (1983).
[31]M. Althoff *et al.*, Z. Phys. C **22**, 307 (1984); Phys. Lett. B **139**, 126 (1984); Preprint DESY 84/093, Hamburg (1984). D. Bender *et al.*, Phys. Rev. D **31**, 1 (1985).
[32]R. Sosnowski in: Hard Hadronic Collisions; International Conference on High Energy Physics, Brighton, UK (1983), p. 628.
[33]A. Breakstone *et al.*, Preprint CERN/EP 83-182, Geneva (1983).
[34]T. Akesson *et al.*, Phys. Lett. B **128**, 354 (1983).
[35]T.Akesson *et al.*, *ibid.* **123**, 133; **118**, 185 (1982).
[36]G. Arnison *et al.* (UA1), Phys. Lett. B **123**, 115, 214, 223 (1983); **136**, 294 (1984). K. Eggert in: Ref. 32, p. 447. A. Honma, Preprint CERN-EP/83-173, Geneva (1983).
[37]P. Bagnaia *et al.* (UA2), Z. Phys. C. **20**, 117 (1983). M. Benner *et al.* (UA2), Phys. Lett. B **115**, 59 (1982); **122**, 322. P. Bagnaia *et al.* (UA2), *ibid.* **138**, 430 (1984); **144**, 283, 291.
[38]C. Rubbia in: Ref. 32, p. 860; Preprint CERN-EP/84-55, Geneva (1984). M. Jacob in: Ref. 24, p. 150.
[39]P. C. Basetti *et al.*, Nucl. Phys. B **149**, 13 (1979). P. Allen *et al.*, *ibid.* **214**, 369 (1983).
[40]J. J. Aubert *et al.*, Phys. Lett. B **100**, 433 (1981); **119**, 233, Preprint CERN-EP-83/164, Geneva (1983). J. P. Albanese *et al.*, Preprint CERN-EP/63, Geneva (1984); Phys. Lett. B **144**, 302 (1984).
[41]W. Bartel *et al.*, Preprint DESY 83-050, Hamburg (1983).
[42]H. Rykaczewski, Preprint DESY 83-085, Hamburg (1983).
[43]M. Althoff *et al.*, Preprint DESY 84-001, Hamburg (1984).
[44]P. Allen *et al.*, Phys. Lett. **112**, 88 (1982).
[45]E. E. Kluge, Phys. Scripta **19**, 109 (1979).
[46]N. G. Antoniou *et al.*, Phys. Lett. B **128**, 257 (1983). J. Owenes and E. Reya, Phys. Rev. D **17**, 3003 (1978).
[47]R. Bayer *et al.*, Z. Phys. C **2**, 265 (1979). Z. Kunszt and E. Pietarinen, Phys. Lett. **132**, 453 (1983). W. Furmanski and H. Kowalski, Preprint CERN-EP/83/21, Geneva (1983).
[48]H. Kowalski, Preprint DESY 83-099, Hamburg (1983).
[49]Z. Kunzst and E. Pietarinen, Nucl. Phys. B **164**, 45 (1980). F. Berendes *et al.*, Phys. Lett. B **103**, 124 (1981). R. Odorico, Preprint CERN TH/3744, Geneva (1983).
[50]J. Dorfan, Preprint SLAC-PUB-3250, Stanford (1983). R. Hollebeek, Preprint SLAC-PUB-3242, Stanford (1983).
[51]J. Janata, Preprint DESY 83-110, Hamburg (1983).
[52]Ya. I. Azimov *et al.*, Yad. Fiz. **40**, 1284 (1984) [Sov. J. Nucl. Phys. **40**, 817 (1984)].
[53]B. I. Ermolaev and V. S. Fadin, Pis'ma Zh. Eksp. Teor. Fiz. **33**, 285 (1981) [JETP Lett. **33**, 269 (1981)].
[54]A. E. Chudakov, Izv. Akad. Nauk SSSR, Ser. Fiz. **19**, 651 (1955) [Bull. Acad. Sci. USSR, Phys. Ser. **19** (1955)].
[55]Ya. I. Azimov *et al.*, in: Proceedings of the 18th Winter School at the Leningrad Institute of Nuclear Physics, LINP of the USSR Academy of Sciences, L., 1983, p. 3.
[56]F. Binon *et al.*, Nuovo Cimento A **80**, 363 (1984).
[57]T. D. Gottschalk, Preprint CERN-TH-3810, Geneva (1983). R. Orava, FERMILAB-Conf.-82/86, Batavia (1982).
[58]R. D. Field and R. P. Feynman, Phys. Rev. **D15**, 2590 (1977); Nucl. Phys. B **138**, 1 (1978).
[59]P. Hoyer *et al.*, *ibid.* **161**, 349 (1979).
[60]A. Ali *et al.*, Phys. Lett. B **93**, 155 (1980). T. Meyer, Preprint DESY 81-46, Hamburg (1981).
[61]B. Andersson *et al.*, Phys. Lett. B **71**, 337 (1977); Nucl. Phys. B **135**, 273 (1978).
[62]B. Andersson *et al.*, Phys. Rept. **97**, 31 (1983).
[63]R. Brandelik *et al.*, Phys. Lett. B **94**, 437 (1980).
[64]R. D. Field and S. Wolfram, Nucl. Phys. B **213**, 65 (1983).
[65]T. D. Gottschalk, *ibid.* **214**, 201.
[66]B. R. Webber, *ibid.* 238, 492 (1984).
[67]R. D. Field, Preprint UFTP-83-17, Florida (1983). G. Marchesini and B. R. Webber, Nucl. Phys. B **238**, 1 (1984).
[68]M. Arneodo *et al.*, Phys. Lett. B **145**, 156 (1984); **149**, 415.
[69]J. J. Aubert *et al.*, *ibid.* **135**, 225.
[70]J. M. Izen, Preprint DESY 84-104, Hamburg (1984).
[71]W. Bartel *et al.*, Phys. Lett. B **146**, 121 (1984).
[72]M. Althoff *et al.*, *ibid.* **138**, 337.
[73]A. Breakstone *et al.*, *ibid.* **135**, 505, 510; Preprint, CERN-EP, 84-53, Geneva (1984).
[74]T. Akesson *et al.*, Preprint CERN-EP, 84-70, Geneva (1984); Z. Phys. C **25**, 13 (1984).
[75]W. Bartel *et al.*, *ibid.* **20**, 187 (1983).
[76]A. Wroblewski, Review Talk at the 16th International Symposium on Multiparticle Dynamics, Granlibakke, Lake Tahoe, USA (1983). M. Bardadin-Otwinowska *et al.*, Z. Phys. C **13**, 83 (1982).
[77]Z. Koba *et al.*, Nucl. Phys. B **40**, 317 (1972). J. D. Bjorken in: Proceedings of the 2nd International Conference on Physics in Collision, Stockholm (1982), p. 343.
[78]B. R. Webber, Phys. Scripta **25**, 198 (1982).
[79]J. F. Gunion and G. Bertsch, Phys. Rev. D **25**, 746 (1982).
[80]L. M. Jones and R. Migneron, Z. Phys. C **16**, 217 (1983).
[81]W. Bartel *et al.*, Phys. Lett. B **123**, 460 (1983).
[82]W. Bartel *et al.*, Preprint DESY 83-080, Hamburg (1983); Preprint DESY 85-036, Hamburg (1985). H. Aihara, Phys. Rev. Lett. **54**, 270 (1985).
[83]H. Albrecht *et al.*, Phys. Lett. B **102**, 291 (1981).
[84]M. Althoff *et al.*, Z. Phys. C **26**, 157 (1984).
[85]K. Alpgard *et al.*, Phys. Lett. B **115**, 65 (1982).
[86]G. Arnison *et al.*, Preprint CERN EP/84-86, Geneva (1984).
[87]G. J. Alner *et al.*, Preprint CERN EP/84-111, Geneva (1984).
[88]C. T. H. Davies and B. R. Webber, Z. Phys. C **24**, 133 (1984).
[89]G. Marchesini and B. R. Webber, Preprint CERN TH/3525, Geneva (1983).
[90]M. Basile *et al.*, Preprints CERN-EP-84/94; CERN-EP-84-95, Geneva (1984).
[91]M. Basile *et al.*, Nuovo Cimento A **79**, 1 (1984).
[92]V. G. Grishin, L. A. Didenko, T. Kanarek, and Z. V. Metreveli, Yad. Fiz. **38**, 967 (1983); **40**, 936 (1984) [Sov. J. Nucl. Phys. **38**, 581 (1983); **40**, 595 (1984). Report No. R1-82-252, Joint Institute of Nuclear Research, Dubna (1982).
[93]R. Gottgens *et al.*, Nucl. Phys. B **178**, 392 (1981); **206**, 349 (1982).
[94]A. M. Baldin and L. A. Didenko, Kr. Soobshch. OIYaI, Dubna, (1984), No. 3-84, p. 5; No. 8, p. 5.

Translated by M. E. Alferieff